A Mathematical Model for the Devolatilization of EPDM Rubber in a Series of Steam Stripping Vessels

by

Angelica Joanne Bernice Francoeur

A thesis submitted to the Department of Chemical Engineering

in conformity with the requirements for

the degree of Master of Applied Science

Queen's University

Kingston, Ontario, Canada

October 2012

Abstract

A steady-state mathematical model for the stripping section of an industrial EPDM rubber production process was developed for a three-tank process, and two four-tank processes. The experiments that were conducted to determine model parameters such as equivalent radius for EPDM particles, as well as solubility and diffusivity parameters for hexane and ENB in EPDM polymer are described. A single-particle multiple-tank model was developed first, and a process model that accounts for the residence-time distribution of crumb particles was developed second. Plant data as well as input data from an existing steady-state model was used to determine estimates for the tuning parameters used in the multiple-particle, multiple-tank model. Using plant data to assess the model's predictive accuracy, the resulting three-tank and four-tank process B models provide accurate model predictions with a typical error of 0.35 parts per hundred resin (phr) and 0.12 phr. The four-tank process A model provides less-accurate model predictions for residual crumb concentrations in the second tank and has an overall typical error of 1.05 phr. Additional plant data from the three- and four-tank processes would increase the estimability of the parameter values for parameter ranking and estimations steps and thus, yield increased model predictive accuracy.

Acknowledgements

I would like to acknowledge a number of friends, family and colleagues who without whom I would not have been able to complete this thesis.

My sincerest thanks go to my funding partners: Queen's University, Lanxess, and MITACs. The financial support provided by these groups was very much appreciated.

I would like to thank my supervisor, role model and friend, Dr. Kim McAuley. Her contagious passion for mathematical modeling ignited my interest in the field and was a continued source of motivation to complete my work. I will forever be thankful for her continuous support, encouraging pep-talks, and sage advice.

I would like to thank my supervisor abroad, Dr. Luigi D'Agnillo. He provided the critical link between the world of academia and industrial research. Without his support, I would not have been able to conduct my research at Lanxess' Research and Development site in Geleen, Netherlands, nor would I have had such accommodating access to quality industrial data.

To my dear friends, housemates, and colleagues from Queen's University and abroad: thank you for the good times in Dupuis Hall and the many other fine establishments in Kingston, Ontario. I hope we can celebrate our successes together again soon.

My parents, Stephen and Anna, and my siblings, Stephen, Michael, & Amanda, deserve a great deal of thanks. Their unconditional love and support for me throughout my arduous, seemingly unending, academic journey was very much appreciated. The strength that each of you demonstrated throughout the various crises our family has faced during my academic career will continue to motivate me to persevere through the tough times and conquer adversity.

Last, but not least, I would like to thank my husband, David. His generous, loving and selfless support for me and my engineering pursuits is truly amazing. He has been my rock throughout my academic ups and downs and continues to motivate me to achieve excellence in all areas of my life. I am extremely lucky to have him by my side.

Table of Contents

List of Figures

List of Tables

Nomenclature

Symbols	
C	Concentration
D	Diffusivity
$\overline{D}$	Diffusivity, taking into account concentration-dependence and residence time distribution
$E(t)$	CFST residence time distribution function
f	Approximations for the first derivatives used in the multivariate Newton's method
F_{crumb}	Mass flowrate EPDM crumb through the tank
$F_{dif,j}$	Molar flowrate of species *j* flowing out of the EPDM particles into the headspace
$F_{pre,j}$	Flowrate of species *j* flowing into the headspace
$F_{in,j,i}$	Flowrate of species *j* entering tank *i* within the crumb
$F_{out,j,i}$	Flowrate of species *j* exiting tank *i*
H	Henry's law constant
$I_{j,0}$	Adjustable factor to tune the inlet concentration of species *j* in the crumb
J	Objective function to minimize for parameter estimation
k	Thermal conductivity
L	Half-thickness of an EPDM plaque
m	Average concentration
$\overline{m}$	Average concentration, taking into account the residence time distribution
M	Fraction of the way for the diluent-EPDM system to reach equilibrium
M_t/M_∞	Fraction of solvent remaining in the diluent-EPDM sample at any time *t*
MW	Molecular weight
p	Adjustable factor to tune the pressure for the three- and four-tank process models
p_{34}	Adjustable factor to tune the pressure in tanks 3 and 4 for the four-tank process model
P	Total pressure
P_j	Partial pressure for diluent *j*
P_W^{sat}	Saturation pressure of water, calculated using the Antoine equation
R	Diffusion distance in an EPDM particle
r_j	Total molar flowrate of species *j* entering the headspace
r_{cc}	Corrected critical ratio used to select the number of parameters to estimate
$R_{1,\,2,\,\ldots\,8}$	Effective diffusion radius for EPDM grades 1 to 8
s	Slope parameter for concentration-dependent diffusivity expression
$s_{m_{j,i}}$	Uncertainty associated with the industrial $m_{j,i}$ data
$s_{\theta_{k0}}$	Estimate of the uncertainty associated with the initial estimates for the parameter values
t	Time
t_{bi}	Average time spent in in tank *i* by particles in the bi^{th} bin
$t_{biL,\,R}$	Time at the left edge and right edge of the bi^{th} bin in tank *i*
t'	Equivalent time

T	Temperature
T_{av}	Average temperature
x	Diffusion distance in an EPDM plaque
y	Mole fractions in gaseous headspace
Y_i	Adjustable factor to tune the residence time in tank *i*
Z	Sensitivity matrix

Subscripts	
0	Indicates the variable at an initial or an inlet condition
A, B	Indicated parameters used in the four-tank processes A and B
bi	Indicates the time bin number
bi'	Indicates the equivalent time bin number
Сб	Used in place of *j* to indicate hexane
ENB	Used in place of *j* to indicate ENB
eq	Indicates a variable at an equilibrium condition
i	Indicates the tank number (e.g. 1, 2, 3, 4)
j	Indicates the diluent species
k	Indicates the multivariate Newton's method iteration
$k\delta$	Indicates the perturbed mole fraction for iteration k in the multivariate Newton's method
min	Indicates minimum in the set
n	Indicates the progression through the infinite sum approximation
N	Used in place of *j* to indicate nitrogen
ref	Indicates the variable at a reference condition
VNB	Used in place of *j* to indicate VNB
W	Used in place of *j* to indicate water

Greek	
α	Activation energy term for the Henry's constant Arrhenius expression
β	Activation energy term for the diffusivity-related Arrhenius expression
Υ	Proportionality factor between molar flowrate and mole fraction in the headspace
δ	Amount of perturbation for iteration *k* in the multivariate Newton's method
$\eta_{m_{j,i,r}}$	Prediction for the measured concentration of diluent *j* in crumb leaving the i^{th} tank from the r^{th} data set
θ	Parameter
ρ	Density
π	Pi
τ	Average residence time
τ'	Calculated equivalent average residence time
ϕ	Fraction of particles within the specified time bin

Chapter 1:
Introduction & Literature Review

The main objective of this research project is to develop a steady-state mathematical model for the stripping section of an industrial EPDM rubber production process. This model should:

- Provide accurate predictions of concentrations of residual solvent and monomers in the rubber particles (crumb) that exit each vessel in a train of three or four stripping vessels.
- Account for diffusion-limited mass-transfer out of the crumb particles as a function of stripper operating conditions, particle size and EPDM properties.
- Account for particle residence time distribution in multiple vessels in series with different operating conditions.

The model equations should be sufficiently simple so that they can be solved on-line to provide information for operators and plant engineers. Basic information about EPDM polymers, production processes and existing mathematical models are provided below, followed by a general outline for this thesis.

1.1 EPDM Structure

EPDM is a type of elastomer which Ver Strate (1990) defines as "a polymeric material that rapidly recovers its shape after removal of a strain of at least 50% and whose entropically derived equilibrium modulus increases with temperature." Terpolymers composed of ethylene, propylene and various diene monomers have the ASTM designation of EPDM (Ver Strate, 1985; Bisio and Tegge, 1984). The 'M' in the name refers to the methyl backbone of the polymer (Noordermeer, 2002) or to the polymer's saturated backbone (Davis et al., 1996). The formula for a generic ethylene-propylene-diene rubber is given in Figure 1 where m = ~1500 (~60 mol%), n = ~975 (~39 mol%), and o = ~25 (~1 mol%). Commercial EPDM is a random terpolymer, although limited quantities of block terpolymers have also

been produced (Ver Strate et al., 1999). Industrial EPDM ranges in total molecular weight from approximately 50,000 g/mol to 300,000 g/mol.

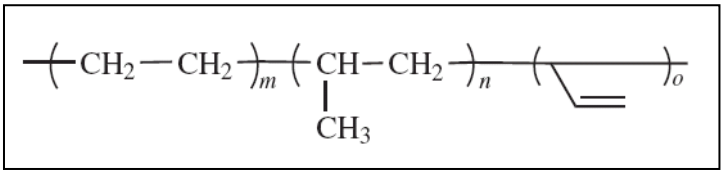

Figure 1: EPDM polymer structure with 1,4-hexadiene as the diene comonomer (Noordermeer, 2002). Note that the various monomers are arranged randomly.

Unlike the majority of other synthetic rubbers, EPDM is mostly a saturated hydrocarbon with a random-coil configuration (Ver Strate, 1990). Exposure of other synthetic rubbers to oxygen, ozone, and ultraviolet light would result in backbone cleavage, due to unsaturation along the backbone. This cleavage leads to the reduction of molecular weight and loss of physical properties (Davis et al., 1996). EPDM's saturated backbone provides it with excellent weatherability and heat resistance (Davis et al., 1996). Bisio and Tegge (1984) summarized some common requirements for third monomers in EPDM. The diene should:

- Be nonconjugated; only one double bond should be polymerizable and the other suitable for sulfur vulcanization, pendant to the main chain to avoid chain scission.
- Be distributed randomly along the polymer chain.
- Exhibit a high copolymerization rate while not interfering with the polymerization of ethylene and propylene.

The pendant double bonds, rather than double bonds within the chain, are especially beneficial so that ozone- and oxygen-attack will occur at the pendant olefin site on the side chain, leaving the main chain undisturbed (Ver Strate, 1985).

Several different diene monomers are used commercially (Noordermeer, 2002) including 5-ethylidene-2-norbornene (ENB), dicyclopentadiene (DCPD), and 5-vinyl-2-norbornene (VNB) (see Figure 2). Several dienes may also be used in combination (Noodermeer, 2002).

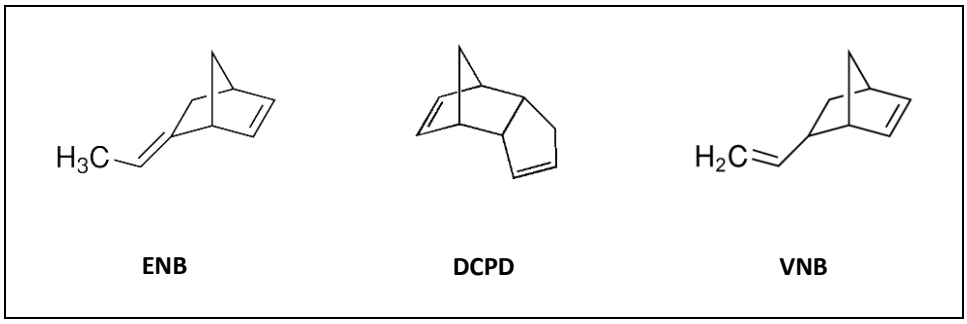

Figure 2: Structure of diene comonomers used in industrial EPDM (Noordermeer, 2002)

The structure of EPDM that results from the addition of ENB is shown in Figure 3. Note that the ring strain makes the double bond in the six-member ring the more active site for polymerization, compared with the secondary olefin.

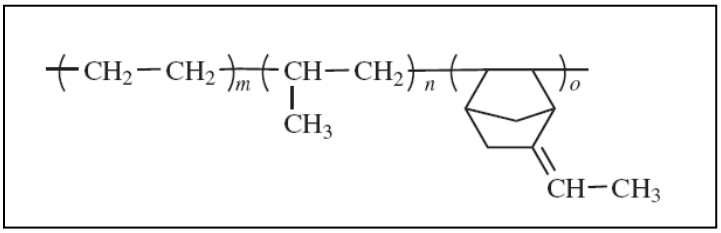

Figure 3: EPDM polymer structure with ENB as the diene comonomer (Noordermeer, 2002)

Dienes are selected to give polymer qualities that are desired for further polymer processing (Bisio and Tegge, 1984). For example, in order to vulcanize EPDM rubber with common sulfur vulcanization processes, it is necessary to have approximately 1 to 2 wt% unsaturation.

1.2 Polymer Properties

EPDM properties are largely determined by the polymer structure; that is, the saturated nature of the backbone, the relative monomer composition, and molecular weight. Other structural factors affecting the rubber's properties include molecular weight distribution, composition distribution, and type of diene (Davis et al. 1996). EPDM is most often compounded with oils, fillers and curatives, then crosslinked using sulfur-based curing systems. Polymer properties that are especially significant for commercial EPDM grade characterization are: Mooney viscosity (an empirical measure of average

molecular weight), molecular weight distribution, ethylene content, and diene type and concentration (Bisio and Tegge, 1984; Davis et al., 1996).

1.3 Industrial Process Overview

EPDM is commercially produced by solution and suspension processes, but gas-phase EPDM processes have also developed (Davis et al. 1996). Most production processes are operated continuously using liquid-phase back-mixed reactors. In industry, production commonly proceeds as a solution process in hexane (Ver Strate, 1990), which is the focus for the modeling work in this thesis. Solution polymerization was at first preferred because of its flexibility in terms of the number of different products that could be produced (Ver Strate, 1985). Ziegler-Natta catalysts are used in combination with aluminum alkyls to scavenge water and other impurities that would deactivate the catalyst (Ver Strate, 1985). The EPDM production process may be simplified into four steps: polymerization, degassing, stripping, and finishing. These steps involve the recycling of three of the process fluids: that is, the unreacted monomers, hexane solvent, and water.

Monomers, hydrogen, Ziegler-Natta catalyst, aluminum alkyl halide cocatalyst and activator streams are continuously fed in an alkane solvent to a CSTR (Davis et al., 1996). While a single reactor can be used, a series of reactors results in higher conversions and higher catalyst efficiencies, and provides flexibility in product properties (Ver Strate, 1985). Polymerization is very fast and extremely exothermic in nature. Temperatures can vary from 20 to 40°C and pressures may range from 1 to 20 atm (Bisio and Tegge, 1984). Residence times range from 30 to 90 minutes (Davis et al., 1996).

The EPDM dissociates from the catalyst and remains in solution. Viscosity increases with conversion and therefore, reduces effective reactor mixing and heat transfer as the process continues; thus, there exists an upper safe limit of polymer concentration in the solution (Bisio and Tegge, 1984) of 5 to 10 wt% (Davis et al., 1996). After the reaction stage, vigorous stirring of the solution with water kills

the catalyst and prevents side reactions from drastically increasing the viscosity (commonly called "Mooney Jumping") (Noordermeer, 2002).

From the polymerization reactor(s), the two-phase mixture containing the product solution and associated water passes continuously into a flash tank where most of the unpolymerized monomers evaporate and are collected to be recycled back to the reactor. To separate the EPDM rubber from solution, a steam stripping method is utilized. The viscous rubber slurry is pumped into either a single vessel, or a series of vessels, containing rubber particles in boiling water (Noordermeer, 2002) shown in Figure 4.

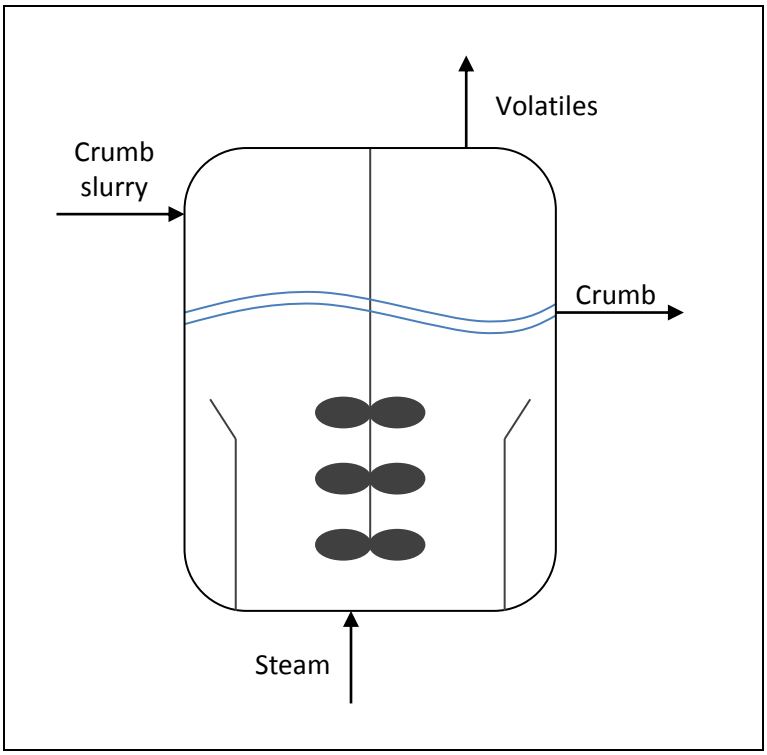

Figure 4: Schematic diagram of a single stripping vessel

On the industrial scale, steam-stripping is usually carried out continuously. Fresh steam is fed to the bottom of each stripper and the contents are agitated such that the rubber crumb particles come into direct contact with water vapour, enabling the majority of the hexane to flash (Quadri, 1998; Noordermeer, 2002). The water and hexane vapour mixture is collected, condensed, separated and recycled. Unpolymerized monomers in the gas phase are also separated and recycled (Noordermeer,

2002). After the stripping phase, the crumb and water mixture enters one or more stirred vessels in a series which are used to store the polymer crumb and capture additional volatiles.

Polymer crumb particles that leave the last vessel are mixed with hot water. The excess water is separated from the solid crumb, usually in a dewatering press, after which up to 15% of the water remains in the crumb. The dewatered crumb can then be fed to an extruder, reaching temperatures up to 150 ^{o}C and pushed through a perforated die plate. The rubber particles are then air-dried either in a fluidized bed or a tunnel drier. In general, residual monomers and moisture are reduced during the dewatering, extrusion and drying processes to below 0.5 wt% (Ver Strate, 1990). Finally, the rubber is pressed into bales (Davis et al., 1996) or, for highly crystalline EPDM, extruded into pellets (Noordermeer, 2002).

1.4 Mathematical Models for EPDM Stripping and Experiments to Obtain Parameter Values

Since residual monomer and solvent removal from polyolefins can sometimes be problematic in industrial processes, several models have been developed to predict the removal of organic penetrants from ethylene propylene rubber (EPR) and/or EPDM particles (van Amerongen, 1964, and references within; Frensdorff, 1964 a, b; Matthews et al., 1986 a, b; Cozewith, 1994; Quadri, 1998). Matthews et al. (1986 a, b) developed a model to describe diffusion of hexane solvent vapors from EPR particles, taking into consideration several phenomena including:

i. A concentration-dependent diffusivity expression that accounts for the influence of solvent concentration (initially as large as 10 wt% in the crumb particles) on the diffusion coefficient.
ii. Influence of residence time distribution on solvent concentrations in particles leaving a single stripping vessel.

Matthews et al. (1986 a) indicated that previous experiments to determine diffusivity of small molecules from polyolefin particles focused on only dry polymer particles; no previous research had been

conducted concerning "organic penetrants in wet, hydrophobic rubbers such as the ethylene-propylene elastomers." Matthews et al. (1986 a) cautioned that "the presence of water in rubbers affects diffusion of organic penetrants significantly. Care must be taken in generalizing results obtained with dry rubber in the laboratory to include wet rubbers encountered in steam-stripping applications."

The following diffusion equation was used by Matthews et al. (1986 a) to model the mass transfer of solvent out of a pressed EPR plaque suspended in either gas or water:

$$\frac{\partial C}{\partial t} = D\frac{\partial^2 C}{\partial x^2} \tag{1}$$

The corresponding boundary conditions are as follows:

i. At depth x = 0 (the centre of their sample), there is no diffusion to or from the plaque. This condition occurs because the concentration profile is symmetrical at the centre-line.

$$\left.\frac{\partial C}{\partial x}\right|_{x=0} = 0 \tag{2}$$

ii. At time zero, the concentration in the sample is equal to the initial concentration at all depths, x; *i.e.*, the solvent concentration is initially uniform throughout the plaque.

$$C|_{t=0} = C_o \tag{3}$$

iii. At depth $x = \pm L$, the surface concentration within the rubber is in equilibrium with the bulk contacting gas and liquid, C_{eq}. This boundary condition requires that there is no liquid-phase or gas-phase resistance to mass transfer.

$$C|_{x=L} = C_{eq} \tag{4}$$

This model could be solved numerically, but an analytical solution is also available. Carslaw and Jaeger (1959) provide the solution to the analogous heat transfer (conduction) problem and the adapted mass transfer (diffusion) model is provided by Crank (1956). The average temperature (T_{av}) within a solid plate undergoing one-dimensional heat transfer (in the x direction only) with heat loss from the top and bottom surfaces is:

$$T_{av}(t) = \frac{8T_0}{\pi^2}\sum_{n=0}^{\infty}\frac{1}{(2n+1)^2}e^{\left(\frac{-kt(2n+1)^2\pi^2}{4L^2}\right)} \quad (5)$$

where T_0 is the initial temperature of the solid, k is the thermal conductivity, L is the half-thickness of the plate, and t is time.

This expression can be rearranged such that the left-hand side of the equation describes the fraction of the way to steady state temperature T_{eq}:

$$\frac{T_{av}(t)-T_0}{T_{eq}-T_0} = 1 - \frac{8}{\pi^2}\sum_{n=0}^{\infty}\frac{1}{(2n+1)^2}e^{\left(\frac{-kt(2n+1)^2\pi^2}{4L^2}\right)} \quad (6)$$

The analogous mass-transfer expression is:

$$M(t) = \frac{m(t)-m_0}{m_{eq}-m_0} = 1 - \frac{8}{\pi^2}\sum_{n=0}^{\infty}\frac{1}{(2n+1)^2}e^{\left(\frac{-Dt(2n+1)^2\pi^2}{4L^2}\right)} \quad (7)$$

where *M(t)* is the fraction of the way to equilibrium, *m(t)* is the average concentration (in mass %) of solvent in the rubber plaque after being exposed to stripping conditions for a time period of duration *t*, m_0 is the initial solvent concentration, m_{eq} is the concentration of the solvent in that would be in "equilibrium" with the contacting gas or liquid phase, and *D* is the diffusivity of the solvent in the rubber.

Matthews et al. (1986a) assumed that hexane diffusivity had a linear dependence on solvent concentration in the rubber, indicated by equation 8:

$$D(C) = D(0)(1 + sC) \quad (8)$$

where *D(C)* is the diffusivity of hexane at concentration, *C,* in the wet rubber in g/cm^3, *D(0)* is the diffusivity at zero hexane concentration in the rubber, and *s* is a slope parameter. Using stripping data from two different initial hexane concentrations, Matthews et al. (1986 a) determined that *D(0)* = 1.796 x 10^{-7} cm^2/s and *s* = 300 cm^3/g.

Based on experiments using plaques pressed from wet and dry rubber particles, Matthews et al. (1986a) concluded that the presence of water in the particles used to produce the plaques reduced *D(0)* by a factor of ~13. They also concluded that the hexane stripping rate is not influenced by the aqueous

phase surrounding the particles, presumably because the main resistance to mass transfer is within the rubber particles, rather than in the liquid phase or gas phase of the stripping vessel.

Matthews et al. (1986 a) modeled the individual crumb particles as "an assemblage of spheres" and determined the "effective" radii for solvent diffusion in industrial EPR crumb particles via three different methods. One method involved a particle-characterization method termed "wet-profile measurement" which determined the number-average radius of the wet regions. The other two methods used lab-scale stripping data, and the following diffusion model:

$$\frac{d}{dt}[ln(1 - M_t/M_\infty)] = -D(0)\pi^2/R^2 \quad (9)$$

where M_t/M_∞ is the fraction of solvent remaining in the sample at any time, t, and R is the effective diffusion radius. They showed that the effective radii determined using the three methods were in reasonable agreement and reported the effective radius to be "on the order of 1 mm for 0.63 and 1.27 cm diameter crumb particles" obtained from an industrial EPR process (Mathews et al., 1986a).

The goal of the second part of the two-part study by Matthews et al. (1986 b) was to model the diffusion of solvent out of EPR crumb exiting a single continuous-flow stripping reactor. Continuing from part one, Matthews et al. extended their model by incorporating overall material and energy balance equations for the stripping vessel. Since mass transfer could be modeled assuming diffusion within an assemblage of small spheres, Fick's Second Law, in spherical coordinates, was applied:

$$\frac{\partial C}{\partial t} = \left(\frac{1}{r^2}\right)\frac{\partial}{\partial r}\left[D(C)r^2\frac{\partial C}{\partial r}\right] \quad (10)$$

Assuming sufficiently low levels of solvent in the stripper, the solvent concentration was replaced by:

$$C = \rho m/100 \quad (11)$$

to obtain an expression in terms of solvent mass percent, m, and the rubber density, ρ. Integration of diffusivity equation 8 to account for changes in concentration with time resulted in the following expression for the average diffusivity within the crumb:

$$\overline{D} = D(0)(1 + 1.5\rho[m_o + m(t)]) \quad (12)$$

where m_0 is the initial concentration of solvent in the crumb, and *m(t)* is the average concentration of solvent in crumb particles after being exposed to stripping conditions for a time period of duration, *t*. The final model equation that they derived to describe mass transfer from individual small particles in the assemblage is:

$$M(t) = \frac{m(t) - m_0}{m_{eq} - m_0} = 1 - \frac{6}{\pi^2} \sum_{n=1}^{\infty} \frac{e^{\left(-\frac{\bar{D} n^2 \pi^2 t}{R^2}\right)}}{n^2} \quad (13)$$

where *t* is the time duration within the stripping vessel.

To account for the fact that the process is operated continuously in a well-mixed vessel, a residence time distribution for a continuous flow stirred tank (CFST) (Himmelbau and Bischoff, 1968; Levenspiel, 1962) was incorporated to account for the different times that crumb particles would spend in the stripping vessel:

$$\frac{\bar{m} - m_0}{m_{eq} - m_0} = 1 - \frac{6}{\pi^2} \sum_{n=1}^{\infty} \frac{1}{(\bar{D}\tau/R^2) n^4 \pi^2 + n^2} \quad (14)$$

where $\bar{m}$ is the average concentration of solvent that remains in a sample of the outlet EPDM crumb leaving a single steam stripping tank, and τ is the crumb residence time in the vessel. The model parameters were determined as follows:

i. m_{eq} was calculated from a Flory-Huggins relationship and the hexane partial pressure in the gas phase.

ii. m_0 and $\bar{m}$ were determined by dissolving a known mass of crumb particles in toluene and then measuring the amount of dissolved hexane by gas chromatography.

Matthews et al. (1986 b) concluded that their model appropriately accounted for the effects of the major operating variables.

More recently, Cozewith (1994) extended the models of Matthews et al. (1986 a, b) in an effort to predict residual concentrations in crumb particles emerging from a series of two or more stripping vessels. Cozewith applied the following assumptions:

- Crumb particles are uniform in size.
- Particles are perfectly mixed in each vessel.
- No particle agglomeration or fragmentation occurs.
- All vessels are CFSTs.

He began his model development by assuming that the residence times, temperatures and gas compositions were the same for all of the tanks in series. He used equation 13 to predict the fractional removal of solvent in the particles leaving the first stripper. Cozewith noted that it is inappropriate to use equations 13 and 14 to predict solvent removal in downstream tanks (with m_0 set at the average inlet concentration for each particle) because a key assumption when deriving these equations is that the concentration of hexane is radially uniform in the particles that enter the tank; that is, particles entering the second stripping tank will have a higher hexane concentration at their centre than near their surface.

Assuming that D is constant and that m_{eq} and τ are the same for all tanks, he developed the following equation to predict $\bar{m}$ leaving the i^{th} tank in series:

$$\frac{\bar{m}-m_0}{m_{eq}-m_0} = 1 - \frac{6i^i}{\pi^2}\sum_{n=1}^{\infty}\frac{1}{\left(\frac{i\tau D\pi^2 n^2}{R^2}+i\right)^i n^2} \tag{15}$$

Cozewith then developed a more complicated expression, which is valid when the multiple tanks have different residence times (*i.e.*, τ_1, τ_2, …, τ_j):

$$\frac{\bar{m}-m_0}{m_{eq}-m_0} = 1 - \frac{6}{\pi^2}\sum_{j=1}^{i}\frac{1}{\prod_{\substack{m=1\\m\neq j}}^{i}\left(1-\frac{\tau_m}{\tau_j}\right)}\sum_{n=1}^{\infty}\frac{1}{\left(\frac{\tau_j D\pi^2 n^2}{R^2}+1\right)n^2} \tag{16}$$

Finally, he developed a model to account for different values of D and m_{eq} in different stripping tanks due to different temperatures and hexane partial pressures. He made the restrictive assumption that m_0 in the particles entering the first tank is much greater than m_{eq} in all tanks (*i.e.*, $m_0 >> m_{eq1}$, $m_0 >> m_{eq2}$, …, $m_0 >> m_{eqj}$) and developed the following equation to predict the average hexane content in particles leaving the i^{th} stripping vessel:

$$\frac{m_0-\bar{m}_i}{m_0} = 1 - \frac{6}{\pi^2}\sum_{n=1}^{\infty} \frac{1}{n^2\left(1+{}^{D_1\pi^2n^2\tau_1}/_{R^2}\right)\left(1+{}^{D_2\pi^2n^2\tau_2}/_{R^2}\right)\cdots\left(1+{}^{D_i\pi^2n^2\tau_i}/_{R^2}\right)} \qquad (17)$$

Using equation 17 for two vessels with R = 0.007 cm, and D = 0.17 x 10^{-5} cm^2/s, Cozewith (1994) concluded that the best stripping results were obtained when the vessels have equal residence times.

Quadri (1998) extended Cozewith's model to include ordinary differential equations that describe a thin well-mixed boundary layer in the liquid phase. These equations are used to account for mass-transfer resistance in the liquid phase. As a result, Quadri's model requires additional mass-transfer parameters. He used the model to study the effectiveness of various solvents and multiple solvents under continuous and batch operation.

In summary, several mathematical models have been developed to describe solvent or residual monomer removal from individual particles under different stripper operating conditions. In addition, models have been developed to predict the average solvent concentration in particles that exit one or more stripping vessels in series. The tanks-in-series model (Cozewith, 1994) requires the user to assume either that stripping conditions (*i.e.*, temperature and solvent partial pressure) are very similar in all tanks, or that the inlet concentration of solvent (or unreacted monomer) is much higher in the initial crumb than would be encountered in the tanks if equilibrium were obtained between particles and the headspace. These assumptions may not be valid during industrial operation of EPDM strippers, particularly for ENB and VNB monomers due to their much lower concentrations. It should also be noted that use of the pre-existing models requires information about the equivalent diameter for diffusion, equilibrium partitioning of the solvent between the gas phase and the rubber particles, and solvent diffusivity within the rubber. This information has not been characterized for EPDM monomers and may not be accurate for the industrial EPDM grades and range of stripping conditions that are the focus for this project.

1.5 Plan of the Thesis

The intent of this thesis is to provide a mathematical model to describe industrial EPDM stripping without relying on the potentially inaccurate assumptions or parameters that were used in pre-existing models. This project will provide an estimation of model parameters and an evaluation of the model's predictive accuracy. Chapter 2 describes the experiments that were conducted to determine key model parameters such as diffusivity, Henry's law constants, and the equivalent radius for EPDM crumb particles. The models that are developed and the techniques used to solve the model equations, are described in following chapters: in Chapter 3, a single-particle multiple-tank model is developed and in Chapter 4, a process model that accounts for the residence-time distribution of the crumb particles is described. Parameter estimation using industrial data and testing of the multiple-tank process model is described in Chapter 5. Finally, conclusions and recommendations are provided in Chapter 6.

Chapter 2:
Experimental Determination of Key Physical Properties for Model Development

This chapter includes a description of the experimentally determined modeling parameters that are required for the stripping model. Diffusion coefficients for hexane and ENB diffusing in and out of EPDM rubber, the Henry's Law constants for hexane and ENB in EPDM rubber, and the characteristic diffusion radius of EPDM crumb particles are determined using gravimetric tests. The experimental procedure, analysis, and results are discussed in the remainder of this chapter.

2.1 Gravimetric Testing Method

Gravimetric testing was conducted for a variety of industrial EPDM samples, at a variety of conditions for two different diluents: hexane and ENB. EPDM samples from five different product grades (with different values of Mooney viscosity, weight fraction of ENB, and degree of long-chain branching) were tested. The various testing conditions were selected to mimic drying conditions in the stripper and buffer tanks of the industrial process (*i.e.*, temperatures ranged from 90°C to 140°C and total pressure was 1 atm). In some tests, EPDM crumb particles were pressed into plaques (to determine diffusivities and Henry's law constants). In others, crumb particles were tested in their normal state (to determine effective radius for diffusion).

For each polymer sample placed in the gravimetric testing apparatus, multiple step tests were conducted wherein a series of step changes in partial pressures of the diluent gas (either hexane or ENB) in contact with the polymer were introduced. Diluent partial pressures ranged from 0 to approximately 900 mbar since these are the concentrations of diluent gas that are typically present in the headspace in industrial stripper and buffer tanks. Experiments were repeated using five selected temperatures between 90 and 140 °C.

When preparing plaques, approximately 2.5 g of wet EPDM rubber was pressed flat using a heated hydraulic press, using a pressing time of 3 minutes, resulting in a sheet with a thickness of ~1 mm. The resulting square samples were then cut with scissors to form a circle with a radius of approximately 25 mm. The mass of the polymer sample and the thickness, *L*, measured with a caliper, was recorded. The samples were placed in 25 mm radius circular tin trays as shown in Figure 5, which were stored in protective plastic bags prior to testing.

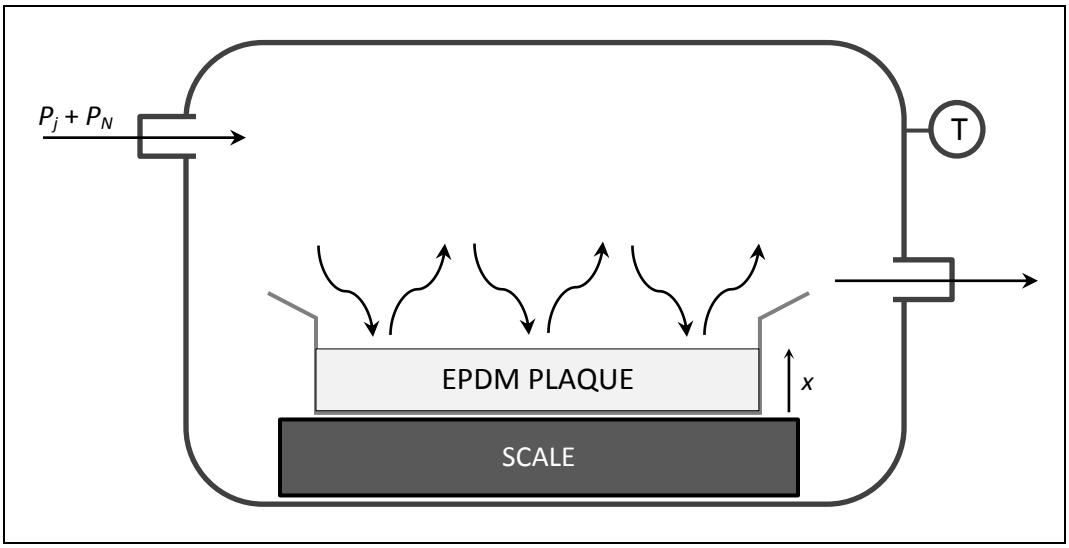

Figure 5: A schematic diagram of the gravimetric testing apparatus (not to scale) at constant temperature, *T* and constant monomer or solvent partial pressure, P_j

The gravimetric testing apparatus was located within a well-ventilated enclosure. The apparatus included a computer control system that regulated experimental conditions and collected temperature, pressure and mass data. Samples were placed in a tray that hangs from a scale within a temperature-controlled, double-walled glass vessel. Temperature was controlled using ethylene glycol, which circulates between the two glass walls. Nitrogen gas and the liquid diluent (either hexane or ENB) were mixed externally, and then passed through the glass vessel to contact the sample. Flowrates of the nitrogen and liquid streams were selected to achieve the desired diluent partial pressure. Sample mass, diluent flowrate, nitrogen flowrate, and temperature measurements were collected throughout each step change experiment.

At the beginning of each experiment, only nitrogen gas was fed to the apparatus to ensure that the rubber sample would start from a diluent-free equilibrium condition. After reaching the initial mass and temperature equilibrium (approximately two hours), the liquid diluent flow was initiated to achieve the desired partial pressure for the first step. After reaching equilibrium, the liquid flowrate was adjusted to the new value required for a second (and sometimes a third) step. After step tests with increasing liquid flowrates were completed, the diluent flowrate was set to zero so that only nitrogen was fed to the tank, resulting in desorption of the diluent from the polymer sample. When the final diluent-free equilibrium was reached, the gravimetric test was complete.

Following the experiment, the sample was allowed to cool to room temperature and the sample thickness was re-measured using calipers. Figure 6 is a plot of the resulting data curves from Run 1 of the hexane experiments. For this data set, there are two upward steps. After reaching an initial mass equilibrium (0 mbar hexane), there is a step change in diluent (hexane) partial pressure to 393 mbar C6. After reaching this second equilibrium, a step change was made to 866 mbar C6 where equilibrium was reached. Finally, the diluent partial pressure returned to zero and the sample weight returned to its original value as the diluent diffused out of the polymer plaque. Note that the mass of the diluent-free plaque has been subtracted from the results shown in Figure 6.

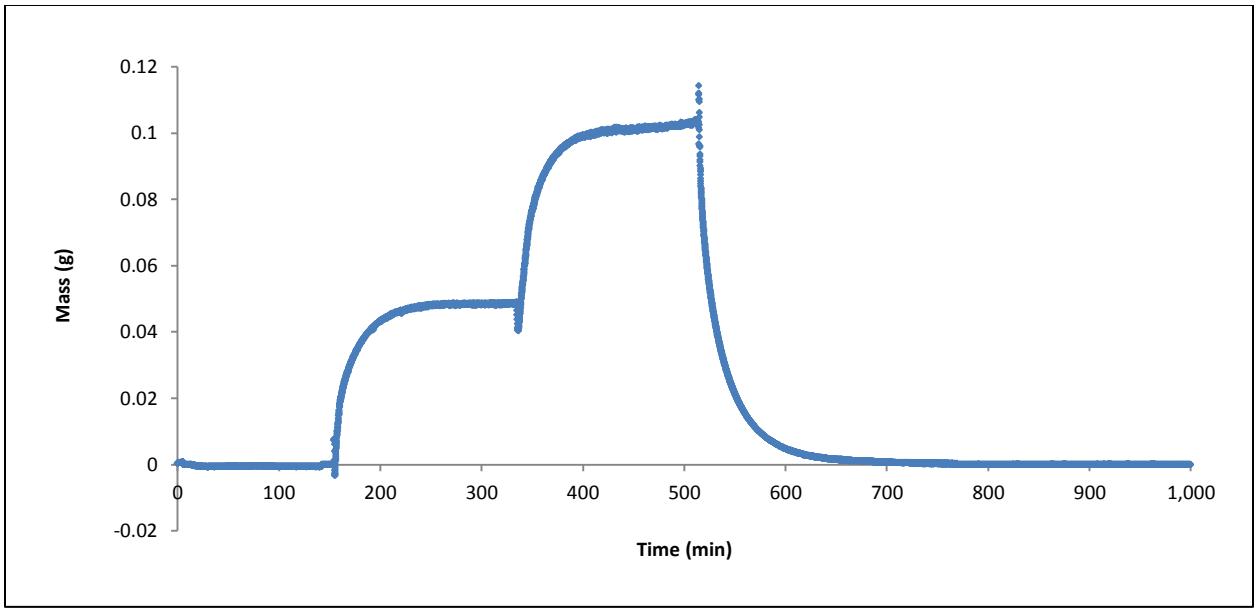

Figure 6: A sample set of data from gravimetric experiments

There is some evidence of an inverse response at the start of each step change, presumably due to jostling of the sample in the apparatus when gas flows are adjusted abruptly. This initial dip in apparent mass was ignored in the data analysis described in this thesis.

2.2 Estimation of Henry's Law Constants and Diffusivities for Hexane and ENB in EPDM

The data were used to estimate diffusivities and Henry's law constants from each adsorption/desorption curve via nonlinear regression. To determine the solubility or Henry's law constant from the steady-state data for each step change the partial pressure of the monomer or solvent in the gas (P_j) is divided by the concentration of monomer or solvent absorbed in the crumb at equilibrium:

$$H_j = \frac{P_j}{m_{eq,j}} \tag{18}$$

Throughout this thesis, the concentration $m_{eq,j}$ is expressed in phr (parts per hundred resin, or g diluent per 100 g EPDM) and the Henry's law constant H_j is in units of mbar/phr. The subscripts *C6*, *ENB* and *VNB* are used in place of *j* to indicate hexane, ENB and VNB, respectively. Diffusivity values were

determined from gravimetric test data obtained using hexane and ENB. No solubility or diffusivity experiments were performed using VNB. The following steps were used to compute D_{C6} and D_{ENB} from the various experiments:

i. The fraction of the way to equilibrium, *M(t),* was calculated for each data point using the initial concentration and equilibrium concentration for each step test, as shown in equation 7. Data from the disturbance at the start of each step change were ignored (see Figure 6).

ii. The *M(t)* data collected for each grade at each temperature were then used to fit diffusivities for hexane and ENB using:

$$M_j(t) = 1 - \frac{8}{\pi^2}\sum_{n=0}^{\infty}\frac{1}{(2n+1)^2}e^{\left(\frac{-D_j t(2n+1)^2\pi^2}{4l^2}\right)} \quad (19)$$

and nonlinear regression. Note that infinite sum in equation 19 was evaluated using only the terms from n = 0 to n = 6 in the summation. Additional terms were not required because convergence to eight decimal places was typically achieved when only the terms from n = 0 to n = 3 were included in the calculation.

2.3 Estimation of Equivalent Radius of EPDM Crumb

To determine the equivalent radius for diffusion, a series of step experiments were conducted using EPDM crumb particles in the sample tray of the gravimetric apparatus. These experiments were conducted using hexane and ENB. Equation 13 was used to compute $M(t)$ for each data point from the step experiments (with points corresponding to the disturbances ignored). An appropriate estimated value of average diffusivity, $\overline{D}$, corresponding to the temperature and polymer grade of interest was substituted into equation 13, and the equivalent radius R was estimated using nonlinear regression. Note that only the terms from n = 0 to n = 6 in the infinite sum were used in equation 13 because use of additional terms had negligible influence.

2.4 Solubility and Diffusivity Results

Similar values of Henry's law constants and diffusivities were obtained when data from individual step tests were used to estimate the parameters (e.g., two Henry's law constants and three diffusivities from data in Figure 6). There was no noticeable trend in plots of Henry's law constant and diffusivity as a function of hexane or ENB concentration for two different EPDM grades. Plots showing the Henry's constants and diffusivities for hexane in EPDM Grade 2 are shown in Figures 7 and 8, respectively. Corresponding results for ENB are not shown, but also showed no trends. Note that the exact temperatures used in the experiments (*i.e.*, T1, T2, … T5) are not provided to protect proprietary data, but T1 > T2 > T3 > T4 > T5.

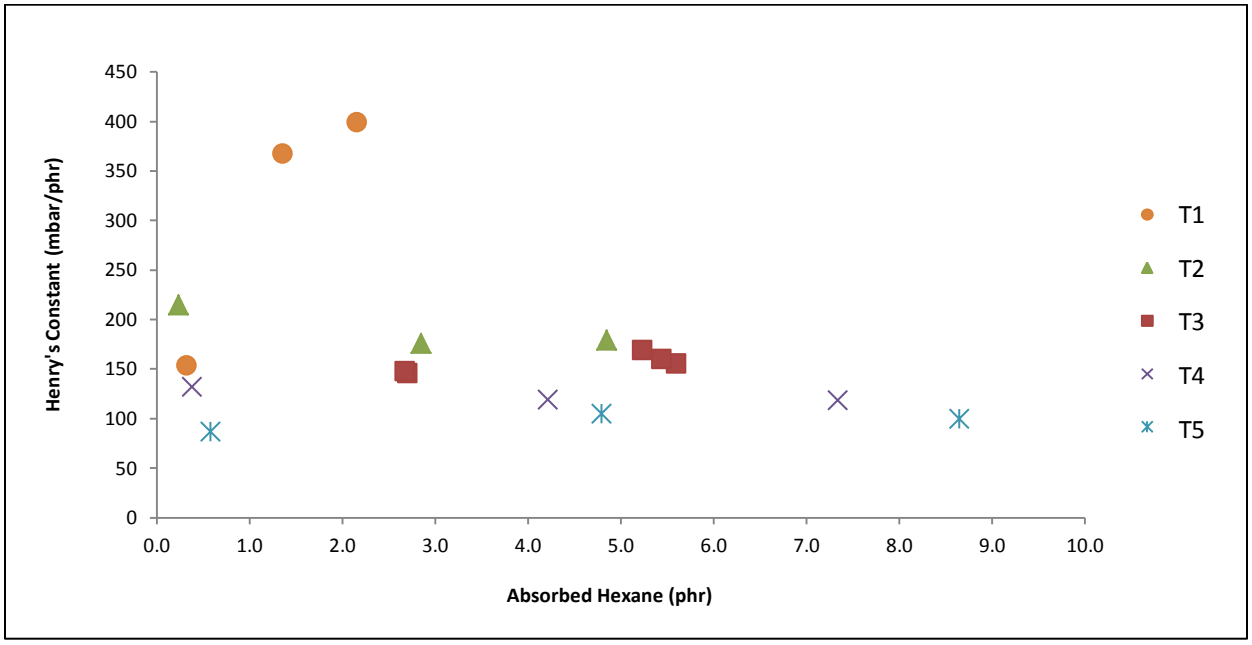

Figure 7: Henry's law constants as a function of absorbed hexane within EPDM grade 2 at various temperatures

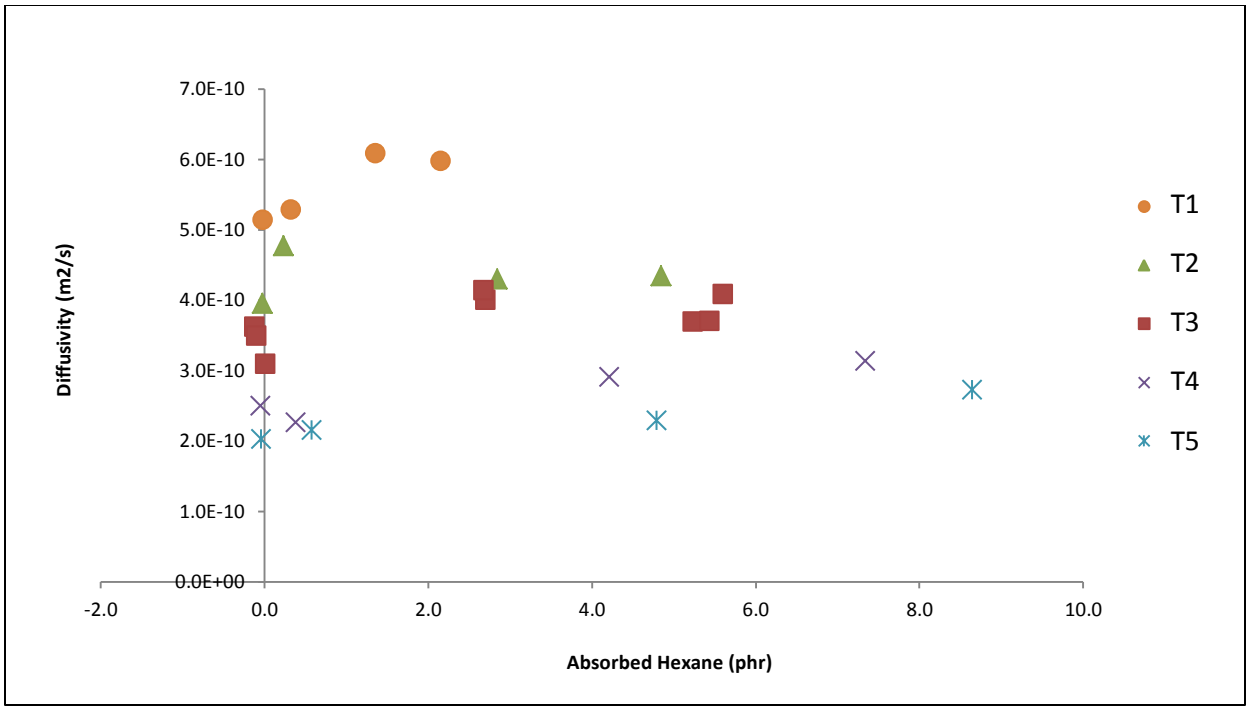

Figure 8: Diffusivity as a function of absorbed hexane within EPDM grade 2 at various temperatures

In summary, there is no apparent effect of absorbed diluent on either Henry's constants or diffusivity values for the two diluents studied, over the concentration range used in the experiments, which is a different result than Matthews et al. (1986 a) obtained in their study.

An overall estimate for Henry's law constant and diffusivity for each EPDM grade was fit via non-linear regression at each experimental temperature. Using these overall estimates for each grade at each test temperature, the temperature and polymer property effects were then analyzed. Using all of the data for EPDM experiments involving product Grade 2, statistically significant temperature effects for the Henry's law constant and diffusivity were observed. The following Arrhenius relationships were fit to the Henry's law constant data and diffusivity data, respectively:

$$H_j(T) = H_{j,ref} \exp\left(\alpha_j \left(\frac{1}{T} - \frac{1}{T_{ref}}\right)\right) \quad (20)$$

$$D_j(T) = D_{j,ref} \exp\left(\beta_j \left(\frac{1}{T} - \frac{1}{T_{ref}}\right)\right) \quad (21)$$

The reference temperature, T_{ref} was set at 381.15 K (108 °C). Table 1 shows the resulting estimated values for the Henry's law constant and diffusivity at 108 °C ($H_{j,ref}$ and $D_{j,ref}$) and the corresponding activation energy parameters (α_j and β_j) for hexane and ENB.

Table 1: Henry's law constant and diffusivity parameters for hexane and ENB in EPDM rubber estimated from gravimetric experiments conducted between 90 °C and 140 °C

	Parameter	Units	Value	Uncertainty at 95% Confidence Level	% Uncertainty
Henry's Law Constant for Hexane in EPDM	$H_{C6,ref}$	mbar/phr	153.48	7.43	5 %
	α_{C6}	K	3503.6	418.9	12 %
Henry's Law Constant for ENB in EPDM	$H_{ENB,ref}$	mbar/phr	10.125	1.790	18 %
	α_{ENB}	K	4719.0	1314.4	28 %
Diffusivity of Hexane in EPDM	$D_{C6,ref}$	m^2/s	3.418×10^{-10}	5.73×10^{-11}	17 %
	β_{C6}	K	2799.5	1373.3	49 %
Diffusivity of ENB in EPDM	$D_{ENB,ref}$	m^2/s	1.468×10^{-10}	1.56×10^{-11}	11 %
	β_{ENB}	K	2922.0	816.7	28 %

Temperature effects were judged to be significant because the 95% confidence intervals for α and β do not include zero. Note that the diffusivity for ENB at 108 °C is lower than the diffusivity for hexane, as expected because ENB is a considerably larger molecule. Note that there may also be a small influence of the EPDM properties (*e.g.*, ENB content within the EPDM polymer chains) on Henry's law constants and diffusivities, but the extent of this influence could not be determined reliably due to limited experimental data. In addition, it was observed that the viscoelastic nature of branched EPDM did not maintain the form of a flat plaque during the cycles in solute partial pressure and made interpretation of the data more difficult. However, more linear samples exhibited little or no dimensional change during the absorption cycle, and there was no significant difference in diffusivity or Henry's coefficient detected as a result of changes in molecular weight or chemical composition. Therefore, diffusivity and Henry's law constant can be considered to be grade-independent.

Estimates for the equivalent diffusion radius from several step tests are summarized in Table 2. Only EPDM grade 1 was used to estimate the characteristic crumb radius and only one gravimetric experiment was conducted.

Table 2: Characteristic radii as determined using a diffusivity value of 5.94×10^{-10} m^2/s for hexane diffusion into EPDM grade 1 at 108 ˚C

Case	Characteristic Radius (mm)
Step change: 0 to 50 mbar H	0.7107
Step change: 50 to 500 mbar H	1.5172
Step change: 500 to 860 mbar H	1.3192
Step change: 860 to 0 mbar H	2.1453
Lumped Estimate	**1.3551**

It should be noted that the lumped estimate is similar to the Matthews et al. (1986) value of approximately 1 mm.

2.5 Conclusions

Gravimetric tests were conducted to determine the Henry's constants and diffusivities for hexane and ENB comonomer in various types of EPDM rubber. It was determined that hexane and ENB concentrations do not influence either the Henry's law constants or diffusivity values appreciably over the range of experimental conditions of interest. An Arrhenius relationship between Henry's law constant and temperature was fitted, as was an Arrhenius relationship between diffusivity and temperature. Effects of product grade on diffusivity and solubility were less significant than the temperature effects and are not shown. A lumped estimate for the characteristic radius of EPDM grade 1 crumb was determined to be 1.36 mm using the experimentally determined hexane diffusivity of 5.94E-10 m^2/s at 108 ˚C.

Chapter 3:
Single-Particle Multiple-Tank Model Development

The main objective of this chapter is to develop a simple model that can predict diluent concentrations in a single particle that spends a certain amount of time t_1 in one well-mixed stripping vessel and then spends time t_2 in a second stripping vessel, with different operating conditions in the two vessels. The results obtained from this simple model are compared with those obtained using a rigorous Partial Differential Equation (PDE) approach to show the effectiveness of the simple model. The simple model developed in this chapter is used in a more complicated model in Chapter 4 that accounts for many particles and the residence time distributions in multiple tanks in series.

3.1 Simplified Equivalent-Time Model

A simplified equivalent-time model was developed that utilizes the analytical solution for mass transfer out of a spherical particle (equation 13).

Consider a single particle leaving the first steam stripper after spending time t_1 hours. The average mass concentration of hexane in the particle, $m_{C6,1}(t_1)$, can be determined using equation 13, given the initial concentration $m_{C6,0}$ and the diffusion coefficient $D_{C6,1}$ and equilibrium concentration $m_{eqC6,1}$ that match the operating conditions in this vessel. Imagine that after t_1 hours in the first steam stripper, the same crumb particle then enters a second steam stripper, which has a different operating temperature and hexane head-space partial pressure than the first vessel, so that $D_{C6,2}$ and $m_{eqC6,2}$ are different than the corresponding values in the first vessel. Unfortunately, equation 13 cannot be used to determine the exiting concentration of hexane from the second tank by simply using $m_{C6,1}(t_1)$ as the initial concentration. The particle leaving the first tank will have a radial concentration profile (with a higher hexane concentration in the centre), whereas use of equation 13 requires a uniform initial concentration throughout the particle.

A rigorous solution to determine $m_{C6,2}$ after t_2 hours in the second stripping vessel requires the solution of a PDE (e.g., equation 10), wherein the boundary conditions at the surface of the particle change abruptly after t_1 hours (and the diffusivity also changes to reflect the new temperature). This complicated method for solving for $m_{C6,2}(t_1+t_2)$ is illustrated using an example in section 3.2.

In an attempt to account for the hexane (or ENB or VNB) gradient in the crumb leaving the first vessel in an approximate fashion, an *equivalent-time* calculation is proposed. The equivalent time t'_2 is defined as the hypothetical amount of time that the particle would have to spend in the second vessel (starting from the uniform concentration $m_{C6,0}$) to achieve the same final average hexane concentration $m_{C6,1}(t_1)$ that was achieved in the first vessel, so that:

$$\frac{m_{C6,1}(t_1)- m_{C6,0}}{m_{eqC6,2}- m_{C6,0}} = 1 - \frac{6}{\pi^2}\sum_{n=1}^{\infty}\frac{e^{\left(-\frac{D_{C6,2}n^2\pi^2 t\prime_2}{R^2}\right)}}{n^2} \qquad (22)$$

Equation 22 is an implicit equation that can be solved iteratively to obtain t'_2.

A good way to approximate the average hexane concentration leaving the second vessel, $m_{C6,2}(t_1+t_2)$, is to assume that a similar concentration profile would be obtained if a particle with initial concentration $m_{C6,0}$ entered the second vessel and spent a total of $t = t'_2 + t_2$ hours:

$$\frac{m_{C6,2}(t_1+t_2)- m_{C6,0}}{m_{eqC6,2}- m_{C6,0}} \cong 1 - \frac{6}{\pi^2}\sum_{n=1}^{\infty}\frac{e^{\left(-\frac{D_{C6,2}n^2\pi^2(t'_2+t_2)}{R^2}\right)}}{n^2} \qquad (23)$$

Equation 23 can be rearranged to solve for $m_{C6,2}(t_1+t_2)$ if t'_2 is known. Figure 9 pictorially shows the use of a hypothetical tank in the simple equivalent-time model for a particle that moves through two tanks. Note that *j* in Figure 9 can be hexane, ENB or VNB. The equivalent time for hexane removal will most likely be different from the equivalent time for ENB or VNB removal, because it will depend on the various partial pressures in the different tanks. Use of equation 23 to predict the average concentration of hexane leaving the second tank will result in some error, because the

radial profile of hexane in the particle leaving the first vessel will be slightly different than the radial profile of hexane in a hypothetical particle that spent the "equivalent time" in the second vessel. The importance of this error is investigated in an example below, by comparing the rigorous PDE solution with the solution from the simple equivalent-time model.

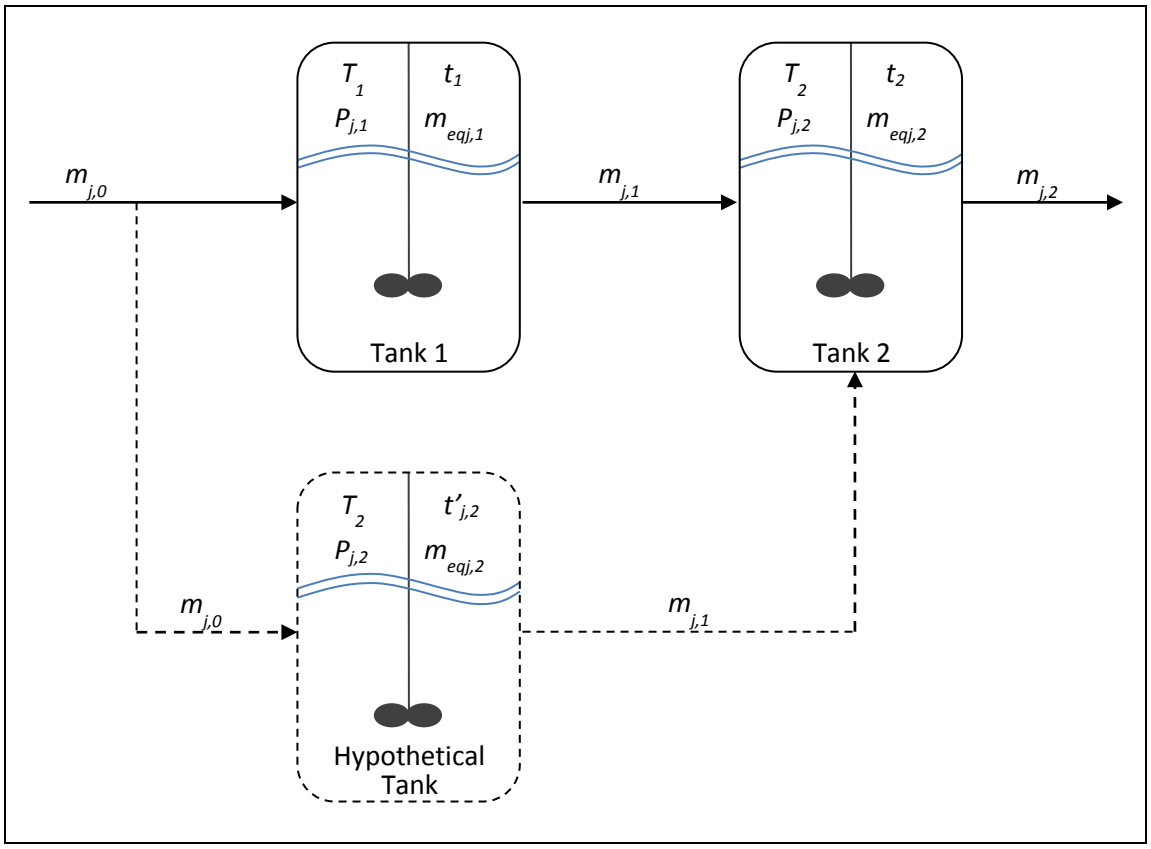

Figure 9: Schematic diagram indicating the methodology of the simple equivalent-time model. The equivalent time $t'_{j,2}$ is determined so that the particle leaving the hypothetical tank has the same average concentration $m_{j,1}$ as the particle when it exits Tank 1.

3.2 Simple Equivalent-Time Model: An Illustrative Example

Table 3 shows the inputs and results for a sample calculation that uses the simple equivalent-time model to calculate the exiting average hexane concentrations within a single EPDM particle passing through a series of two stripping tanks, using the method described in Table 4. For this example, the hexane concentration in the particle is 1.4753 phr when it leaves the second tank. As expected, this value is higher than 1.3611 phr, which would have been obtained from a naïve calculation wherein the

radial concentration profile in the particle exiting tank 1 was ignored (*i.e.,* if equation 13 were used with $m_{C6,0}$ = 19.5375 phr and $t = t_2$ = 0.5 hr).

Table 3: Process settings and results obtained using the simple equivalent-time model when a particle with R = 1.3551 x 10^{-3} m and $m_{C6,0}$ = 35 phr is fed to the series of two stripping vessels

Property	Units	Equation Used	Tank 1	Tank 2
T_i	°C	-	108	115
$P_{C6,i}$	mbar	-	800	200
t_i	hr	-	0.05	0.5
$H_{C6,i}$	mbar/phr	20	153.48	181.16
$D_{C6,i}$	m^2/hr	21	1.23 x 10^{-6}	1.40 x 10^{-6}
$m_{eqC6,i}$	phr	18	5.2124	1.1040
$t'_{C6,i}$	hr	22	n/a	0.0320
$m_{C6,i}(t'_{C6,i} + t_i)$	phr	13 for Tank 1 23 for Tank 2	19.5375	1.4753

Table 4: Simple equivalent-time model method for calculating the average hexane concentration exiting two stripping vessels in series

1	Use the temperatures and hexane partial pressures in the tanks to determine the equilibrium hexane concentrations (*i.e.*, $m_{eqC6,1}$ and $m_{eqC6,2}$) using equations 18 and 20, and the hexane diffusivity values (*i.e.*, $D_{C6,1}$ and $D_{C6,2}$) using equation 21 for a particle in each tank.
2	Use $m_{eqC6,1}$, $D_{C6,1}$, t_1, $m_{C6,0}$, and equation 13 to determine $m_{C6,1}$, the concentration of hexane in the particle when it exits tank 1.
3	Determine the equivalent amount of time $t'_{C6,2}$ that a particle with initial concentration $m_{C6,0}$ would need to spend in tank 2 with $m_{eqC6,2}$ and $D_{C6,2}$ to reach a hexane concentration of $m_{C6,1}$ using equation 22, which is an implicit equation that needs to be solved iteratively.
4	Compute $m_{C6,2}$ the approximate concentration of the particle after it leaves tank 2, using $m_{eqC6,2}$, $D_{C6,2}$ and a total time of $t = t'_{C6,2} + t_2$ in equation 23.

In section 3.2.2, this same example will be used to compute $m_{C6,2}$ using a rigorous PDE solution.

Using the simple equivalent-time model, the average hexane concentration exiting any number of tanks in series may be calculated by repeating steps 3 and 4 from Table 4 for each additional tank. Table 5 shows the inputs and results for a sample calculation that uses the simple equivalent-time model to calculate the exiting average hexane concentrations within a single EPDM particle passing through a series of four stripping tanks, using the method described in Table 6.

Table 5: Process settings and results obtained using the simple model when a single particle with R = 1.3551 x 10^{-3} m and $m_{C6,0}$ = 35 phr is fed to the series of four stripping vessels

Property	Units	Equation Used	Tank 1	Tank 2	Tank 3	Tank 4
T_i	°C	-	108	115	105	100
$P_{C6,i}$	mbar	-	800	200	100	5
t_i	hr	-	0.05	0.5	1.0	2.0
$H_{C6,i}$	mbar/phr	20	153.48	181.16	142.69	126.03
$D_{C6,i}$	m^2/hr	21	1.23×10^{-6}	1.40×10^{-6}	1.16×10^{-6}	1.05×10^{-6}
$m_{eqC6,i}$	phr	18	5.2124	1.1040	0.7008	0.0397
$t'_{C6,i}$	hr	22	n/a	0.0320	0.5278	0.6138
$m_{C6,i}(t'_{C6,i} + t_i)$	phr	13 for Tank 1 23 for other tanks	19.5375	1.4753	0.7023	0.0397

Table 6: Simple equivalent-time model method for calculating the average hexane concentration exiting four stripping vessels in series

1	Use the temperatures and hexane partial pressures in the tanks to determine the equilibrium hexane concentrations (*i.e.*, $m_{eqC6,1}$, $m_{eqC6,2}$, $m_{eqC6,3}$ and $m_{eqC6,4}$) using equations 18 and 20, and the hexane diffusivity values (*i.e.*, $D_{C6,1}$, $D_{C6,2}$, $D_{C6,3}$ and $D_{C6,4}$) using equation 21 for a particle in each tank.
2	Use $m_{eqC6,1}$, $D_{C6,1}$, t_1, $m_{C6,0}$, and equation 13 to determine $m_{C6,1}$, the concentration of hexane in the particle when it exits tank 1.
3	Determine the equivalent amount of time $t'_{C6,2}$ that a particle with initial concentration $m_{C6,0}$ would need to spend in tank 2 with $m_{eqC6,2}$ and $D_{C6,2}$ to reach a hexane concentration of $m_{C6,1}$ using equation 22, which is an implicit equation that needs to be solved iteratively.
4	Compute $m_{C6,2}$, the approximate concentration of the particle after it leaves tank 2, using $m_{eqC6,2}$, $D_{C6,2}$ and a total time of $t = t'_{C6,2} + t_2$ in equation 23.
5	Determine the equivalent amount of time $t'_{C6,3}$ that a particle with initial concentration $m_{C6,0}$ would need to spend in tank 3 with $m_{eqC6,3}$ and $D_{C6,3}$ to reach a hexane concentration of $m_{C6,2}$ using equation 22, which is an implicit equation that needs to be solved iteratively.
6	Compute $m_{C6,3}$, the approximate concentration of the particle after it leaves tank 3, using $m_{eqC6,3}$, $D_{C6,3}$ and a total time of $t = t'_{C6,3} + t_3$ in equation 23.
7	Determine the equivalent amount of time $t'_{C6,4}$ that a particle with initial concentration $m_{C6,0}$ would need to spend in tank 4 with $m_{eqC6,4}$ and $D_{C6,4}$ to reach a hexane concentration of $m_{C6,3}$ using equation 22, which is an implicit equation that needs to be solved iteratively.
8	Compute $m_{C6,4}$, the approximate concentration of the particle after it leaves tank 4, using $m_{eqC6,4}$, $D_{C6,4}$ and a total time of $t = t'_{C6,4} + t_4$ in equation 23.

3.3 Rigorous PDE Model

Since diffusivity is constant throughout the particle, equation 10 can be written in terms of the diluent mass fraction m as:

$$\frac{\partial m}{\partial t} = -D\left(\frac{2}{r}\frac{\partial m}{\partial r} + \frac{\partial^2 m}{\partial r^2}\right) \tag{24}$$

The corresponding initial and boundary conditions are as follows:

i. At time zero, the concentration in the particle is the initial concentration at all depths, *r*; *i.e.*, the solvent concentration is initially uniform throughout the spherical particle.

$$m(r,0) = m_0 \tag{25}$$

ii. At depth *r* = 0 (the centre of the particle), there is no diffusion. This condition occurs because the concentration profile is symmetrical at the centre-line.

$$\left.\frac{\partial m}{\partial r}\right|_{r=0} = 0 \tag{26}$$

iii. At *r* = *R*, the surface concentration within the rubber is in equilibrium with the headspace gas and liquid, m_{eq}. The value of m_{eq} changes from $m_{eq,1}$ to $m_{eq,2}$ when the particle moves into the second tank so that:

$$m(R,t) = m_{eq,1} \qquad 0 \le t < t_1$$

$$m(R,t) = m_{eq,2} \qquad t_1 \le t \le t_2 \tag{27}$$

Using these equations and the parameter values in Table 3, the concentration profile of diluent within the spherical particle can be calculated using the Matlab™ solver *pdepe*. The *pdepe* solver options were set to the default convergence criterion values of meeting the larger of either a relative error tolerance of 0.1 % or an absolute error tolerance of 1 x 10^{-6} phr. The average concentration can then be calculated from the radial profile using the trapezoidal rule. Using this method, with 100 equally spaced trapezoids gives a value of 1.4579 phr for the example in Table 3. Note that this value is consistent with the result obtained using the simplified model.

The following is a list of assumptions required to use the PDE model:

- The only components present in the system include: water, EPDM crumb, hexane, ENB, and VNB. All other components are negligible in quantity and can be ignored in the model.
- All resistances to mass transfer are in the solid crumb phase. Mass transfer resistances in the gas phase and in the water are negligible.

- Hexane, ENB and VNB in the EPDM crumb begin to be desorbed out of the crumb immediately upon entering the first tank in the series of stripping vessels. Further desorption occurs in the stripping vessels that follow and no desorption occurs in the pipes between tanks, due to the short residence time in the pipes.
- Heat transfer is typically much faster than mass transfer of diluents in polymer particles (e.g., Yao et al., 2001); thus, the temperature throughout the crumb particle is assumed to reach the water (and headspace) temperature instantaneously upon entering a stripping tank.
- The gas headspace in every vessel behaves like an ideal gas and the headspace concentrations are at steady state.
- The particles entering the first tank in the stripping section have uniform radial distribution of volatile components.
- At the particle surface, the volatiles dissolved in the polymer are in equilibrium with the vapour phase.
- Diluent concentrations in the particle are sufficiently low so that Henry's law applies (between the particle surface and the gas phase).
- Henry's law coefficients and diffusion coefficients depend only on temperature and not on the type of EPDM or on diluent concentrations.
- The particle radius R remains constant as the diluent is removed.

Note that the only additional model assumption in the simple equivalent-time model is that:

- The radial concentration profile for a particle that spends time t_1 in vessel 1 is similar enough to that of a particle that spends t'_2 in vessel 2 so that the approach in Table 4 will give reliable results.

3.4 Simple Model and PDE Model Comparison

Figure 10 shows a comparison between predictions from the simplified model and the rigorous PDE model for different values of t_1 and t_2. Figure 10 indicates that the PDE and simple model predictions are similar (*i.e.*, differing by less than 5%) for a variety of times spent in tank 1 and tank 2. The largest difference between the PDE and simple model predictions is indicated when t_1 is largest, t_1 = 0.15 hr and when t_2 is shortest, t_2 = 0.125 hr. In this extreme case the simple model differs by 10%. The smallest difference between the PDE and simple model predictions is indicated when t_1 is smallest and when t_2 is largest. When the particle spends longer times in tank 2, the hexane in the particle approaches equilibrium and the effect of the concentration profile on the average concentration of hexane in the particle leaving tank 2 is reduced. Similar results were observed for PDE and simple model predictions of ENB concentrations. These results are not shown.

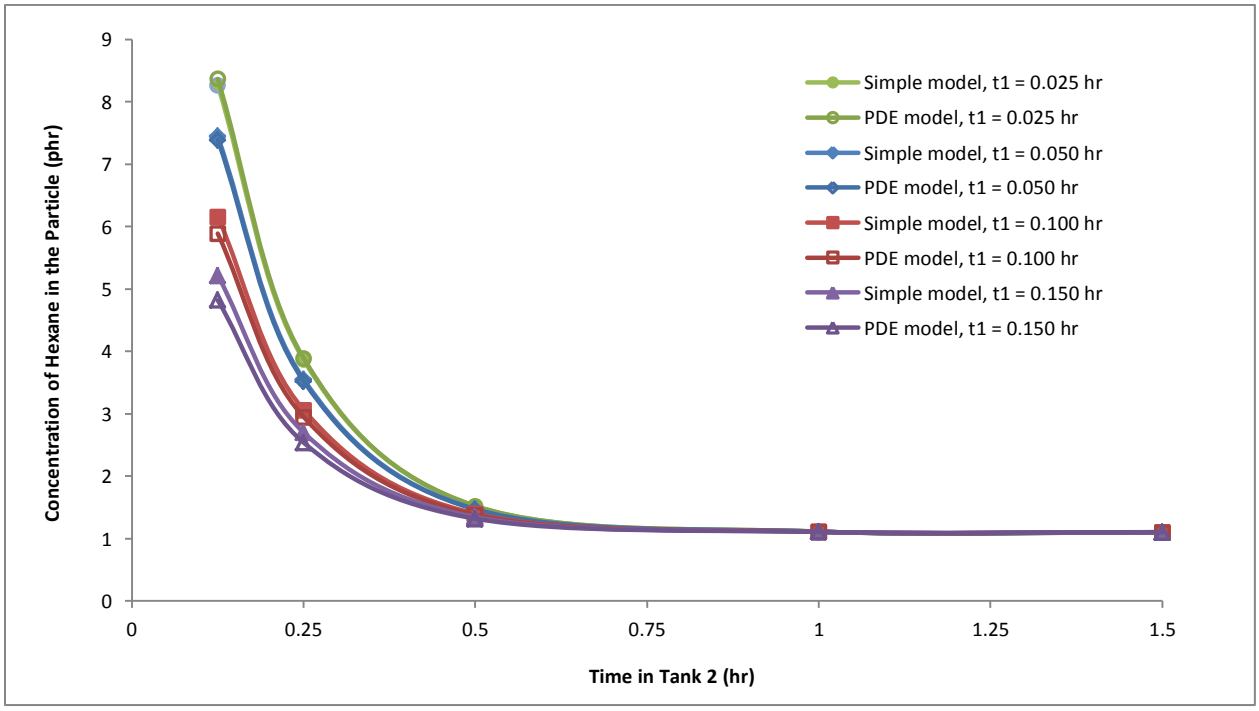

Figure 10: Resulting hexane concentrations remaining in the spherical EPDM particle after spending various times in tank 1 and tank 2

Table 7 compares predictions of the full PDE model, the simple model, and a "naïve" model that neglects the radial concentration profile in particles that leave tank 1 (*i.e.*, predictions obtained using t_2 in equation 13 with $m_{C6,0}$ = 14.8864 phr, the exit concentration from tank 1). As expected the simplified model gives better predictions than the naïve model, with an average error of only 3.26 %, compared with -16.96 % for the naïve model for the results shown in Table 7.

Table 7: PDE model, Simple model and Naïve model predictions for the average hexane concentration in a particle passing through two stripping vessels at the conditions given in Table 3. Note that the PDE and Simple model results correspond to the points on the red curve with squares in Figure 10.

Time in Tank 1, t_1 (hr)	Time in Tank 2, t_2 (hr)	PDE Model Prediction, $m_{C6,2}$ (phr)	Simple Model Prediction, $m_{C6,2}$ (phr)	Naïve Model Prediction, $m_{C6,2}$ (phr)
0.1	0.125	5.8893	6.1604	4.4131
0.1	0.250	2.9515	3.0651	2.3742
0.1	0.500	1.3827	1.4010	1.2962

3.5 Single Particle Model Conclusions

A simplified single-particle model was developed and its predictions were compared to those from a rigorous PDE model. Both models, which predict the average hexane (or ENB or VNB) concentration in a single particle that passes through two stripping vessels in series, account for the radial concentration profile in particles that exit the first vessel. As a result, they predict higher hexane concentrations for particles leaving the second vessel than a naïve model that neglects this concentration profile. Predictions from the simple equivalent-time model match the PDE model predictions well, particularly for particles with short residence times in tank 1 and long residence times in tank 2. The reduced computational effort required to use the simplified model make it useful for predicting concentrations in the more advanced model developed in Chapter 4 that accounts for the residence time distribution of particles in up to four stripping vessels in series.

Chapter 4:
CFST-Distribution Multiple-Tank Model Development

The main objective of this chapter is to develop model equations that predict the overall average diluent concentrations for a population of EPDM particles. These particles travel through a series of stream-stripping vessels, with different particles spending different amounts of time in each vessel. This CFST (continuous flow stirred tank) distribution model uses equations from the simple single-particle model (developed in Chapter 3) as well as additional equations that account for the influence of diluent evaporation rates on the headspace concentrations. The model equations also account for the residence time distributions of the particles in the three and four tanks.

4.1 Method for Determining the Headspace Concentrations

To use the model equations developed in Chapter 3, the headspace composition in each vessel must be known to determine the mass transfer driving force. Unfortunately, the process data available for this thesis project did not include measured headspace compositions in any of the tanks. Therefore, it was necessary to develop equations for determining the headspace concentrations in each of the stripping vessels.

The sum of the mole fractions of the various species in the headspace is one:

$$1 = y_W + y_{C6} + y_{ENB} + y_{VNB} \tag{27}$$

where y_{C6}, y_{ENB}, y_{VNB} are the mole fractions of each of the diluent species in the headspace and y_W is the mole fraction of water present in the headspace. To determine y_W, the Antoine equation and the measured temperature, T, can be used to calculate the saturation pressure of water (P_W^{sat}) in the particular tank, which is then divided by the absolute pressure (Smith, Van Ness and Abbott, 2005):

$$P_W^{sat} = 10 \times e^{\left(16.3872 - \left(3885.7/(T+230.17)\right)\right)} \tag{28}$$

$$y_W = \frac{P_W^{sat}}{P} \tag{29}$$

The remaining gas-phase mole fractions can be calculated, knowing that their respective mole fractions in the headspace are proportional to their molar flowrates into the headspace. As a result, the diluent mole fractions are related to each other by a proportionality factor, Υ:

$$\gamma = \frac{y_{C6}}{r_{C6}} = \frac{y_{ENB}}{r_{ENB}} = \frac{y_{VNB}}{r_{VNB}} \tag{30}$$

where r_{C6}, r_{ENB} and r_{VNB} are the total molar flowrates of the respective species into the headspace. The total molar flowrate for each species, *j*, may be calculated according to:

$$r_j = F_{difj} + F_{prej} \tag{31}$$

where $F_{dif\,j}$ is the molar flowrate of species *j* diffusing out of the EPDM particles in the tank, and $F_{pre\,j}$ is the molar flowrate of species *j* flowing into the headspace from any other source (e.g., sometimes the gas from the headspace of one stripping vessel flows into the headspace of a subsequent stripping vessel). Combining and rearranging equations 27, 30, and 31 yields equations 32 and 33 for tank *i*:

$$\gamma_i = \frac{1 - y_{W,i}}{\sum_j \left(F_{difj,i} + F_{prej,i}\right)} \tag{32}$$

$$y_{j,i} = \gamma_i \left(F_{difj,i} + F_{prej,i}\right) \tag{33}$$

$F_{dif\,j,i}$ can be determined from a material balance on species j in the crumb in the i^{th} tank:

$$F_{difj,i} = F_{inj,i} - F_{outj,i} \tag{34}$$

where $F_{inj,i}$ is the molar flowrate of species *j* entering the tank within the crumb and F_{outj} is the molar flowrate of species *j* in the crumb exiting the tank. F_{inj} and F_{outj} can be computed using:

$$F_{inj,i} = \left(\frac{\overline{m}_{j,i-1}\, F_{crumb}}{100}\right) / MW_j \tag{35}$$

$$F_{outj,i} = \left(\frac{\overline{m}_{j,i}\, F_{crumb}}{100}\right) / MW_j \tag{36}$$

where $\overline{m}_{j,i-1}$ is the average concentration of species *j* (in phr) in the crumb entering the i^{th} tank, $\overline{m}_{j,i}$ is the average concentration of species *j* in the crumb exiting the i^{th} tank, F_{crumb} is the mass flowrate of EPDM crumb, and MW_j is the molecular weight of species *j*. If the exiting average concentrations of each

species ($\overline{m}_{C6,i}$, $\overline{m}_{ENB,i}$, $\overline{m}_{VNB,i}$) are known, these equations may be used to calculate the corresponding mole fractions in the headspace.

Table 6 in Chapter 3 shows how to use the equivalent-time method to estimate $m_{j,i}$ for a fraction of the crumb that spends time t_i in the tank (given t_i, $D_{j,i}$, $m_{j,i-1}$ and $m_{eqj,i}$). Determining $\overline{m}_{j,i}$ for the overall population of particles (that spend different amounts of time in tank *i*) will be described in section 4.2. Note that $m_{eqj,i}$ can be calculated using equation 18, given the tank pressure P_i, Henry's constant for the tank $H_{j,i}$, and a guess value for $y_{j,i}$:

$$m_{eqj,i} = \frac{P_i\, y_{j,i}}{H_{j,i}} \tag{37}$$

Thus, $y_{j,i}$ values may be solved iteratively, after guessing initial values for $y_{C6,i}$, $y_{ENB,i}$, and $y_{VNB,i}$, as described in Table 8.

Table 8: Iterative method used for calculating the gaseous headspace concentrations of each species in tank *i* in a series of stripping vessels

1	Compute $y_{W,i}$ using equations 28 and 29, and assume initial molar fractions for other species in the headspace (*i.e.*, $y_{C6,i,guess}$, $y_{ENB,i,guess}$, $y_{VNB,i,guess}$) so that the mole fractions add to one.
2	Use P_i, $y_{C6,i,guess}$, $y_{ENB,i,guess}$, $y_{VNB,i,guess}$, $H_{C6,i}$, $H_{ENB,i}$, $H_{VNB,i}$ and equation 37 to determine $m_{eqC6,i}$, $m_{eqENB,i}$, $m_{eqVNB,i}$.
3	Use $m_{eqj,i}$, $D_{j,i}$, t, $\overline{m}_{j,i-1}$, and Table 6 in section 3.1.2 to determine $\overline{m}_{j,i}$ for each species.
4	Compute the mass flowrate of each species entering the tank within the crumb (*i.e.*, $F_{inC6,i}$, $F_{inENB,i}$, $F_{inVNB,i}$) using $\overline{m}_{C6,i-1}$, $\overline{m}_{ENB,i-1}$, $\overline{m}_{VNB,i-1}$, F_{crumb}, MW_{C6}, MW_{ENB}, MW_{VNB}, and equation 35. Also compute the mass flowrate of each species exiting the tank within the crumb (*i.e.*, $F_{outC6,i}$, $F_{outENB,i}$, $F_{outVNB,i}$) using $\overline{m}_{C6,i}$, $\overline{m}_{ENB,i}$, $\overline{m}_{VNB,i}$, and equation 36.
5	Using $F_{inC6,i}$, $F_{inENB,i}$, $F_{inVNB,i}$, $F_{outC6,i}$, $F_{outENB,i}$, $F_{outVNB,i}$, and the mass balance equation 34, determine the flowrate of each species diffusing out of the crumb and into the gas headspace (*i.e.*, $F_{difC6,i}$, $F_{difENB,i}$, $F_{difVNB,i}$).
6	Using $y_{W,i}$, $F_{difC6,i}$, $F_{difENB,i}$, $F_{difVNB,i}$, the inlet gaseous flowrates for each species (*i.e.*, $F_{preC6,i}$, $F_{preENB,i}$, $F_{preVNB,i}$) and the material balance equation 32, determine Υ_i.
7	Use Υ_i, $F_{difC6,i}$, $F_{difENB,i}$, $F_{difVNB,i}$, $F_{preC6,i}$, $F_{preENB,i}$, $F_{preVNB,i}$ and equation 33 to determine new headspace concentrations: $y_{C6,i,new}$, $y_{ENB,i,new}$, $y_{VNB,i,new}$.

*Note that step 3 will be further described in section 4.2 wherein $\overline{m}_{j,i}$ values are calculated using a discretized residence-time distribution method.

4.1.1 Multivariate Newton's Method to Solve for Headspace Concentrations

The three mole fractions ($y_{C6,i}$, $y_{ENB,i}$, and $y_{VNB,i}$) must be solved for simultaneously because equation 32 uses the molar flowrates for all the three species diffusing out of the EPDM particles (F_{difC6}, F_{difENB} and F_{difVNB}), which depend on the mole fractions of each diluent in headspace. Functions of the following form are used to solve for these mole fractions:

$$f_{C6}(y_{C6,i}, y_{ENB,i}, y_{VNB,i}) = y_{C6,i} - y_{C6,i,new}(y_{C6,i}, y_{ENB,i}, y_{VNB,i}) = 0 \quad (38)$$

$$f_{ENB}(y_{C6,i}, y_{ENB,i}, y_{VNB,i}) = y_{ENB,i} - y_{ENB,i,new}(y_{C6,i}, y_{ENB,i}, y_{VNB,i}) = 0 \quad (39)$$

$$f_{VNB}(y_{C6,i}, y_{ENB,i}, y_{VNB,i}) = y_{VNB,i} - y_{VNB,i,new}(y_{C6,i}, y_{ENB,i}, y_{VNB,i}) = 0 \quad (40)$$

where Table 8 describes how to calculate new $y_{j,i,new}$ values as a function of the initial guess values for $y_{j,i}$. To solve these equations iteratively, a multivariate Newton's method was used. For this method, the first derivatives of each function f_j with respect to each unknown mole fraction variable are required. Since analytical first derivative expressions are not easy to derive based on the calculations in Table 8, they were estimated using difference approximations shown in the Jacobian matrix below:

$$Jac = \begin{bmatrix} \left(\frac{f_{C6,1}-f_{C6,2}}{y_{C6,i,k}-y_{C6,i,k\delta}}\right) & \left(\frac{f_{C6,1}-f_{C6,3}}{y_{ENB,i,k}-y_{ENB,i,k\delta}}\right) & \left(\frac{f_{C6,1}-f_{C6,4}}{y_{VNB,i,k}-y_{VNB,i,k\delta}}\right) \\ \left(\frac{f_{ENB,1}-f_{ENB,2}}{y_{C6,i,k}-y_{C6,i,k\delta}}\right) & \left(\frac{f_{ENB,1}-f_{ENB,3}}{y_{ENB,i,k}-y_{ENB,i,k\delta}}\right) & \left(\frac{f_{ENB,1}-f_{ENB,4}}{y_{VNB,i,k}-y_{VNB,i,k\delta}}\right) \\ \left(\frac{f_{VNB,1}-f_{VNB,2}}{y_{C6,i,k}-y_{C6,i,k\delta}}\right) & \left(\frac{f_{VNB,1}-f_{VNB,3}}{y_{ENB,i,k}-y_{ENB,i,k\delta}}\right) & \left(\frac{f_{VNB,1}-f_{VNB,4}}{y_{VNB,i,k}-y_{VNB,i,k\delta}}\right) \end{bmatrix} \quad (41)$$

Note that $y_{C6,i,k}$, $y_{ENB,i,k}$ and $y_{VNB,i,k}$ are the current guesses for the gas-phase mole fractions, and the perturbed mole fractions (*i.e.*, $y_{C6,i,k\delta}$, $y_{ENB,i,k\delta}$, $y_{VNB,i,k\delta}$) for ENB and VNB were determined by:

$$y_{ENB,i,k\delta} = 1.1 \times y_{ENB,i,k} \quad (42)$$

$$y_{VNB,i,k\delta} = 1.1 \times y_{VNB,i,k} \quad (43)$$

The perturbed mole fraction $y_{C6,i,k\delta}$ was then obtained from equation 27, with $y_{W,i}$ held fixed at the value obtained from equation 29. A series of Newton iterations were then used to compute updated mole fraction estimates:

$$\begin{bmatrix} y_{C6,i} \\ y_{ENB,i} \\ y_{VNB,i} \end{bmatrix}_{k+1} = -Jac_k{}^{-1} \begin{bmatrix} f_{C6}(y_{C6,i}, y_{ENB,i}, y_{VNB,i}) \\ f_{ENB}(y_{C6,i}, y_{ENB,i}, y_{VNB,i}) \\ f_{VNB}(y_{C6,i}, y_{ENB,i}, y_{VNB,i}) \end{bmatrix}_k + \begin{bmatrix} y_{C6,i} \\ y_{ENB,i} \\ y_{VNB,i} \end{bmatrix}_k \quad (44)$$

where the subscript *k* is the iteration counter. Iterations ceased when the relative errors in all mole fractions were less than 1% or when the absolute error was within 1 x 10^{-4}.

4.2 Computing the Overall Diluent Mole Fraction for all Particles Exiting the *i*th Tank

This section describes the method to solve for the average concentration ($\overline{m}_{j,i}$) of each species *j* in particles that spend different amounts of time in tank *i* due to the residence time distribution. Matthews et al. (1986 b) incorporated a residence time distribution for a CFST into equation 13 to solve for the average concentration of a species exiting in the crumb, given the residence time, τ (indicated as equation 14 in section 1.4). Like Matthews et al., the same residence time distribution is utilized but this distribution is discretized here to permit a simple extension for multiple tanks in series without using complex integral functions.

Consider the particles within a discrete time bin that all spend approximately the same of amount of time, t_{bi}, in tank *i*. Particles that spend significantly different amounts of time are categorized in other discrete bins. If one considers the particles in one specific bin, equation 13 is appropriate to solve for the concentration of species *j* that remains in the particles after the period of time, t_{bi}, in tank *i* (*i.e.*, $m_{bi,j,i}$). Diluent concentrations of particles in each bin can then be combined to compute the overall or average concentration (*i.e.*, $\overline{m}_{j,i}$) for each diluent.

4.2.1 Use of Time Bins for a Single Tank

After conducting a sensitivity analysis, it was determined that using 48 discrete time bins within the time range from $0\tau_i$ to $12\tau_i$ was sufficient to accurately calculate the resulting $\overline{m}_{j,i}$ values. To

improve the accuracy of the calculations, bins were not evenly spaced. The 48 bins are divided into six subsections, each with time widths larger than the previous. Table 9 shows the six bin subsections and the corresponding time bin widths (see Appendix H for an example of the CFST residence time distribution and time bin edges).

Table 9: Time bin subsections and time bin widths

Bin Section	Number of Bins	Bin Width (hr)
$0\tau_i$ to $\tau_i/10$	9	$\tau_i/90$
$\tau_i/10$ to $\tau_i/2$	12	$\tau_i/30$
$\tau_i/2$ to τ_i	12	$\tau_i/24$
τ_i to $3\tau_i$	9	$\tau_i/4.5$
$3\tau_i$ to $6\tau_i$	3	τ_i
$6\tau_i$ to $12\tau_i$	3	$2\tau_i$

The representative time corresponding to particles in a particular bin was the average value:

$$t_{bi} = \frac{t_{biL}+t_{biR}}{2} \tag{43}$$

where t_{biL} corresponds to the time at the left edge of the b^{th} bin in tank i, t_{biR} corresponds to the time at the right edge of the b^{th} bin. The CFST residence-time distribution for a single tank, $E(t)$:

$$E(t) = \frac{1}{\tau_i} e^{-\left(\frac{t}{\tau_i}\right)} \tag{44}$$

is integrated to calculate the fraction of particles in each bin (Himmelbau and Bischoff, 1968; Levenspiel, 1962). The fraction of particles that spend between t_{b1L} and t_{b1R} in the first tank is:

$$\phi_{b1} = e^{-\left(\frac{t_{b1L}}{\tau_1}\right)} - e^{-\left(\frac{t_{b1R}}{\tau_1}\right)} \tag{45}$$

The overall or average concentration of species j exiting the 1^{st} tank, $\bar{m}_{j,1}$, is:

$$\bar{m}_{j,1} = \sum_{b1=1}^{48} \left(\phi_{b1} m_{b1,j,1}\right) \tag{46}$$

where $m_{b1,j,1}$ is the species concentration within the population of crumb in the $b1^{th}$ bin. $m_{b1,j,1}$ is calculated using $m_{eqj,1}$, $D_{j,1}$, t_{b1} and equation 13. Table 10 summarizes the steps and equations used to calculate average species concentrations exiting tank 1 (*i.e.*, $\bar{m}_{j,1}$ values) using the discretized bin method.

Table 10: Discretized bin method for calculating the average concentration of diluent *j* in particles leaving the first tank

1	Calculate the average residence time τ_1 time for particles in tank 1.
2	Using Table 9, make an array of time bins for the total population of particles experiencing residence times from 0 to 12τ_1, keeping track of the times associated with the left and right edge of each bin (*i.e.*, t_{b1L} and t_{b1R}).
3	Calculate the average time, t_{b1}, associated with each bin using equation 43.
4	Calculate the fraction of particles, Φ_{b1}, associated with each bin using t_{b1L}, t_{b1R}, τ_1 and equation 45.
5	Use $m_{eqj,1}$, $D_{j,1}$, t_{b1} and equation 13 to calculate $m_{b1,j,1}$ for each bin and for each species.
6	Use equation 46, $m_{b1,j,1}$ and Φ_{b1} for all bins to calculate $\bar{m}_{j,1}$ for each species.

4.2.2 Use of Time Bins for Multiple Tanks in Series

To extend the discretized bin method for a two, three or four-tank model, a similar procedure is conducted. However, instead of considering a single array of time bins corresponding to the fractions of particles in each bin, one must consider a two, three or four-dimensional array of bins, with each element in the array corresponding to the fraction of particles in that bin. For example, consider a model for two tanks in series. Each element in the array corresponds to the fraction of particles that spends between t_{b1L} to t_{b1R} amount of time in tank 1 and between t_{b2L} to t_{b2R} hours in tank 2. To calculate the fraction of particles in each element of the 2D array, equation 44 is used first used to calculate the $E(t_{b1L})$, $E(t_{b1R})$, $E(t_{b2L})$ and $E(t_{b2R})$. Next, the two-dimensional trapezoidal rule is used to calculate the fraction of particles in each element of the 2D array:

$$\phi_{b1,b2} = (t_{b1R} - t_{b1L})(t_{b2R} - t_{b2L}) \frac{E(t_{b1R})+E(t_{b1L})+E(t_{b2R})+E(t_{b2L})}{4} \quad (47)$$

where *b1* and *b2* refer to the time bins in tanks 1 and 2, respectively. Analogous to equation 46, the average concentration for each species in the crumb, $\bar{m}_{j,2}$ is:

$$\bar{m}_{j,2} = \sum_{b2=1}^{48} \sum_{b1=1}^{48} \left(\phi_{b1,b2} m_{b1,b2,j,2}\right) \quad (48)$$

where $m_{b1,b2,j,2}$ is the overall concentration of species *j* within the crumb corresponding to bin *b1* in tank 1 and bin *b2* in tank 2. $m_{b1,b2,j,2}$ is calculated using the steps described in Table 6. Table 11 describes the method used to calculate average species concentrations exiting tank 2 (*i.e.*, $\bar{m}_{j,2}$ values) using the discretized bin method.

Table 11: Discretized bin method for calculating the average concentration of species *j* in particles exiting the second tank

1	Calculate the average residence time τ_1 time for particles in tank 1. Use Table 9 to determine t_{b1L}, t_{b1R} and use equation 43 to calculate t_{b1}. Next use Table 8 to determine $y_{j,1}$, $m_{b1,j,1}$ and $\overline{m}_{j,1}$ for each species and for each bin in tank 1. Use equation 44 and $\tau = \tau_1$ to determine $E(t_{b1L})$, $E(t_{b1R})$ for each bin in tank 1.
2	Calculate the average residence time τ_2 time for particles in tank 2. Use Table 9, equation 43 and $\tau = \tau_2$ to determine t_{b2L}, t_{b2R}, t_{b2}. Use equation 44 to determine $E(t_{b2L})$ and $E(t_{b2R})$ for each bin in tank 2. Use equation 44 and $\tau = \tau_1$ to determine $E(t_{b1L})$, $E(t_{b1R})$ for each bin in tank 1.
3	Calculate the fraction of particles, $\Phi_{b1,b2}$, associated with each element in the 2D array using $E(t_{b1L})$, $E(t_{b1R})$, $E(t_{b2L})$, $E(t_{b2R})$ and equation 47.
4	Perform steps 1 to 3 from Table 6 to determine the equivalent time $t'_{b1,j}$ for each bin in tank 1, for each species, using $m_{eqj,2}$, $m_{b1,j,1}$, $D_{j,2}$, T_2, and $m_{j,0}$.
5	Perform step 4 from Table 6 for each element in the 2D array of bins to determine $m_{b1,b2,j,2}$ for each element, for each species, using $t_{b1,b2,j,2} = t'_{b1,j,} + t_{b2}$, $m_{eqj,2}$, $D_{j,2,}$ T_2, and $m_{j,0}$.
6	Use equation 48 $m_{b1,b2,j,2}$ and $\Phi_{b1,b2}$ for all bins to obtain $\overline{m}_{j,2}$ for each species.

Extending the discretized bin method for three or more tanks in series involves an additional step. Unlike the crumb particles exiting the first tank (that have been lumped using a single array of 48 time bins), the particles exiting the second tank have been lumped using a 2D array of time bins (48 x 48 bins). This method would require the cataloguing of 48^3 separate bins for particles exiting the third tank and 48^4 separate bins for particles exiting the fourth tank. To prevent this bin dimensionality explosion, the particles in the 48 x 48 bins exiting tank two were further lumped into a single array of 48 bins. The 2D array of $m_{b1,b2,j,2}$ values was condensed into a 1D array (see Table 12) of $m_{b2',j,2}$ values so that the methodology described in Table 10 can be used to calculate the resulting $m_{b2',b3,j,3}$ and $\overline{m}_{j,3}$ values.

Table 12: Sorting method used to convert a 2D matrix of $m_{b1,b2,j,2}$ values into a 1D array of $m_{b2',j,2}$ values

1	Calculate the average residence time τ_1 time for particles in tank 1. Use equation 13, $m_{eqj,1}$, $D_{j,1}$, $m_{j,0}$ and $t = \tau_1$ to determine the concentration of species *j* in a typical particle spending τ_1 time in tank 1. Perform this calculation for each species.
2	Determine the equivalent amount of time $\tau'_{j,2}$ that a particle with initial concentration $m_{j,0}$ would need to spend in tank 2 with $m_{eqj,2}$ and $D_{j,2}$ to reach a concentration of $m_{j,1}$ using equation 22, which is an implicit equation that needs to be solved iteratively. Perform this calculation for each species.
3	Determine the minimum of $\tau'_{C6,2}$, $\tau'_{ENB,2}$ and $\tau'_{VNB,2}$ (*i.e.*, $\tau'_{min,2}$).
4	Perform steps 1 and 3 using $\tau = \tau_2 + \tau'_{min,2}$, and use Table 10 to determine $t_{b2'L}$, $t_{b2'R}$, $t_{b2'}$, $E(t_{b2'L})$ and $E(t_{b2'R})$ for each bin.
5	For each of the new equivalent time bins in tank 2, search for all values of $t_{b1,b2,j,2}$ that satisfy: $t_{b2'L} < t_{b1,b2,j} < t_{b2'R}$. Sum the fractional concentrations of species *j* in the crumb (i.e., $m_{b1,b2,j,2} \times \Phi_{b1,b2}$) for all of the bins sorted into the $t_{b2'}$ bin to estimate $m_{b2',j,2}$ for each bin.

4.3 Three-Tank Model Preliminary Simulation Results and Conclusions

Three-tank simulation results were compared with industrial data to see if predictions using the initial parameter values are reasonable and to check for any model errors or inconsistencies. Process operating conditions and resulting crumb concentrations were collected on 14 different days where the stripping vessels were operating at steady state. Note that data are also available from two plants with a four-tank stripping process (*i.e.*, five from process 'A' and six from process 'B'). For the three-tank process, outlet crumb concentrations were only available from the second and third tanks due to process limitations. For the four-tank processes crumb concentration data were available from tank 2 for some operating conditions, and from tanks 3 and 4.

Process data and predictions from an existing upstream process model in Aspen^{TM} were used to determine appropriate input variables for use in the current model. Table 13 provides a list of these input variables.

Table 13: Industrial input variables for three- and four-tank models

Symbol	Description	Source	Units
F_{crumb}	EPDM crumb mass flowrate	Process data	kg/hr
$m_{C6,0}$, $m_{ENB,0}$, $m_{VNB,0}$	Inlet concentrations of hexane, ENB and VNB in the crumb	Existing model	phr
F_{preC6}, F_{preENB}, F_{preVNB}	Inlet gaseous molar flowrates of hexane, ENB and VNB	Existing model	mol/hr
T_1, T_2, T_3, T_4	Temperature in tanks 1, 2 and 3	Process data	K
P_1, P_2, P_3, P_4	Pressure in tanks 1, 2, 3 and 4	Process data	mbar
τ_1, τ_2, τ_3, τ_4	Crumb residence time in tanks 1, 2, 3 and 4	Model and data	hr

Figure 11 compares predictions from the three-tank model with measured values for $\overline{m}_{C6,2}$, $\overline{m}_{C6,3}$, $\overline{m}_{ENB,2}$, $\overline{m}_{ENB,3}$, $\overline{m}_{VNB,2}$ and $\overline{m}_{VNB,3}$ for one of the 14 three-tank data sets. Corresponding plots for the remaining data are provided in Appendix A. The effective radius used for these simulations was 1.3551 x 10^{-3} m and the Henry's law and diffusivity parameters used to compute the model predictions are shown in Table 1. Note that no diffusion and solubility experiments were conducted for VNB (see Chapter 2). Predictions in Figure 11 and in Appendix A were made assuming that VNB has the same diffusivity and solubility behavior as ENB. The model predicts outlet crumb concentrations for hexane,

ENB and VNB that are of the correct order of magnitude. As expected, the model and data show a decrease in concentrations as the crumb particles move through the three tanks.

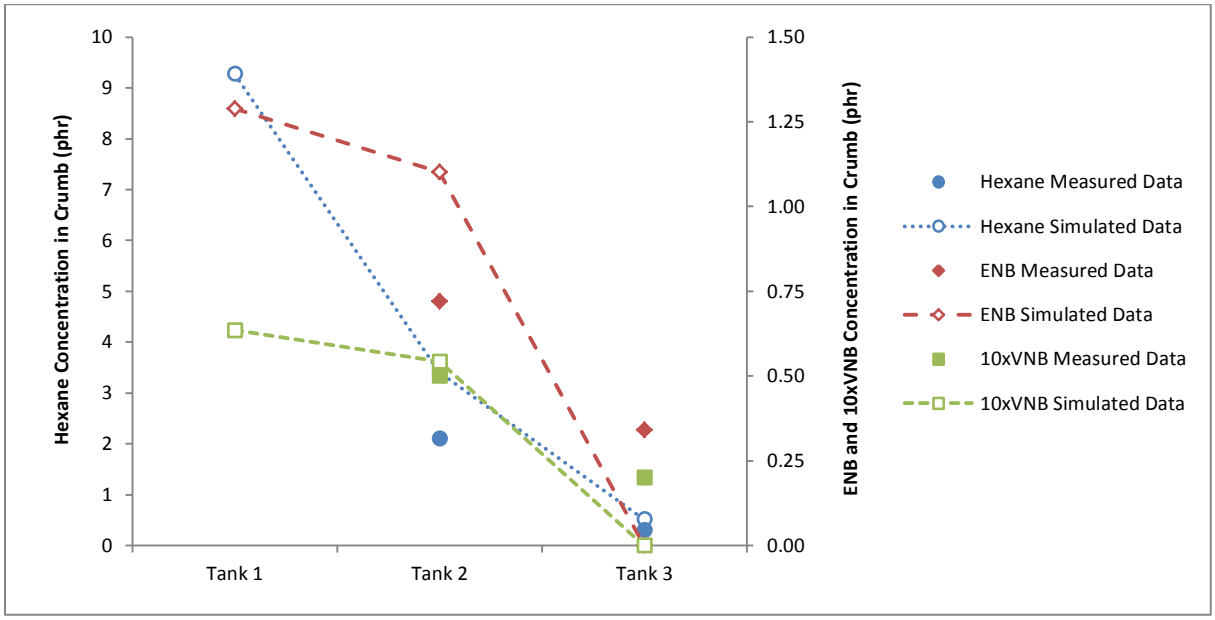

Figure 11: Three-Tank simulation results for outlet crumb concentrations, $\bar{m}_{j,i}$, compared to measured data for data set one, using the original set of model parameters. Dashed lines are used to guide the eye. Note that this plot is representative of the corresponding plots for data sets two to 14 (see Appendix A).

One problem that was encountered while calculating the model predictions in Fig. 11 and Appendix A is that the measured pressure in the third tank tended to be lower than the vapour pressure of water calculated using the Antoine equation. As a result, Table 8 could not be used to calculate $y_{C6,i}$, $y_{ENB,i}$, and $y_{VNB,i}$ values. Whenever this problem occurred, the mole fractions of hexane, ENB and VNB in the third tank were set to zero so that $\bar{m}_{C6,3}$, $\bar{m}_{ENB,3}$ and $\bar{m}_{VNB,3}$ could be calculated. To correct this underestimation problem, a tuning parameter, p_3, was used to adjust the pressure in the third tank, P_3. Similarly, tuning parameters were added to the model to account for large uncertainties in the initial diluent concentrations in the crumb ($m_{C6,0}$, $m_{ENB,0}$, and $m_{VNB,0}$), which are calculated using a previously-existing Aspen™ model that contains assumptions that may not be valid. Additional tuning parameters were added to each tank's residence-time calculation since crumb-flow phenomena were estimated

with limited knowledge, especially for the first tank. A complete list of the model's tuning parameters and updated simulation results are discussed in Chapter 5.

Chapter 5:
Parameter Tuning for Three- and Four-Tank Models

The main objective of this chapter is to fine-tune the three- and four-tank models described in Chapter 4 such that the model predictions for the diluent concentrations in the crumb exiting each tank are more accurate. Tuning parameters and existing model parameters (*i.e.*, effective radius, solubility and diffusion parameters) are first ranked using a sensitivity-based estimability analysis procedure (Yao et al., 2003; Thompson et al., 2009; Wu et al., 2011; McLean and McAuley, 2011), and then adjusted systematically such that the model predictions better match the measured industrial data. The tuning method, the updated parameter estimates, and the improved model predictions are described below.

5.1 Preliminary Model Tuning Using Data from Three-Tank Process

The method used for parameter tuning in this thesis is the orthogonalisation method as described by Wu et al. (2011). In this method, the parameters are first ranked in order of most to least estimable based on their relative effects on the model predictions and the uncertainty of their initial values, while taking parameter correlation into account. Next, the optimal number of parameters to be estimated is selected based on the anticipated mean-squared error (MSE) of the model predictions. Preliminary model tuning was first conducted for the three-tank model only, to test model efficacy and to ensure that the orthogonalisation method was selecting reasonable parameters for estimation. Table 14 summarizes the adjustable parameters in the three-tank model, along with their initial guesses and their uncertainty bounds. Note that the parameters are listed in no particular order.

Table 14: Initial Three-Tank Model Tuning Parameters

Symbol	Description	Units	Value	Lower Bound	Upper Bound
Y_1	Adjustable factor to tune the residence time in tank 1 for the three-tank process model	-	1	0.5	1.5
Y_2	Adjustable factor to tune the residence time in tank 2 for the three-tank process model	-	1	0.95	1.05
Y_3	Adjustable factor to tune the residence time in tank 3 for the three-tank process model	-	1	0.95	1.05
$H_{C6,ref}$	Henry's constant for hexane in EPDM at the reference temperature (108 °C)	mbar/phr	1.5348×10^{2}	1.4640×10^{2}	1.6091×10^{2}
α_{C6}	Activation energy term for Henry's constant Arrhenius expression for hexane in EPDM	K	-3.5036×10^{3}	-3.9224×10^{3}	-3.0847×10^{3}
$H_{ENB,ref}$	Henry's constant for ENB in EPDM at the reference temperature (108 °C)	mbar/phr	10.123	8.6035	11.9148
α_{ENB}	Activation energy term for Henry's constant Arrhenius expression for ENB in EPDM	K	-4.7190×10^{3}	-6.0333×10^{3}	-3.4046×10^{3}
$H_{VNB,ref}$	Henry's constant for VNB in EPDM at the reference temperature (108 °C)	mbar/phr	10.123	1.1740	19.075
α_{VNB}	Activation energy term for Henry's constant Arrhenius expression for VNB in EPDM	K	-4.7190×10^{3}	-7.3477×10^{3}	-2.0902×10^{3}
$D_{C6,ref}$	Diffusivity for hexane in EPDM at the reference temperature (108 °C)	m^2/s	3.4177×10^{-10}	2.9273×10^{-10}	3.9903×10^{-10}
β_{C6}	Activation energy term for diffusivity-related Arrhenius expression for hexane in EPDM	K	-2.7995×10^{3}	-4.1729×10^{3}	-1.4262×10^{3}
$D_{ENB,ref}$	Diffusivity for ENB in EPDM at the reference temperature (108 °C)	m^2/s	1.4679×10^{-10}	1.3266×10^{-10}	1.6241×10^{-10}
β_{ENB}	Activation energy term for diffusivity-related Arrhenius expression for ENB in EPDM	K	-2.9220×10^{3}	-3.7388×10^{3}	-2.1053×10^{3}
$D_{VNB,ref}$	Diffusivity for VNB in EPDM at the reference temperature (108 °C)	m^2/s	1.4679×10^{-10}	6.8655×10^{-11}	2.2492×10^{-10}
β_{VNB}	Activation energy term for diffusivity-related Arrhenius expression for VNB in EPDM	K	-2.9220×10^{3}	-4.5555×10^{3}	-1.2886×10^{3}
p_1	Adjustable factor to tune the pressure in tank 1 for the three-tank process model	-	1	0.98	1.02

p_2	Adjustable factor to tune the pressure in tank 2 for the three-tank process model	-	1	0.95	1.25
p_3	Adjustable factor to tune the pressure in tank 3 for the three-tank process model	-	1	0.95	1.25
$I_{C6,0}$	Adjustable factor to tune the inlet concentration of hexane in the crumb for the three-tank process model	-	1	0.4	1.6
$I_{ENB,0}$	Adjustable factor to tune the inlet concentration of ENB in the crumb for the three-tank process model	-	1	0.4	1.6
$I_{VNB,0}$	Adjustable factor to tune the inlet concentration of VNB in the crumb for the three-tank process model	-	1	0.4	1.6
R_1	Effective diffusion radius for EPDM grade 1	m	1.3551×10^{-3}	2.0000×10^{-3}	6.3551×10^{-3}
R_2	Effective diffusion radius for EPDM grade 2	m	1.3551×10^{-3}	2.0000×10^{-3}	6.3551×10^{-3}
R_3	Effective diffusion radius for EPDM grade 3	m	1.3551×10^{-3}	3.551×10^{-4}	2.3551×10^{-3}

*Note that the EPDM grade numbers in this table do not necessarily correspond to the grade numbers that are described in Chapter 2.

These upper and lower bounds indicate the range of plausible values that are permitted during the parameter tuning process. These bounds were set according to a variety of factors:

- Residence times in tanks 2 and 3 were thought to be calculated accurately within ± 5%; however, the crumb flow phenomena in tank 1 were not as well-known and bounds were set to within ± 50%.
- Boundaries for the Henry's law constant and diffusivity parameters for hexane and ENB were estimated using 95% confidence intervals determined in Chapter 2. For VNB, the Henry's law constant and diffusivity parameters were initially set at the values for ENB, with the error bounds set five times larger than those determined for ENB, since no diffusivity or solubility experiments were performed using VNB.

- As previously discussed in Chapter 4, it was determined that the total pressure needed to be increased in cases where the calculated saturation pressures of water were larger than the measured total pressure in the tank. Upper and lower bounds of 1.25 and 0.95, respectively, were assigned to multiplicative pressure tuning parameters for tanks 2 and 3. Since this calculation problem does not occur in tank 1, upper and lower bounds were set more conservatively at 1.02 and 0.98, respectively.
- Initial diluent crumb concentrations were considered to be uncertain by ± 60% based on advice from our industrial sponsor, due to lack of confidence in the pre-existing Aspen^{TM} model predictions (e.g., due to thermodynamic parameters and phase equilibrium assumptions that may not be valid for the diluent concentrations in the entering crumb).
- The value for effective radius for EPDM grade 3 was experimentally estimated to be 1.36×10^{-3} m (see Chapter 2). It is estimated to be accurate to within approximately ± 1 mm. For other EPDM grades that have different particle morphology (*i.e.*, EPDM grades 1 and 2), the upper boundary was increased to 6.36×10^{-3} m and the lower boundary was reduced to 2.00×10^{-3} m.

In accordance with the orthogonalisation method, the parameters were first ranked in order from most estimable to least estimable using the deflation algorithm first proposed by Yao et al. (2003), and using the uncertainty-based scaling suggested by Thompson et al. (2009). This method ranks parameters by taking into account: the magnitude of the influence of parameters on predictions of the data available for parameter estimation, the uncertainty associated with the initial parameter values, the uncertainty in the measured values and the correlated effects of parameters. Parameters that have large initial uncertainty and a large influence on model predictions tend to be ranked at the top of the list and parameters with smaller uncertainty ranges and that have little influence on model predictions are ranked at the bottom of the list.

To perform the ranking, parametric sensitivity coefficients were calculated and were scaled to determine elements of the sensitivity matrix, *Z*:

$$\frac{\partial \eta_{m_{j,i,r}}}{\partial \theta_k} \frac{s_{\theta_{k0}}}{s_{m_{j,i}}} \tag{49}$$

where $\eta_{m_{j,i,r}}$ is the prediction of the measured concentration of diluent *j* in crumb leaving the i^{th} tank from the r^{th} data set and θ_k is the k^{th} parameter in the model. The values of $s_{\theta_{k0}}$ are set at half the difference between the upper and lower bounds of the uncertainty range for the k^{th} parameter (see values of bounds in Table 14). The uncertainties associated with the industrial data, $s_{m_{j,i}}$, were estimated by taking into account measurement error and reproducibility (see Table 15).

Table 15: Uncertainty associated with measured data from the three-tank process

Data	Uncertainty (phr)
$m_{C6,2}$	0.31
$m_{ENB,2}$	0.18
$m_{VNB,2}$	0.02
$m_{C6,3}$	0.11
$m_{ENB,3}$	0.09
$m_{VNB,3}$	0.01

The $s_{m_{j,i}}$ values are the same measurement uncertainty values used to weight the objective function:

$$J = \sum_r \sum_i \sum_j \left(\frac{\eta_{m_{j,i,r}} - m_{j,i,r}}{s_{m_{j,i}}} \right)^2 \tag{50}$$

Following parameter ranking, parameters from the ranked list were estimated using weighted least-squares regression. Using the ranked list (shown in Table 16), the first parameter (R_2) was estimated while holding all of the others constant at their original guess values, then the first two parameters (R_2 and p_3) were estimated, and so on. When each regression had converged, the objective function value was recorded. See Figure 12 for a plot of the resulting objective function values as a function of number of estimated parameters.

Table 16: Ranked list of the three-tank model parameters

Parameter Rank, *k*	Symbol	Parameter Rank, *k*	Symbol
1	R_2	13	α_{VNB}
2	p_3	14	Y_1
3	R_1	15	α_{C6}
4	p_2	16	$D_{C6,ref}$
5	$H_{VNB,ref}$	17	β_{VNB}
6	$I_{ENB,0}$	18	α_{ENB}
7	$D_{VNB,ref}$	19	β_{C6}
8	R_3	20	p_1
9	$I_{VNB,0}$	21	$D_{ENB,ref}$
10	$I_{C6,0}$	22	Y_2
11	$H_{C6,ref}$	23	β_{ENB}
12	$H_{ENB,ref}$	24	Y_3

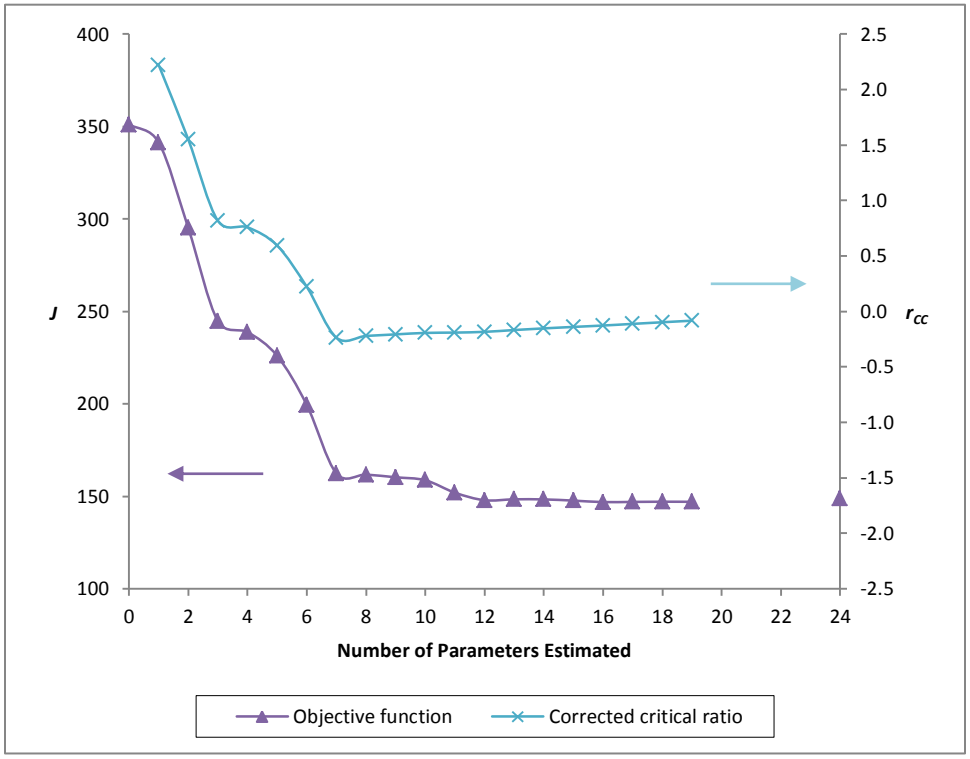

Figure 12: Objective function and corrected critical ratio as a function of number of parameters estimated for the three-tank model

Next, the MSE-based procedure described by Wu et al. (2011) was used to determine the optimal number of parameters to estimate. The corrected critical ratio, r_{CC}, computed using this method is lowest when estimating additional parameters would not improve the model predictions. Note that the minimum r_{CC} value calculated for the three-tank model parameters

occurs when seven parameters are estimated, as shown in Figure 12. Estimating 8 or more parameters would reduce the bias in model predictions but would increase the variance in the predictions by a larger amount. As a result, estimating 8 or more parameters would cause the MSE to be worse than when 7 parameters are estimated.

Using the seven updated parameter estimates (see Table 17) and the initial guesses for the other 17 parameters in the three-tank model (see Table 14), the 14 data sets were simulated. Figure 13 compares the predictions from the three-tank model with measured values of $\overline{m}_{C6,2}$, $\overline{m}_{C6,3}$, $\overline{m}_{ENB,2}$, $\overline{m}_{ENB,3}$, $\overline{m}_{VNB,2}$ and $\overline{m}_{VNB,3}$ for one of the 14 three-tank data sets. Corresponding plots for the remaining updated simulations are provided in Appendix B.

Table 17: List of the seven updated three-tank model parameters

Parameter Rank, *k*	Symbol	Units	Initial Value	Updated Value
1	R_2	m	1.3551×10^{-3}	1.1058×10^{-3}
2	p_3	-	1	1.0816
3	R_1	m	1.3551×10^{-3}	5.2869×10^{-2}
4	p_2	-	1	0.98493
5	$H_{VNB,ref}$	mbar/phr	10.125	14.607
6	$I_{ENB,0}$	-	1	0.64896
7	$D_{VNB,ref}$	m^2/s	1.4679×10^{-10}	1.9207×10^{-10}

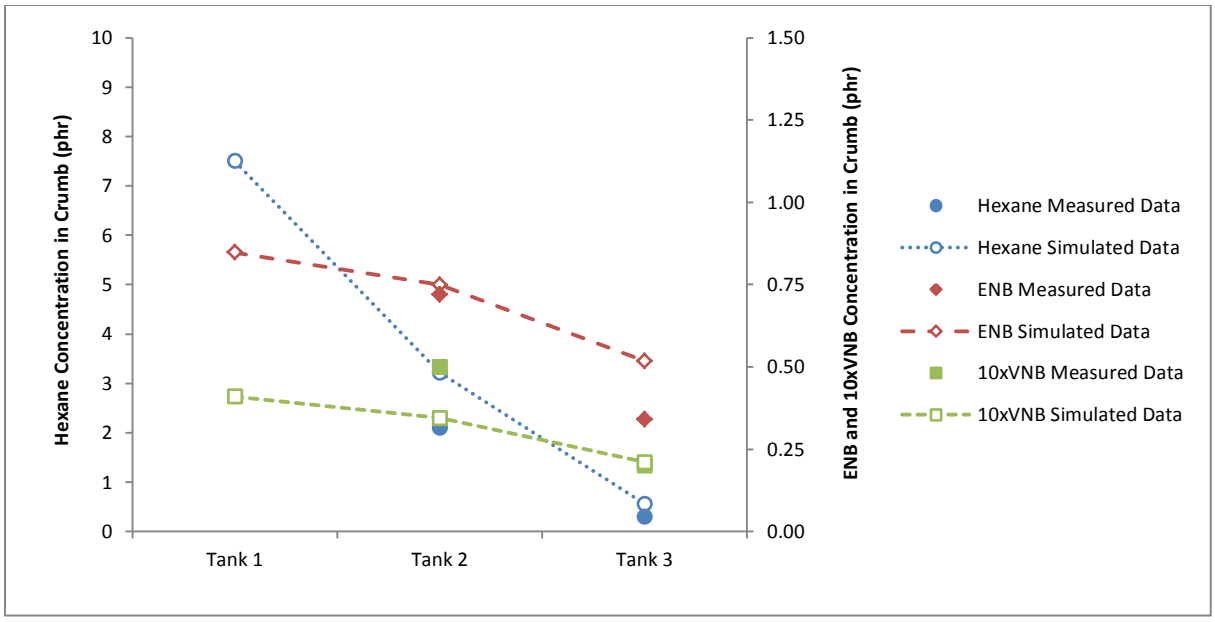

Figure 13: Three-Tank simulation results for outlet crumb concentrations, $\bar{m}_{j,i}$, compared to measured data for data set one, using the updated set of model parameters. Dashed lines are used to guide the eye. Note that this plot is representative of the corresponding plots for data sets two to 14 (see Appendix B).

As expected, predictions in Figure 13 and in Appendix B more closely match the measured data than the simulations in Figure 11 wherein the initial guesses for the parameter values were used to predict outlet crumb concentrations. Note that the tuning parameter p_3, estimated to a value of 1.0816, effectively adjusted the pressure in the third tank so that predicted mole fractions of hexane, ENB, and VNB in the headspace are greater than zero.

The residuals for all 14 data sets were plotted versus each of the 18 input variables used in the three-tank model. Plots were examined to determine whether or not any phenomena were inadequately accounted for in the model with the seven updated parameter values. Appendix C includes the residual plots and discussion of the possible trends that were observed. It was determined that the trends in Appendix C were minor except for perhaps some trends associated with H_{VNB} or D_{VNB}. Note that the parameter estimation method already increased the values of the $H_{VNB,ref}$ and $D_{VNB,ref}$ parameters. As neither parameter is at its upper bound, further adjustment using additional data from the four-tank processes might occur.

5.2 Parameter Tuning Using Data from Four-Tank Processes A and B

In the second phase of parameter tuning, the number of estimable parameters in each of the four-tank models (process A and B) were ranked and estimated. The parameters were ranked in order of most to least estimable based on their relative effects on the model predictions and the uncertainties of their initial values, while taking correlation into account. The optimal number of parameters to be estimated was selected based on the anticipated MSE of the model predictions. The initial set of parameters used for this stage of parameter estimation did not include the parameters that are common to both the three-tank and the four-tank processes: the Henry's law constants and diffusivity parameters (see Table 18). Fine-tuning of the common parameters as well as other highly-ranked parameters is conducted in a final stage of parameter tuning (section 5.3) using all of the available data from the three- and four-tank processes. The Henry's law constants and diffusivity coefficients were held at the values from the three-tank data. Tables 19 and 20 summarize the adjustable parameters in the four-tank models, processes A and B, along with their initial guesses and their uncertainty bounds. The parameters are listed in no particular order.

Table 18: Henry's Law Constant and Diffusivity Parameters used in Four-Tank Model Parameter Estimation

Symbol	Description	Units	Value
$H_{C6,ref}$	Henry's constant for hexane in EPDM at the reference temperature (108 °C)	mbar/phr	1.5348×10^{2}
α_{C6}	Activation energy term for Henry's constant Arrhenius expression for hexane in EPDM	K	-3.5036×10^{3}
$H_{ENB,ref}$	Henry's constant for ENB in EPDM at the reference temperature (108 °C)	mbar/phr	10.123
α_{ENB}	Activation energy term for Henry's constant Arrhenius expression for ENB in EPDM	K	-4.7190×10^{3}
$H_{VNB,ref}$	Henry's constant for VNB in EPDM at the reference temperature (108 °C)	mbar/phr	14.607
α_{VNB}	Activation energy term for Henry's constant Arrhenius expression for VNB in EPDM	K	-4.7190×10^{3}
$D_{C6,ref}$	Diffusivity for hexane in EPDM at the reference temperature (108 °C)	m^2/s	3.4177×10^{-10}
β_{C6}	Activation energy term for diffusivity-related Arrhenius expression for hexane in EPDM	K	-2.7995×10^{3}
$D_{ENB,ref}$	Diffusivity for ENB in EPDM at the reference temperature (108 °C)	m^2/s	1.4679×10^{-10}
β_{ENB}	Activation energy term for diffusivity-related Arrhenius expression for ENB in EPDM	K	-2.9220×10^{3}
$D_{VNB,ref}$	Diffusivity for VNB in EPDM at the reference temperature (108 °C)	m^2/s	1.9207×10^{-10}
β_{VNB}	Activation energy term for diffusivity-related Arrhenius expression for VNB in EPDM	K	-2.9220×10^{3}

Table 19: Initial Four-Tank Model Tuning Parameters for Process A

Symbol	Description	Units	Value	Lower Bound	Upper Bound
R_4	Effective diffusion radius for EPDM grade 4	m	1.3551×10^{-3}	2.0×10^{-3}	1.1355×10^{-2}
R_5	Effective diffusion radius for EPDM grade 5	m	1.3551×10^{-3}	2.0×10^{-3}	1.1355×10^{-2}
R_6	Effective diffusion radius for EPDM grade 6	m	1.3551×10^{-3}	2.0×10^{-3}	1.1355×10^{-2}
Y_{1A}	Adjustable factor to tune the residence time in tank 1	-	1	0.95	1.05
Y_{2A}	Adjustable factor to tune the residence time in tank 2	-	1	0.95	1.05
Y_{3A}	Adjustable factor to tune the residence time in tank 3	-	1	0.5	1.5
Y_{4A}	Adjustable factor to tune the residence time in tank 4	-	1	0.5	1.5
p_{1A}	Adjustable factor to tune the pressure in tank 1	-	1	0.98	1.02
p_{2A}	Adjustable factor to tune the pressure in tank 2	-	1	0.95	1.5
p_{34A}	Adjustable factor to tune the pressure in tanks 3 and 4	-	1	0.95	1.5
$I_{C6,0A}$	Adjustable factor to tune the inlet concentration of hexane in the crumb	-	1	0.4	1.6
$I_{ENB,0A}$	Adjustable factor to tune the inlet concentration of ENB in the crumb	-	1	0.4	1.6
$I_{VNB,0A}$	Adjustable factor to tune the inlet concentration of VNB in the crumb	-	1	0.4	1.6

Table 20: Initial Four-Tank Model Tuning Parameters for Process B

Symbol	Description	Units	Value	Lower Bound	Upper Bound
R_7	Effective diffusion radius for EPDM grade 7	m	1.3551×10^{-3}	2.0000×10^{-3}	1.1355×10^{-2}
R_8	Effective diffusion radius for EPDM grade 8	m	1.3551×10^{-3}	2.0000×10^{-3}	1.1355×10^{-2}
Y_{1B}	Adjustable factor to tune the residence time in tank 1	-	1	0.95	1.05
Y_{2B}	Adjustable factor to tune the residence time in tank 2	-	1	0.95	1.05
Y_{3B}	Adjustable factor to tune the residence time in tank 3	-	1	0.5	1.5
Y_{4B}	Adjustable factor to tune the residence time in tank 4	-	1	0.5	1.5
p_{1B}	Adjustable factor to tune the pressure in tank 1	-	1	0.98	1.02
p_{2B}	Adjustable factor to tune the pressure in tank 2	-	1	0.95	1.5
p_{34B}	Adjustable factor to tune the pressure in tanks 3 and 4	-	1	0.95	1.5
$I_{C6,0B}$	Adjustable factor to tune the inlet concentration of hexane in the crumb	-	1	0.4	1.6
$I_{ENB,0B}$	Adjustable factor to tune the inlet concentration of ENB in the crumb	-	1	0.4	1.6
$I_{VNB,0B}$	Adjustable factor to tune the inlet concentration of VNB in the crumb	-	1	0.4	1.6

The upper and lower bounds indicate the range of plausible values that are permitted during the parameter tuning process. Note that a single tuning parameter is used to adjust the pressure in the third and fourth tanks due to the fact that these tanks have a common headspace and common pressure. The four-tank parameters and parameter bounds were the same for processes A and B and were set to the same respective initial values and bounds that were used or the three-tank process. The values for effective radii for EPDM grades 4, 5, 6, 7 and 8 from the four-tank processes had different particle morphology than grades 1, 2 and 3 from the three-tank process. Since the initial guesses for their values are less certain, the upper bound was increased to 1.14×10^{-2} m and the lower bound was reduced to 2.00×10^{-3} m.

Figure 14 compares predictions from the four-tank model with measured values for $\overline{m}_{C6,3}$, $\overline{m}_{C6,4}$, $\overline{m}_{ENB,3}$, $\overline{m}_{ENB,4}$, $\overline{m}_{VNB,3}$ and $\overline{m}_{VNB,4}$ for one of the eleven four-tank data sets. Corresponding

plots for the additional data sets are provided in Appendix D. Predictions in Figure 14 and in Appendix D were made using the initial parameter values in Tables 19 and 20. Before tuning, the four-tank model predicts outlet crumb concentrations for hexane, ENB and VNB are considerably smaller than the measured concentration. As expected, the model and data show a decrease in concentrations as the crumb particles move through the four tanks.

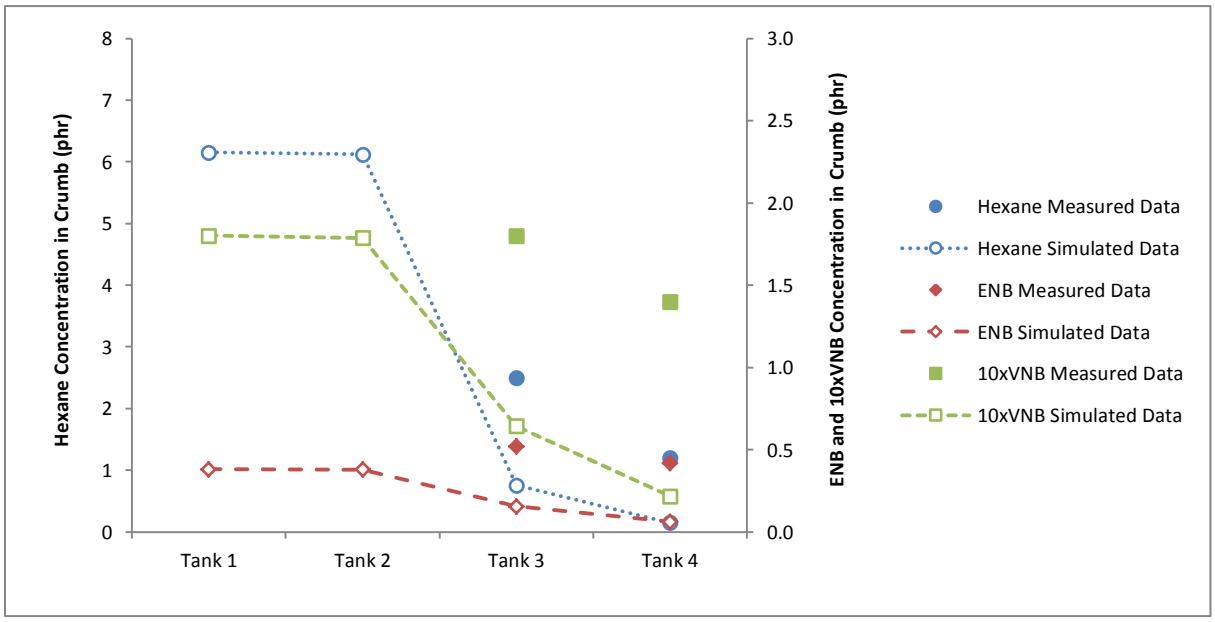

Figure 14: Four-Tank simulation results for outlet crumb concentrations, $\bar{m}_{j,i}$, compared to measured data for data set one (process A), using the initial set of model parameters in Tables 19 and 20. Dashed lines are used to guide the eye. Note that this plot is representative of the corresponding plots for data sets two to eleven (see Appendix D).

Two major problems are shown in Figure 14 and Appendix D. Similar to the original three-tank model, the four-tank model predictions are lower than the measured values in the third and fourth tanks because the measured pressure in the third and fourth tanks tended to be small relative to the vapour pressure of pure water, calculated using the Antoine equation. Secondly, the first-tank predictions for ENB and VNB are lower than the ENB and VNB concentrations that are measured in the third tank, indicating that inlet ENB and VNB concentrations in the crumb might be larger than the values approximated by the Aspen™ model and used as inputs into the four-tank models. It is expected that parameter tuning will correct these two problems; that is, the associated tuning parameters used to

adjust the third and fourth tank's pressure and the inlet ENB and VNB concentrations will be adjusted and the predictions will more closely match the data.

The four-tank model parameters from process A and process B were separately ranked in order from most estimable to least estimable using the othogonalization method. To perform the ranking, parametric sensitivity coefficients were calculated and were scaled to determine elements of the sensitivity matrix, Z (see equation 49). The values of $s_{\theta_{k0}}$ are set at half the difference between the upper and lower bounds of the uncertainty range for the k^{th} parameter (see values of bounds in Tables 19 and 20). The uncertainties associated with the industrial data, $s_{m_{j,i}}$, were estimated by taking into account measurement error and reproducibility, as shown in Table 21.

Table 21: Uncertainty associated with measured data from the four-tank processes

Data	Uncertainty (phr)
$m_{C6,2}$	0.80
$m_{ENB,2}$	0.01
$m_{VNB,2}$	0.54
$m_{C6,3}$	0.30
$m_{ENB,3}$	0.09
$m_{VNB,3}$	0.01
$m_{C6,4}$	0.15
$m_{ENB,4}$	0.06
$m_{VNB,4}$	0.01

Following parameter ranking, parameters from the ranked list were estimated using weighted least-squares regression (see Tables 22 and 23 for the ranked lists). Using the ranked lists, the first parameters (p_{34A} and $I_{C6,0B}$, respectively) were estimated while holding all of the others constant at their original guess values, then the first two parameters in each list were estimated, and so on. When each regression had converged, the objective function value was recorded. See Figures 15 and 16 for plots of the objective function values as a function of number of estimated parameters for processes A and B, respectively.

Table 22: Ranked list of the four- tank model, process A parameters

Parameter Rank, *k*	Symbol
1	p_{34A}
2	R_5
3	$I_{VNB,0A}$
4	$I_{C6,0A}$
5	R_4
6	R_6
7	$I_{ENB,0A}$
8	Y_{3A}
9	Y_{4A}
10	Y_{1A}
11	p_{1A}
12	p_{2A}
13	Y_{2A}

Table 23: Ranked list of the four-tank model, process B parameters

Parameter Rank, *k*	Symbol
1	$I_{C6,0B}$
2	$I_{VNB,0B}$
3	$I_{ENB,0B}$
4	R_8
5	R_7
6	p_{2B}
7	p_{34B}
8	Y_{3B}
9	p_{1B}
10	Y_{3B}
11	Y_{1B}
12	Y_{2B}

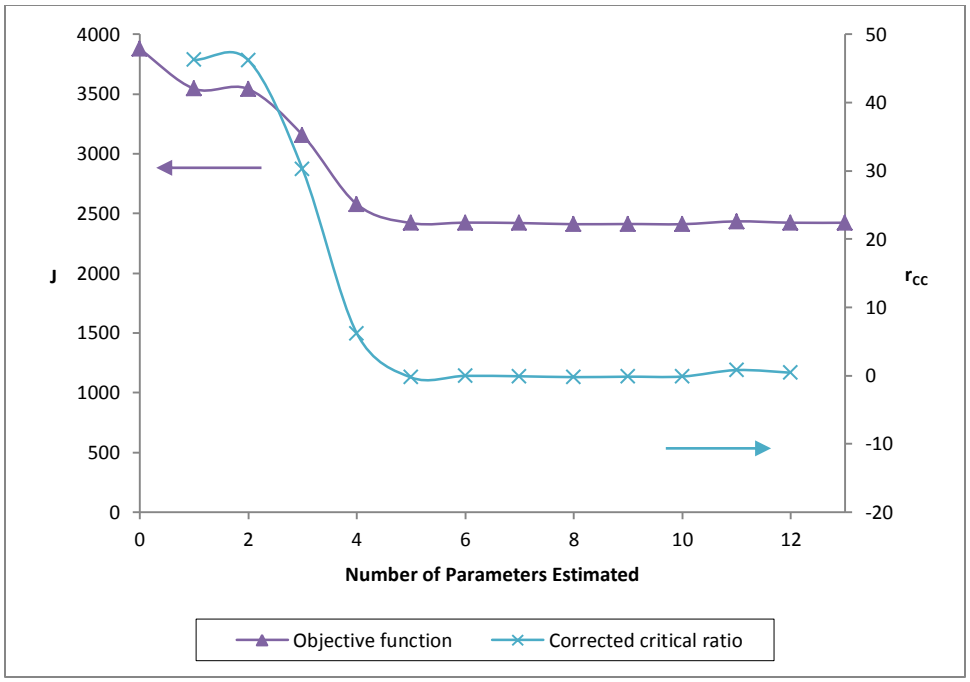

Figure 15: Objective function and corrected critical ratio as a function of the number of parameters estimated for the four-tank model, process A

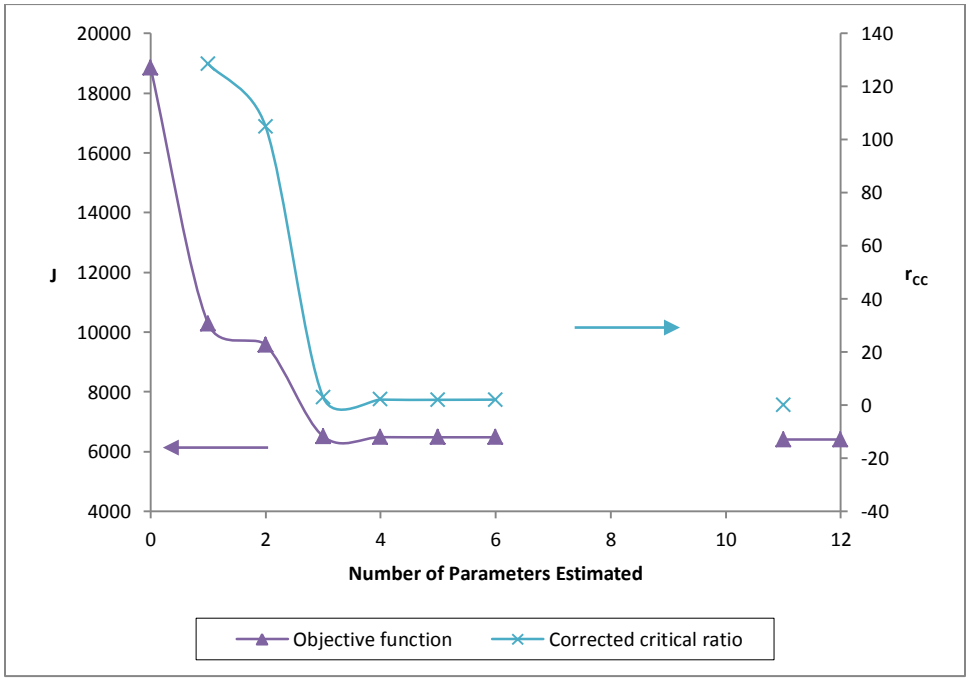

Figure 16: Objective function and corrected critical ratio as a function of the number of parameters estimated for the four- tank model, process B

The MSE-based procedure described by Wu et al. (2011) was used to determine the optimal number of parameters to estimate for both process models based on r_{CC}. Note that the

minimum r_{CC} value calculated occurs when five parameters are estimated for process A, as shown in Figure 15. For process B, the minimum r_{CC} value is occurs between four to eleven parameters are estimated; unfortunately, however, the objective value could not be determined when seven, eight, nine, and ten parameters were estimated because the numerical methods used to solve the model equations experienced convergence difficulties for parameter values encountered during parameter estimation. It was possible to estimate 11 and 12 parameters, as shown in Figure 16. Several attempts were made to estimate seven, eight, nine, and ten parameters from the list starting from different initial guesses but these attempts failed. As such, the six top-ranked parameters were selected as the optimal parameters for estimation. The updated parameters are shown in Tables 24 and 25.

Table 24: List of the five updated four-tank model, process A parameters

Parameter Rank, *k*	Symbol	Units	Initial Value	Updated Value
1	p_{34A}	-	1.3	1.1221
2	R_5	m	1.3551×10^{-3}	1.3722×10^{-3}
3	$I_{VNB,0A}$	-	1	1.2586
4	$I_{C6,0A}$	-	1	0.71966
5	R_4	m	1.3551×10^{-3}	4.6438×10^{-3}

Table 25: List of the six updated four-tank model, process B parameters

Parameter Rank, *k*	Symbol	Units	Initial Value	Updated Value
1	$I_{C6,0B}$	-	1	0.45606
2	$I_{VNB,0B}$	-	1	1.582
3	$I_{ENB,0B}$	-	1	1.583
4	R_8	m	1.3551×10^{-3}	0.32283×10^{-3}
5	R_7	m	1.3551×10^{-3}	0.31238×10^{-3}
6	p_{2B}	-	1	0.95245

Note that for the parameter ranking and parameter estimation steps, the initial parameter values for p_{34A} and p_{34B} were 1.3 and 1.1, respectively, rather than 1. A higher total pressure in the third and fourth tanks would allow for higher pressure supplied by the volatiles in the headspace; therefore, reducing the driving force, resulting in a larger concentration of each volatile within the crumb. Appendix E includes plots of the model predictions compared to the measured data for the

11 four-tank datasets. As anticipated, the model predictions more closely matched the measured data with the updated parameters.

5.3 Final Parameter Tuning Using Combined Datasets

To determine better estimates for the common parameters in the three- and four- tank models (*i.e.*, the Henry's law constant and diffusivity parameters) and to ensure that all of the critical parameters were included together in parameter tuning, a final round of parameter estimation was conducted, including all of the data from the three- and four-tank processes simultaneously. The 18 parameters that had been previously selected as the optimal parameters to be estimated for each of the processes were preselected to be included in the final stage of parameter estimation. The preselected parameters (in no particular order) are summarized in Table 26. The remaining 31 parameters that had not been previously selected were ranked in order of most to least estimable using the same method described in the previous sections, assuming that the 18 parameters were preselected. The ranked list is shown in Table 27.

Table 26: Preselected three- and four- tank model parameters used in final stage of parameter tuning

Common Parameters	Three-Tank Process Parameters	Four-Tank Process A Parameters	Four-Tank Process B Parameters
$H_{VNB,ref}$	R_2	p_{34A}	$I_{C6,0B}$
$D_{VNB,ref}$	p_3	R_5	$I_{VNB,0B}$
	R_1	$I_{VNB,0A}$	$I_{ENB,0B}$
	p_2	$I_{C6,0A}$	R_8
	$I_{ENB,0}$	R_4	R_7
			p_{2B}

Table 27: Ranked list of the previously unselected three- and four- tank model parameters considered for the final stage of estimation

Parameter Rank, *k*	Symbol	Parameter Rank, *k*	Symbol
19	p_{34B}	35	p_{1A}
20	R_6	36	α_{ENB}
21	$I_{ENB,0A}$	37	β_{VNB}
22	$I_{VNB,0}$	38	$D_{ENB,ref}$
23	Y_{4A}	39	p_{1B}
24	$I_{C6,0}$	40	β_{C6}
25	Y_{3A}	41	Y_{1B}
26	$H_{ENB,ref}$	42	Y_{1A}
27	α_{VNB}	43	Y_2
28	$H_{C6,ref}$	44	Y_3
29	R_3	45	Y_{4B}
30	Y_1	46	β_{ENB}
31	$D_{C6,ref}$	47	p_2
32	Y_{3B}	48	Y_{2A}
33	α_{C6}	49	Y_{2B}
34	p_1		

Following parameter ranking, parameters from the ranked list were estimated using weighted least-squares regression. The method used for estimating parameters was the same method described in the previous two sections; however, the 18 preselected parameters were first estimated simultaneously while holding all of the other parameters constant at their original values. Next, the 18 preselected parameters and the top-ranked parameter from Table 27 were estimated, and so on. See Figure 17 for a plot of the objective function values as a function of the number of estimated parameters. The objective value could not be determined when 23, 24 and 25 parameters were estimated simultaneously due to convergence difficulties.

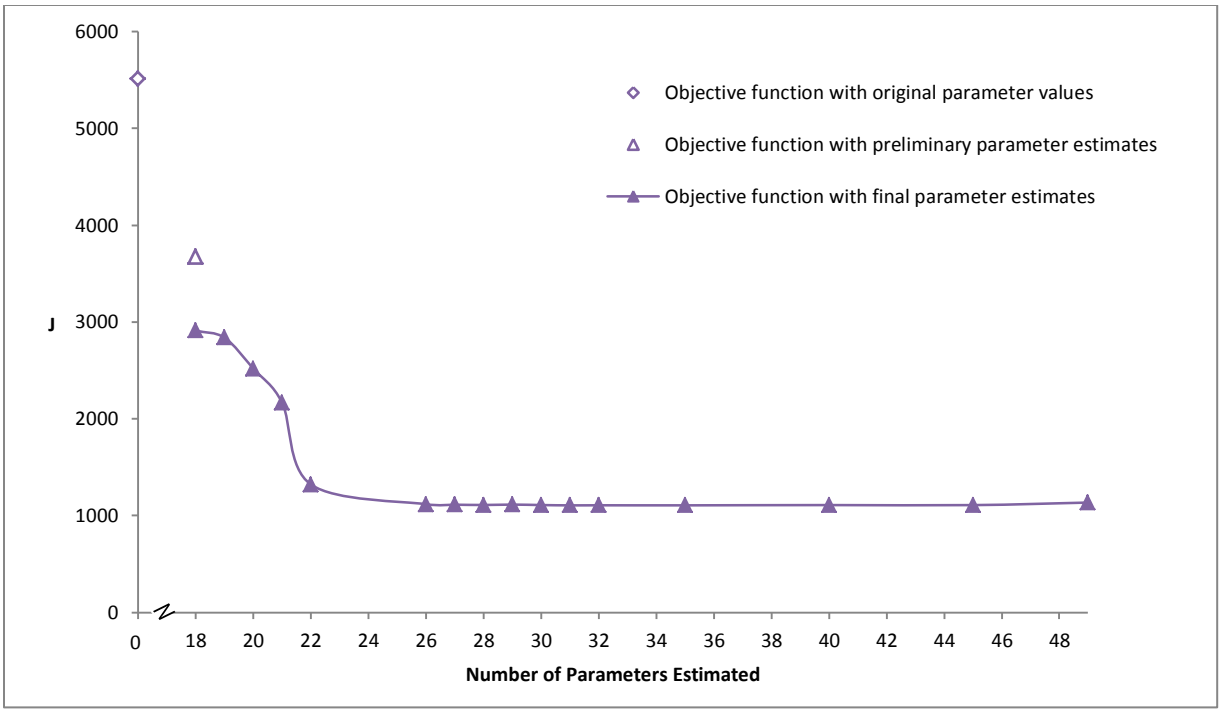

Figure 17: Objective function as a function of the number of parameters estimated from the three- and four-tank processes

Note that the objective function had a value of 5513.94 with the original parameter values (see Tables 14, 19 and 20 for values) and improved to a value of 3675.01 after preliminary tuning of the 18 top-ranked parameters in the separate three- and four-tank models. After combining all of the datasets and re-estimating the 18 parameters, the value of the objective function decreased to a value of 2910.7.

The MSE-based procedure described by Wu et al. (2011) was used to determine the optimal number of parameters to estimate using all of the data. The minimum value of r_{CC} occurs when 26 parameters are estimated. As such, these 26 were estimated to provide the parameter shown in Table 28.

Table 28: List of the 26 updated three- and four-tank parameters

Symbol	Units	Initial Value	Updated Value
R_2	m	1.1058×10^{-3}	1.5304×10^{-3}
p_3	-	1.0816	1.0444
R_1	m	5.2869×10^{-2}	7.8069×10^{-4}
p_2	-	0.98493	0.98126
$H_{VNB,ref}$	mbar/phr	14.607	6.9922
$I_{ENB,0}$	-	0.64896	0.65870
$D_{VNB,ref}$	m^2/s	1.9207×10^{-10}	7.2942×10^{-11}
p_{34A}	-	1.1221	1.1573
R_5	m	1.3722×10^{-3}	6.3490×10^{-4}
$I_{VNB,0A}$	-	1.2586	1.56658
$I_{C6,0A}$	-	0.71966	0.41148
R_4	m	4.6438×10^{-3}	2.2118×10^{-4}
$I_{C6,0B}$	-	0.45606	0.99609
$I_{VNB,0B}$	-	1.582	0.44550
$I_{ENB,0B}$	-	1.583	1.49096
R_8	-	3.2283×10^{-4}	9.2452×10^{-4}
R_7	m	3.1238×10^{-4}	1.0427×10^{-3}
p_{2B}	-	0.95245	0.98499
p_{34B}	-	1	1.02051
R_6	m	1.3551×10^{-3}	8.7824×10^{-3}
$I_{ENB,0A}$	-	1	1.4062
$I_{VNB,0}$	-	1	0.65848
Y_{4A}	-	1	1.4969
$I_{C6,0}$	-	1	0.85260
Y_{3A}	-	1	0.56835
$H_{ENB,ref}$	mbar/phr	10.123	9.1735

It is interesting to note some of the trends observed in the final parameter estimates. $H_{VNB,ref}$ and $D_{VNB,ref}$ decreased from their initial guess values, which were based on the experimentally determined values for ENB. The decreased estimates for the Henry's law constant and diffusivity suggest that VNB is less soluble and diffuses less readily in EPDM than ENB in EPDM.

For the three-tank process and for the four-tank process B, the p parameters changed only slightly from their original values; the p_2 parameters reduced slightly from the original value of 1 and the p_3 and p_{34B} parameters increased slightly from the original value of 1. For the four-tank process A, however, the p_{34A} parameter was estimated to larger value of 1.1573. Additionally, the residence time parameters for the four-tank process A, (Y_{3A} and Y_{4A}) decreased and increased to their lower and upper bounds, respectively. Similarly, for the three-tank process and for the four-

tank process B, the effective radius parameters only changed slightly from their initial guess values; R_1 decreased slightly, R_2 increased slightly, R_7 decreased slightly, and R_8 decreased slightly. However, for the four-tank process A, R_4 approached its lower bound, R_5 decreased, and R_6 increased to a very large effective radius. The larger change in magnitude between the original guess parameter values and the final parameter estimates for the four-tank process A, might indicate that the four-tank process A results in EPDM crumb with different particle morphology than the other two processes or that the parameter estimator had difficulty fitting the model parameters such that the model predictions would fit the four-tank process A data. Additional four-tank process A data as well as additional gravimetric testing to determine effective radius would aid in providing improved parameter estimates.

The inlet concentration parameters for all three volatile components and for all three processes changed from their initial values, perhaps indicating poor estimates for the inlet concentrations models for all three processes. For the three-tank process, all inlet concentration parameters decreased. In contrast, the four-tank process parameters both increased and decreased, sometimes reaching their estimation bounds. For the four-tank process A, the hexane inlet concentration parameter decreased almost to its lower bound, whereas the ENB and VNB inlet concentration parameters increased to their upper bounds. For the four-tank process B, the hexane inlet concentration parameter decreased slightly, the ENB inlet concentration parameter nearly increased to its upper bound and the VNB inlet concentration parameter nearly decreased to its lower bound.

Figures 18, 19 and 20 show the model predictions compared to the measured data for the first datasets from the three-tank process, four-tank process A, and four-tank process B, respectively. Appendix F and G includes similar plots for the 22 other three- and four-tank datasets.

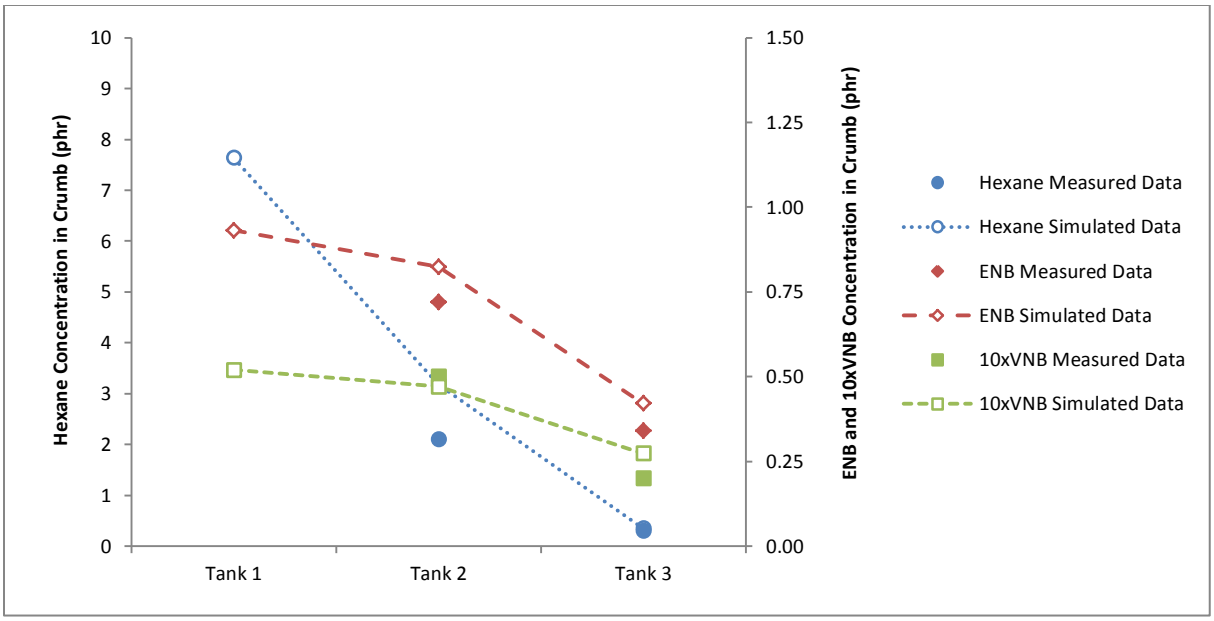

Figure 18: Three-Tank simulation results for outlet crumb concentrations, $\bar{m}_{j,i}$, compared to measured data for data set one, using the updated set of model parameters. Dashed lines are used to guide the eye.

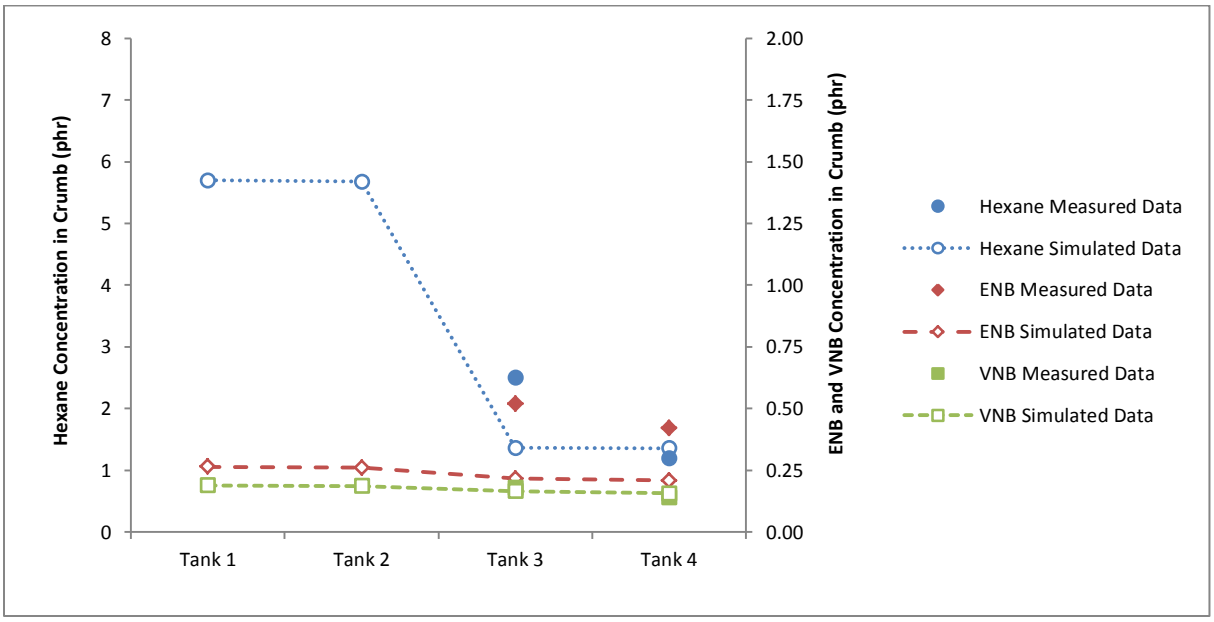

Figure 19: Four-Tank Process A simulation results for outlet crumb concentrations, $\bar{m}_{j,i}$, compared to measured data for data set one, using the updated set of model parameters. Dashed lines are used to guide the eye.

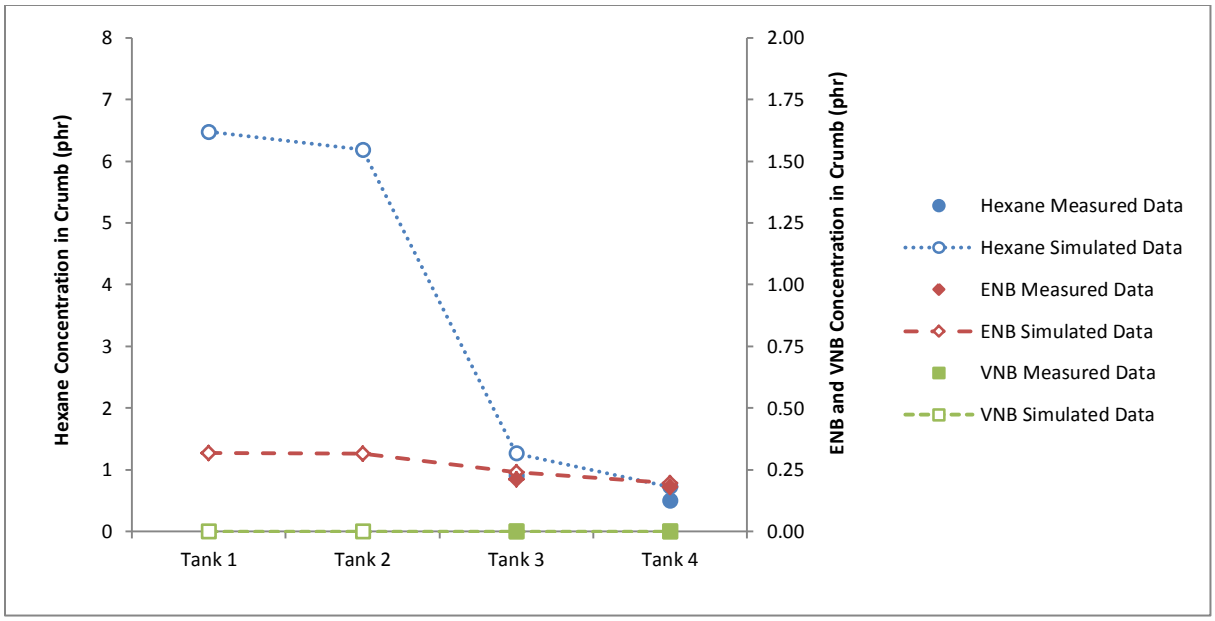

Figure 20: Four-Tank Process B simulation results for outlet crumb concentrations, $\bar{m}_{j,i}$, compared to measured data for data set six, using the updated set of model parameters. Dashed lines are used to guide the eye.

This final stage of parameter tuning resulted in improved model predictions, in most cases. For the three-tank model, the model predictions slightly improved from the preliminary parameter tuning with the exception of datasets 12 and 13 where the model predictions for the volatile concentrations in the third tank are slightly worse.

The fit of four-tank process A model's was slightly worse. Unfortunately, using the data from the combined three- and four- tank datasets resulted in poorer fit, especially for datasets four and five. Dataset four is the only four-tank dataset with measured volatile concentration data from the second tank. The estimated effective radius for the fourth and fifth datasets, R_6, was 8.7824×10^{-3} m whereas in the preliminary round of parameter estimation, the value was 1.1335×10^{-3} m. The much larger effective radius obtained in the final round of parameter estimation resulted in slightly better estimates for fourth and fifth datasets but resulted in poorer match-up for the other datasets. The four-tank, process A data only includes 24 data values out of 120 data values included in the combined three- and four-tank datasets. If more measured data from the four-tank process A model were available, the parameter estimator would have focused more on

obtaining a used in the four-tank process A model would have attributed to more error summed in the objective function, and better parameter estimates would have resulted during the final stage of parameter estimation. The final stage of parameter estimation yielded improved fit with measured data for the four-tank, process B model. The model predictions matched the data well.

5.4 Final Model Evaluation

In addition to the visual inspection of the model's fit to measured data for each of the datasets, the residual plots and calculated typical errors were assessed. Figures 21 to 25 indicate the residual error between the simulation predictions and the measured data from the three- and four-tank processes, as a function of measured concentrations for each species. The figures indicate that the residual error is evenly distributed above and below the zero line, indicating that there is unbiased variance in each of the model's fit to the data.

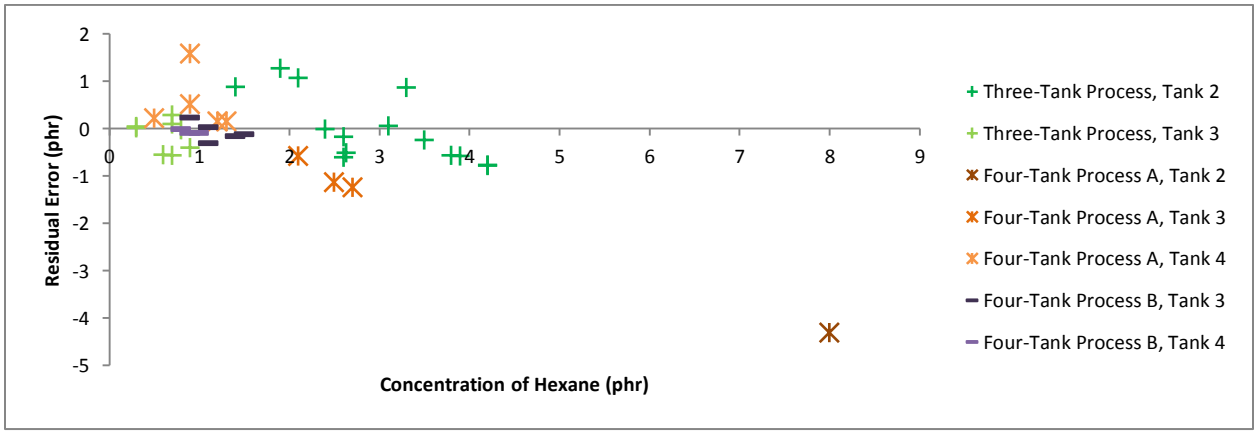

Figure 21: Residual error between the simulation predictions for the hexane concentrations in the outlet crumb, $\bar{m}_{H,i}$, and the measured data from the three- and four-tank processes, as a function of measured hexane concentration.

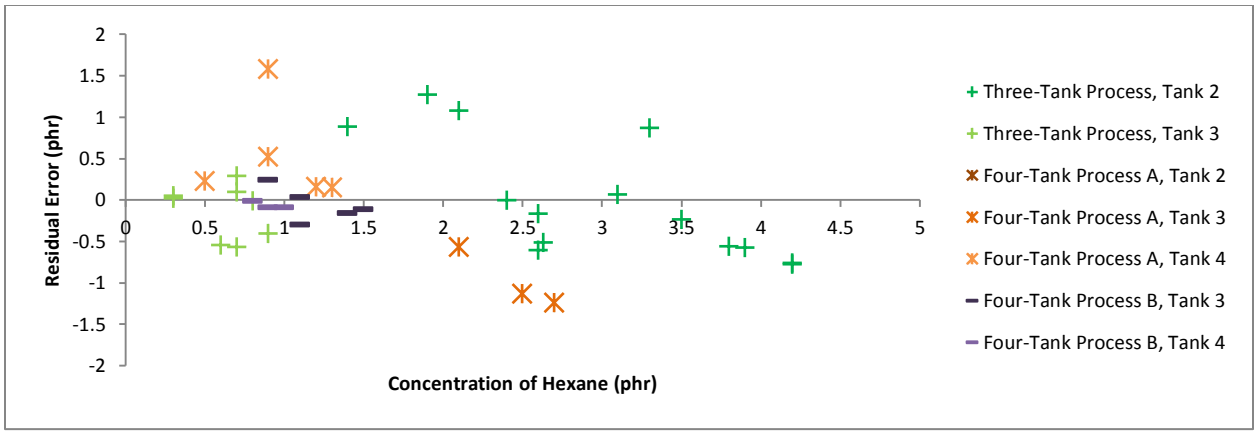

Figure 22: Residual error between the simulation predictions for the hexane concentrations in the outlet crumb, $\bar{m}_{H,i}$, and the measured data from the three- and four-tank processes, as a function of measured hexane concentration. Note that this figure does not include the outlying data point shown in Figure 21.

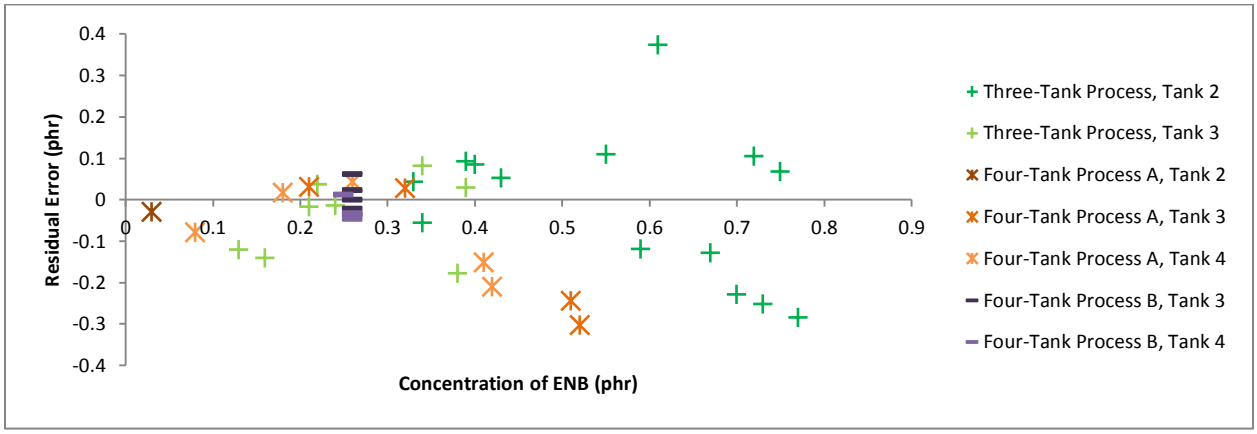

Figure 23: Residual error between the simulation predictions for the ENB concentrations in the outlet crumb, $\bar{m}_{E,i}$, and the measured data from the three- and four-tank processes, as a function of measured ENB concentration.

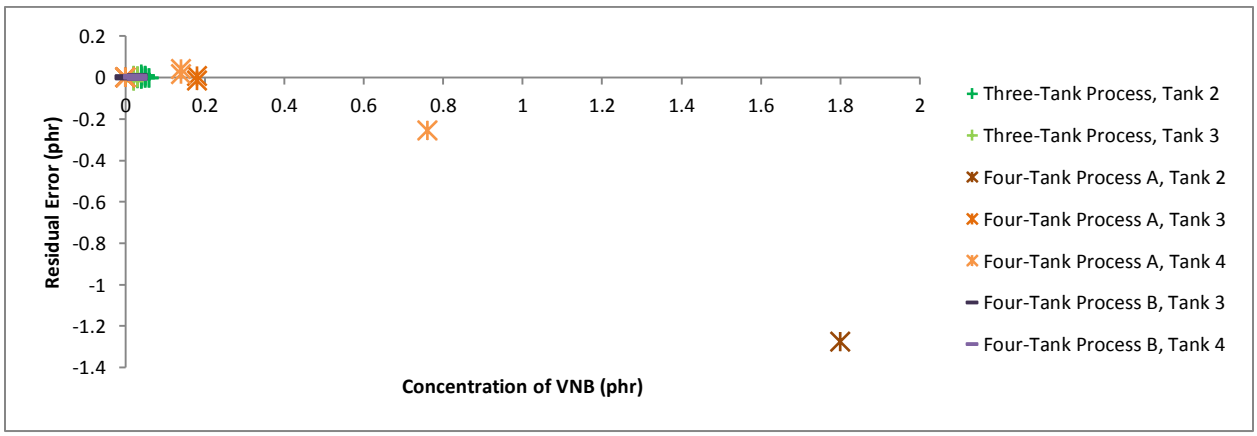

Figure 24: Residual error between the simulation predictions for the VNB concentrations in the outlet crumb, $\bar{m}_{V,i}$, and the measured data from the three- and four-tank processes, as a function of measured VNB concentration.

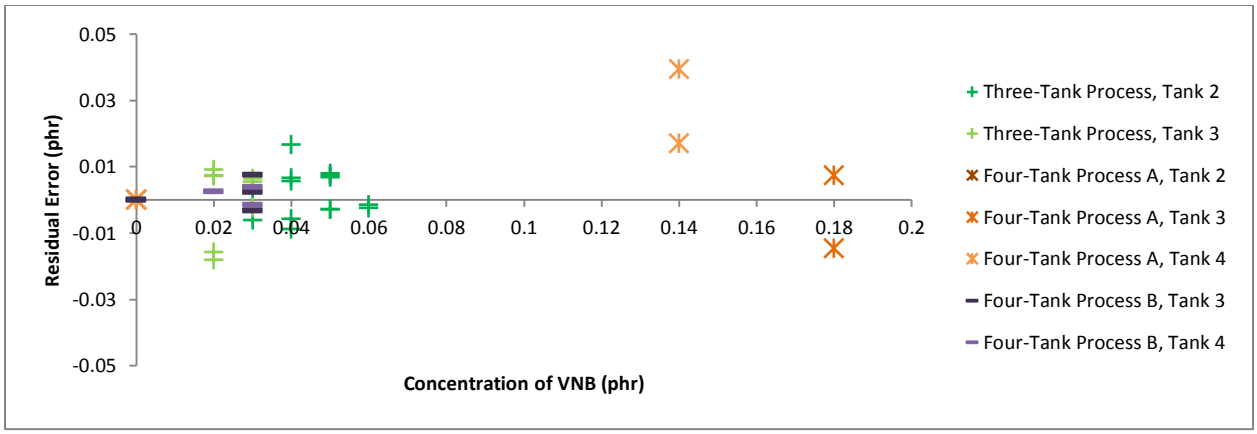

Figure 25: Residual error between the simulation predictions for the VNB concentrations in the outlet crumb, $\bar{m}_{V,i}$, and the measured data from the three- and four-tank processes, as a function of measured VNB concentration. Note that this figure does not include the outlying data points shown in Figure 24.

Figures 21 to 25 indicate that there may be smaller residual errors for lower species concentrations than for higher species concentrations. That is, for the last tanks in the series for the three- and four-tank processes, there is better model fit to data than for the earlier tanks in series. Additionally, Figures 21 and 24 show residual error data points much larger in magnitude that correspond to larger concentrations of hexane and VNB; it is not clear as to whether or not these data points are outliers or if they indicate that there is poor model fit for large hexane and VNB concentrations in the four-tank process A model.

The calculated roots of average squared-error indicate the typical error for each of the species in each tank, for each species overall, and for each of the three models, are shown in Table 29. Note that the lowest amount of typical error is for ENB, and for the Four-Tank Process B model, indicating that the Four-Tank Process B model predictions will be most accurate and the ENB model predictions will be the most accurate. The largest typical error was calculated for the Four-Tank Process A, second tank predictions. As previously mentioned, the typical error for the four-tank model, second tank predictions was based on only one data set which may include outlier data.

Table 29: Typical error associated with each $\bar{m}_{j,i}$ value, each species, and each of the three- and four-tank models. Note that the typical error is in units of phr.

	Three-Tank Process	Four-Tank Process A	Four-Tank Process B	Typical error associated with each species
Hexane				0.9040
$\bar{m}_{H,2}$	0.7001	4.3102		
$\bar{m}_{H,3}$	0.3316	1.0265	0.2307	
$\bar{m}_{H,4}$		0.8394	0.1291	
ENB				0.1355
$\bar{m}_{E,2}$	0.1729	0.0300		
$\bar{m}_{E,3}$	0.0971	0.2256	0.0339	
$\bar{m}_{E,4}$		0.1381	0.0310	
VNB				0.2058
$\bar{m}_{V,2}$	0.0070	1.2746		
$\bar{m}_{V,3}$	0.0103	0.0094	0.0035	
$\bar{m}_{V,4}$		0.1299	0.0025	
Typical error associated with each model	**0.3533**	**1.0504**	**0.1150**	

Finally, it was of interest to compare the predictions calculated using the previously-discussed "naïve" model (see sections 3.4 and 3.5) and those using the developed equivalent-time or "bin" model. Provided the same input and parameter values, the naïve model predictions were compared to the finalized three-tank model. Comparison of the four-tank naïve and equivalent-time models was deemed unnecessary due to the fact that the fourth tanks' predictions are closer to reaching equilibrium and do not provide any additional value for comparison. Figures 26 and 27 indicate the predictions using the naïve and equivalent-time models using the input data from datasets one and eight from the three-tank process.

As expected, the naïve model under-predicts the concentrations of diluent for the first and third tanks in series. The difference between the naïve and equivalent-time models decreases for the second tank in series due to the fact that the naïve model is using a smaller initial diluent concentration (i.e. the diluent concentration leaving the first tank is smaller for the naïve model).

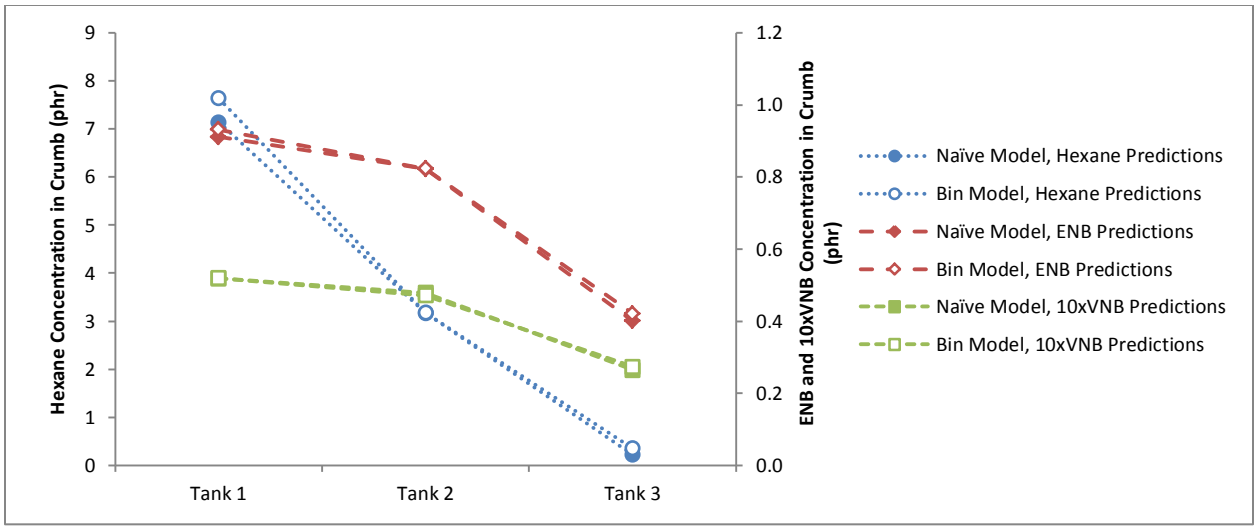

Figure 26: The simulation predictions for hexane, ENB and VNB concentrations in the outlet crumb, using the naïve and equivalent-time models for dataset one of the three-tank process. Dashed lines are used to guide the eye.

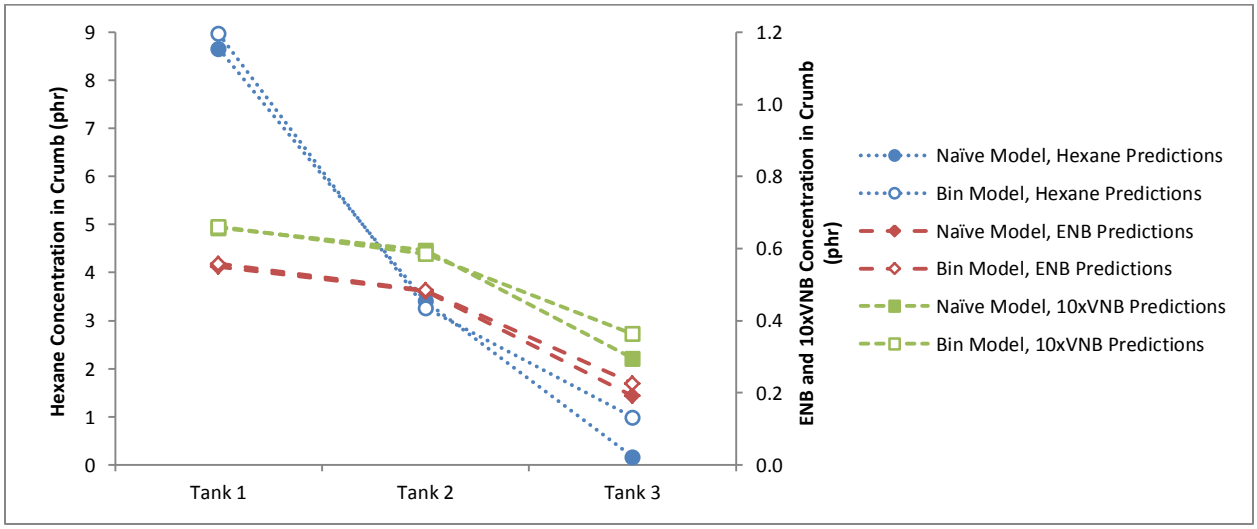

Figure 27: The simulation predictions for hexane, ENB and VNB concentrations in the outlet crumb, using the naïve and equivalent-time models for dataset eight of the three-tank process. Dashed lines are used to guide the eye.

Although the indicated difference between the predictions provided by the naïve and equivalent-time models is quite small, the developed equivalent-time model will provide more accurate predictive information that would be critical for de-bottlenecking analyses or other operational optimization of the stripping section of the production process.

Chapter 6:
Conclusions and Recommendations

The main objective of this research project was achieved; that is, a steady-state mathematical model for the stripping section of an industrial EPDM rubber production process was developed for a three-tank, and two four-tank processes. As a part of the model development, experiments were conducted to determine model parameters such as equivalent radius for EPDM particles, as well as solubility and diffusivity parameters for hexane and ENB in EPDM polymer. First, a single-particle multiple-tank model was developed and second, a process model that accounts for the residence-time distribution of the crumb particles was developed. Data from the plant as well as input data from an existing steady-state model were used to determine estimates for the tuning parameters used in the multiple-particle, multiple-tank model. Finally, the model's predictive accuracy was assessed against plant data.

The final three- and four-tank models satisfy the following criteria:

- The models account for diffusion-limited mass-transfer out of the crumb particles as a function of stripper operating conditions, particle size and EPDM properties.
- The models account for particle residence time distribution in multiple vessels in series with different operating conditions.
- The model equations are sufficiently simple so that they can be solved on-line to provide information for operators and plant engineers.
- The models provide accurate predictions of concentrations of residual solvent and monomers in the rubber particles (crumb) that exit each vessel in a train of three or four stripping vessels.

Specifically, the three-tank model and the four-tank process B model provide accurate model predictions, as indicated by the residual error plots as a function of measured concentrations (Figures 21, 22, and 23) and the typical error value determined to be 0.35 phr and 0.12 phr,

respectively. The four-tank process A model provides less accurate model predictions with a typical error of 1.05 phr; however, provided more data and additional parameter tuning, model predictions would improve.

Although the model equations are sufficiently simple and may be solved online, the amount of time the model requires to converge to a solution could be reduced. To reduce the model run-time, other regression methods could be investigated. Additionally, the models' predictive accuracy could possibly improve via the following recommended model improvements:

- Additional plant datasets from the three- and four-tank processes would increase the estimability of the parameter values for parameter ranking and estimation steps and thus, increase model predictive accuracy.
- Measurements of the residual volatile concentrations in the crumb in the first and second tanks would allow for improved parameter estimates and yield a better fit with measured data. Without volatile concentration data from these tanks, it is impossible to validate or improve the model's predictive accuracy for these preliminary tanks.
- Measurements of the volatile concentrations in the headspace would greatly improve model predictions since $m_{eq,j}$ values would not have to be solved iteratively. Using the measured volatile concentrations would reduce the solution speed of the model and improve model accuracy.
- Improved accuracy of the initial volatile concentrations in the EPDM crumb would result in improved parameter values and improved model predictive ability.
- Additional gravimetric experimentation to estimate the effective radii for other EPDM grades would improve model accuracy and further tuning of effective radii would be more reliable.

References

van Amerongen, G. J. “Diffusion in Elastomers.” *Rubber Chemistry and Technology* **37**, no. 5: 1065-1152, 1964.

Bisio, A. L. & B. R. Tegge. “Ethylene-Propylene Elastomers,” *Encyclopedia of Chemical Processing and Design,* edited by J. J. McKetta, 338-353. New York: Marcel Dekker, 1984.

Carslaw, H. S. & J. C. Jaeger. *Conduction of Heat in Solids*. New York: Oxford University Press, 1959.

Cozewith, C. “Diffusion from Spherical Particles in a Continuous Flow Stirred Tank Train.” *Industrial & Engineering Chemistry Product Research and Development* **33**: 2712-2716, 1994.

Crank, J. *The Mathematics of Diffusion*. Oxford University Press: Cambridge, 1956.

Levenspiel, O. *Chemical Reaction Engineering*. 2nd ed. Toronto: John Wiley & Sons, 1972.

Dean, J. A. “Formulas and Advantages of Rubbers,” *Lange’s Handbook of Chemistry,* 15th ed., 60. New York: McGraw Hill, 1998.

Himmelbau, D. M. & K. B. Bischoff. *Process Analysis and Simulation: Deterministic Systems*. New York: John Wiley and Sons, 1968.

Noordermeer, J. W. M. “Ethylene-propylene Diene Rubber.” *Kirk-Othmer Encyclopedia of Chemical Technology* **10**: 704-719, 2002.

Matthews, F. J., J. R. Fair, J. W. Barlow, D. R. Paul & C. Cozewith. “Solvent Removal from Ethylene-Propylene Elastomers. 1. Determination of Diffusion Mechanism.” *Industrial & Engineering Chemistry Product Research and Development* **25**: 58-64, 1986a.

Matthews, F. J., J. R. Fair, J. W. Barlow, D. R. Paul & C. Cozewith. “Solvent Removal from Ethylene-Propylene Elastomers. 2. Modeling of Continuous-Flow Stripping Vessels.” *Industrial & Engineering Chemistry Product Research and Development* **25**: 65-68, 1986b.

McLean, K. & K. B. McAuley. “Mathematical Modelling of Chemical Processes – Obtaining the Best Model Predictions and Parameter Estimates Using Identifiability and Estimability Procedures.” *The Canadian Journal of Chemical Engineering* **90**, no. 2: 351-366, 2011.

Quadri, G. P. “Purification of Polymers from Solvents by Steam or Gas Stripping.” *Industrial & Engineering Chemistry Product Research and Development* **37**, no. 7: 2850-2863, 1998.

Smith, J. M., H. C. Van Ness & M. M. Abbott. *Introduction to Chemical Engineering Thermodynamics*. McGraw Hill: New York, 2005.

Thompson, D. E., K. B. McAuley & P. J. McLellan. “Parameter Estimation in a Simplified MWD Model for HDPE Produced by a Ziegler-Natta Catalyst”. *Macromolecular Reaction Engineering* **3**, no. 4: 160-177, 2009.

Ver Strate, G. “Coordination Polymerization,” *Concise Encyclopedia of Polymer Science and Engineering*, edited by J. I. Kroschwitz, 359-362. New York: Wiley-Interscience, 1990.

Ver Strate, G. “Ethylene-Propylene Elastomers,” *Encyclopedia of Polymer Science and Engineering,* edited by J. I. Kroschwitz, 523-563. New York: Wiley-Interscience, 1985.

Wu, S., K. McLean, T. J. Harris & K. B. McAuley. “Selection of Optimal Parameter Set Using Estimability Analysis and MSE-based Model Selection Criterion.” *International Journal of Advanced Mechatronic Systems* **3**, no. 3: 188-197, 2011.

Yao, K. Z., B. M. Shaw, B. Kou, K. B. McAuley & D. W. Bacon. “Modeling Ethylene/Butene Copolymerization with Multi-Site Catalysts: Parameter Estimability and Experimental Design.” *Polymer Reaction Engineering* **11**, no. 3, 563-588, 2003.

Yao, K. Z., K. B. McAuley, D. Berg & E. K. Marchildon. “A dynamic mathematical model for continuous solid-phase polymerization of nylon 6,6.” *Chemical Engineering Science* **56**, 4801-4814, 2001.

Appendix A:
Three-Tank Model Preliminary Simulation Results

Shown in Figures 1a to 1m are model predictions and measured data for $\overline{m}_{j,i}$ values from the three-tank process for 13 industrial data sets. Figure 11 in Chapter 4 provides information about the 14th data set. The model predictions shown were determined using the initial parameter values in Table 1 and R = 1.3551 x 10^{-3} m. Dashed lines are used to guide the eye.

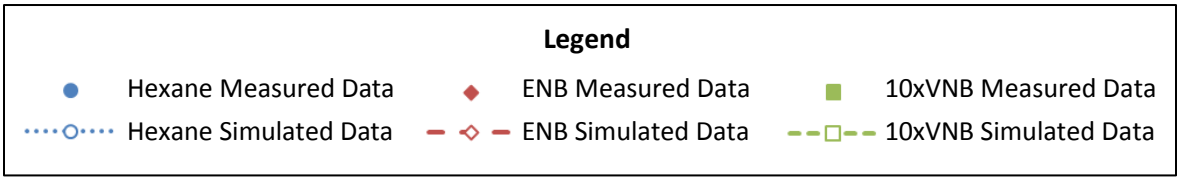

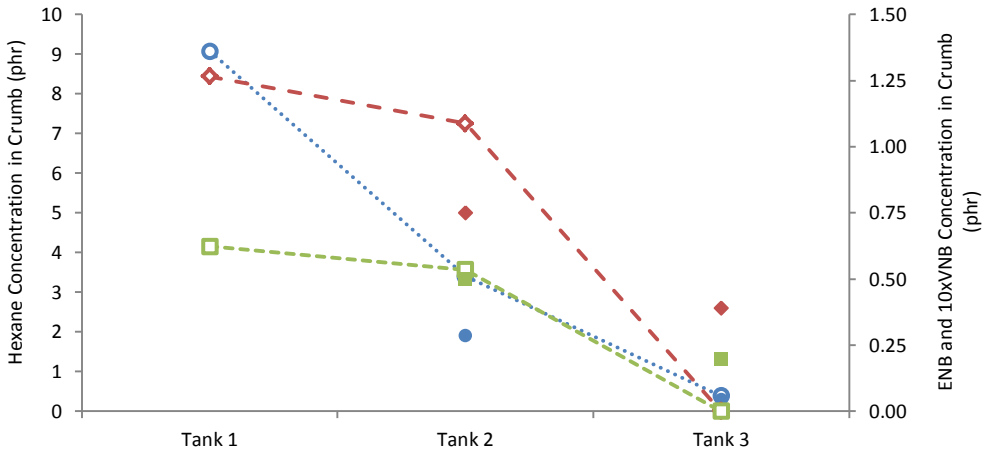

Figure 1a: Model predictions and measured results for data set 2

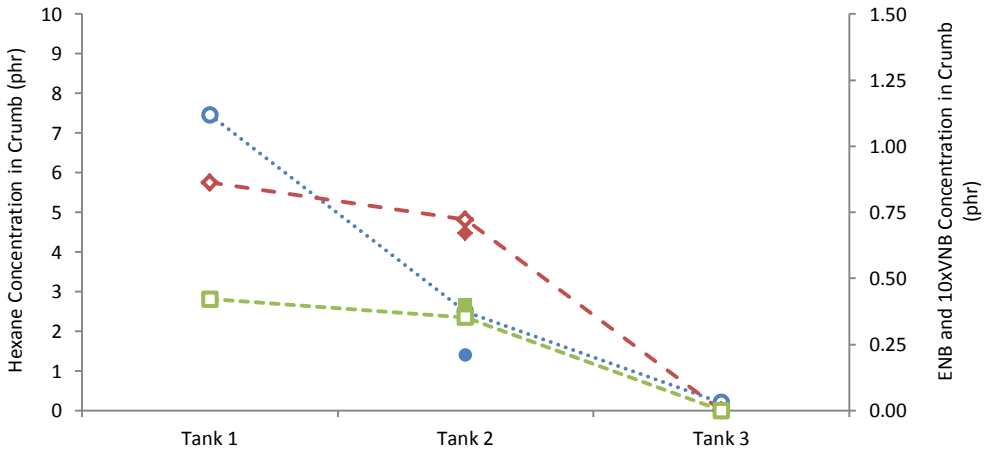

Figure 1b: Model predictions and measured results for data set 3

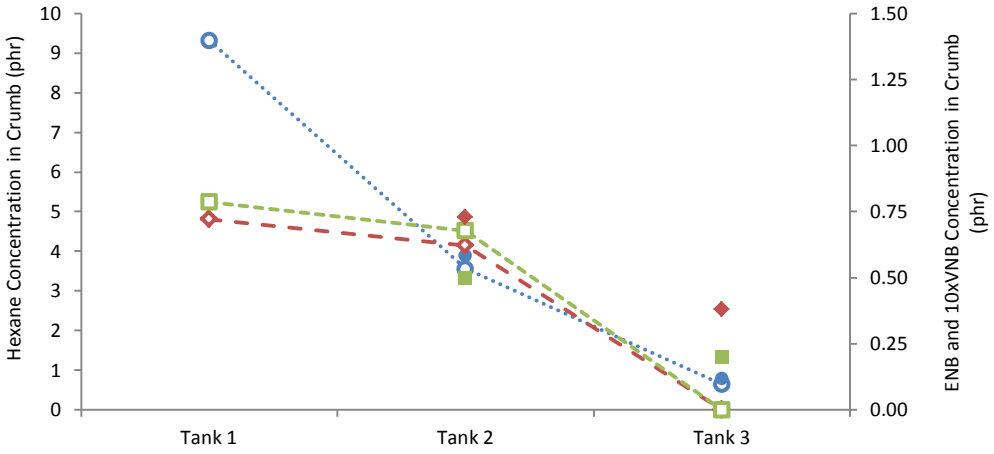

Figure 1c: Model predictions and measured results for data set 4

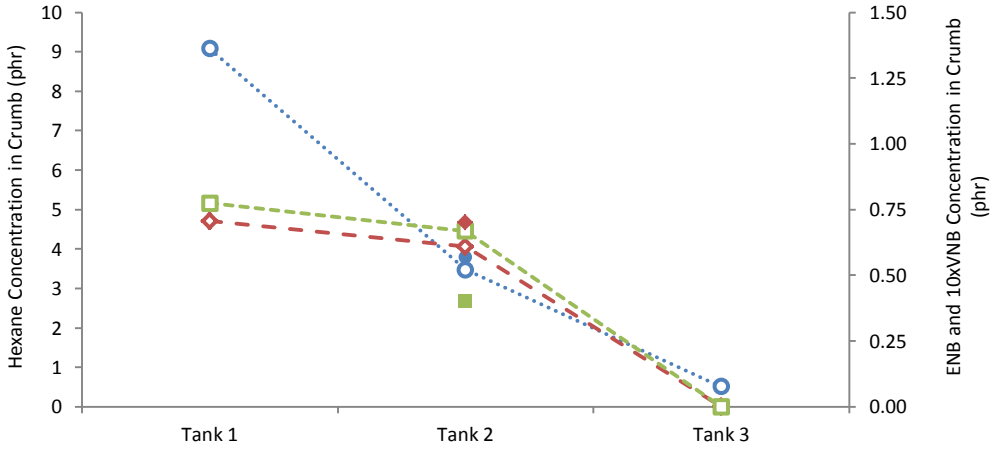

Figure 1d: Model predictions and measured results for data set 5

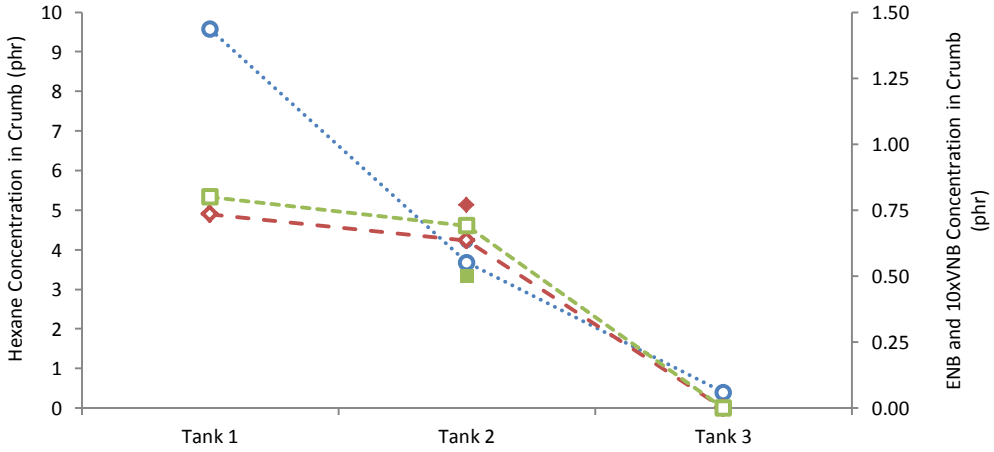

Figure 1e: Model predictions and measured results for data set 6

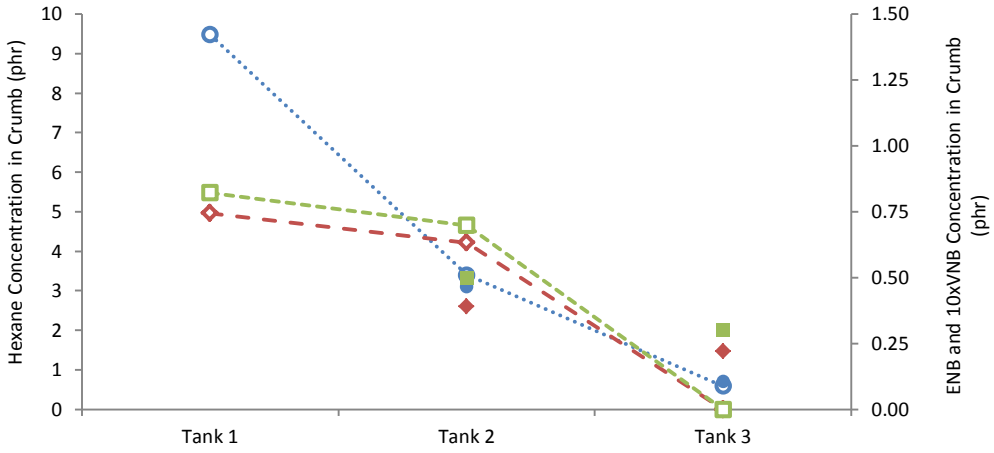

Figure 1f: Model predictions and measured results for data set 7

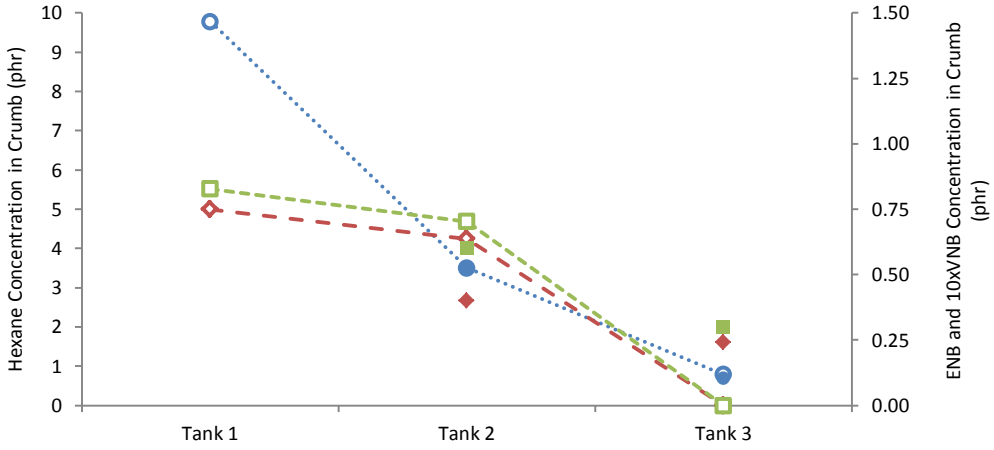

Figure 1g: Model predictions and measured results for data set 8

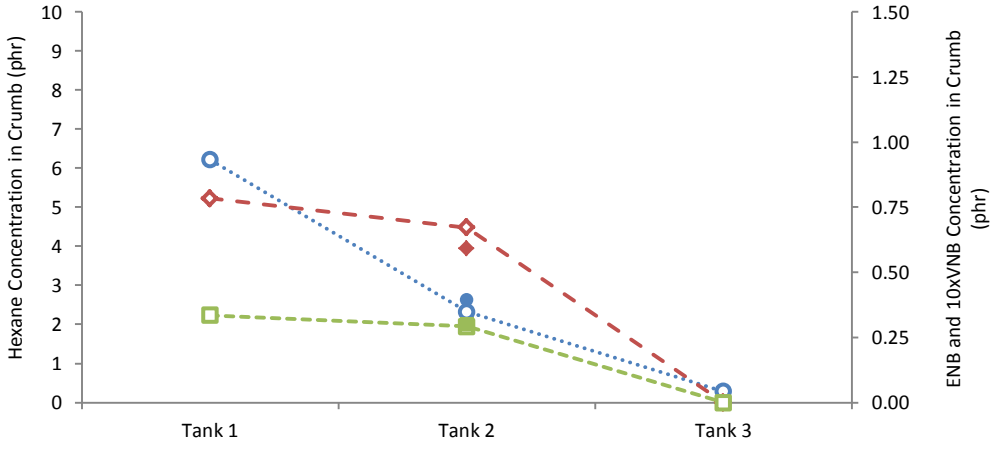

Figure 1h: Model predictions and measured results for data set 9

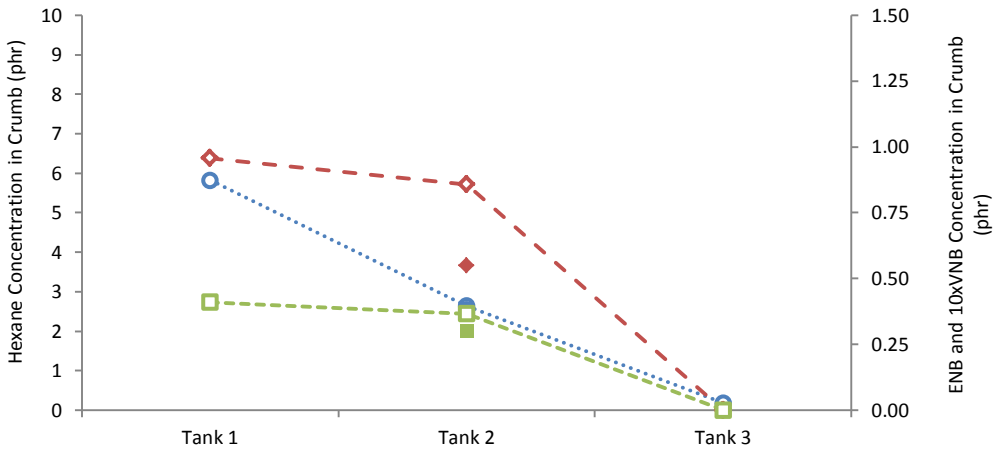

Figure 1i: Model predictions and measured results for data set 10

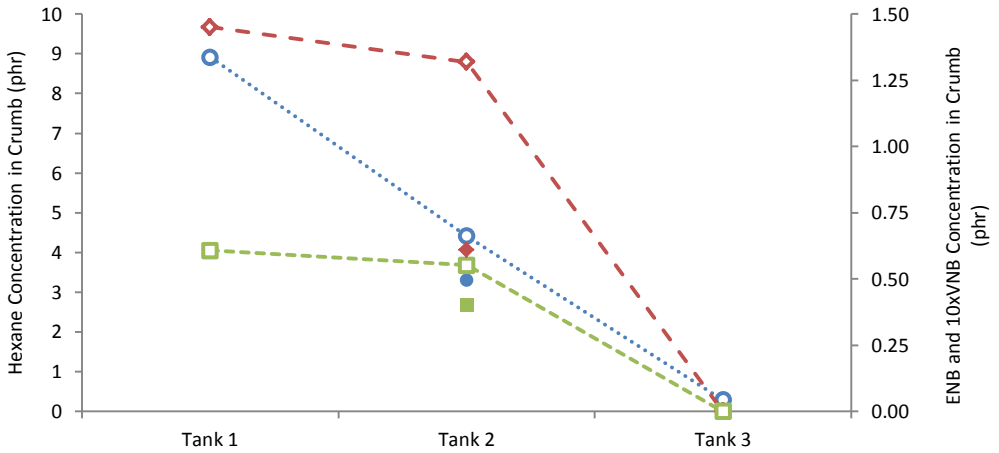

Figure 1j: Model predictions and measured results for data set 11

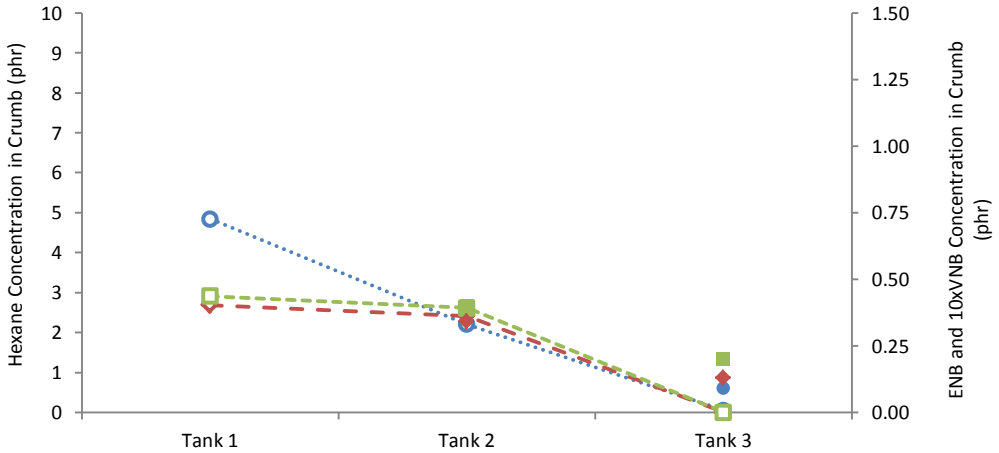

Figure 1k: Model predictions and measured results for data set 12

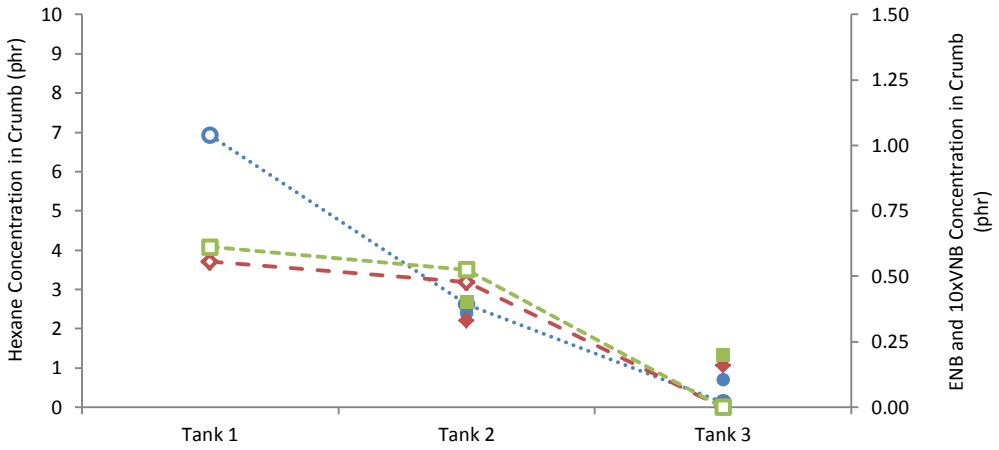

Figure 1l: Model predictions and measured results for data set 13

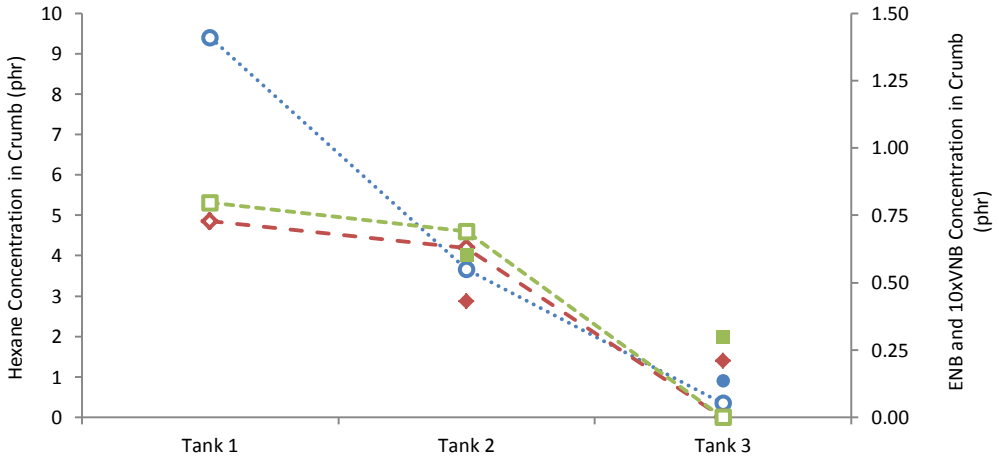

Figure 1m: Model predictions and measured results for data set 14

Appendix B:
Three-Tank Model Simulation Results after Preliminary Parameter Tuning

Shown in Figures 2a to 2m are model predictions and measured data for $\overline{m}_{j,i}$ values from the three-tank process for 13 industrial data sets. Figure 13 in Chapter 5 provides information about the 14th data set. The model predictions shown were determined using initial parameter values in Table 14 and the seven updated tuning parameters in Table 17. Dashed lines are used to guide the eye.

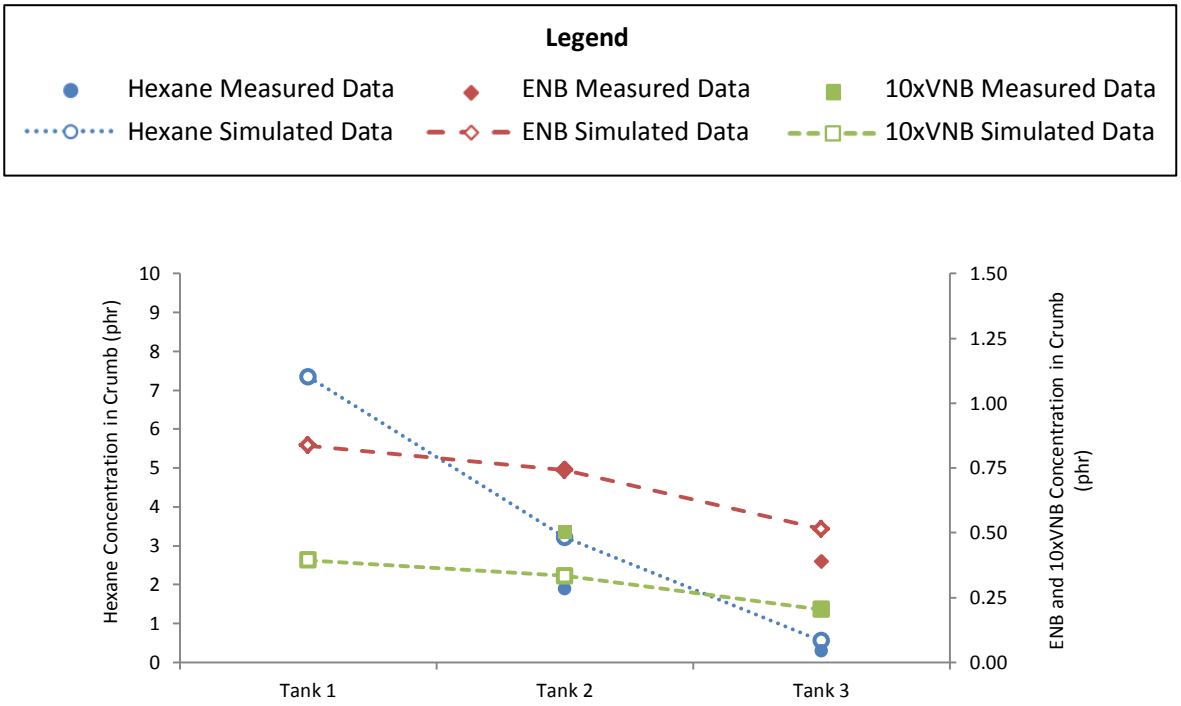

Figure 2a: Updated model predictions and measured results for data set 2

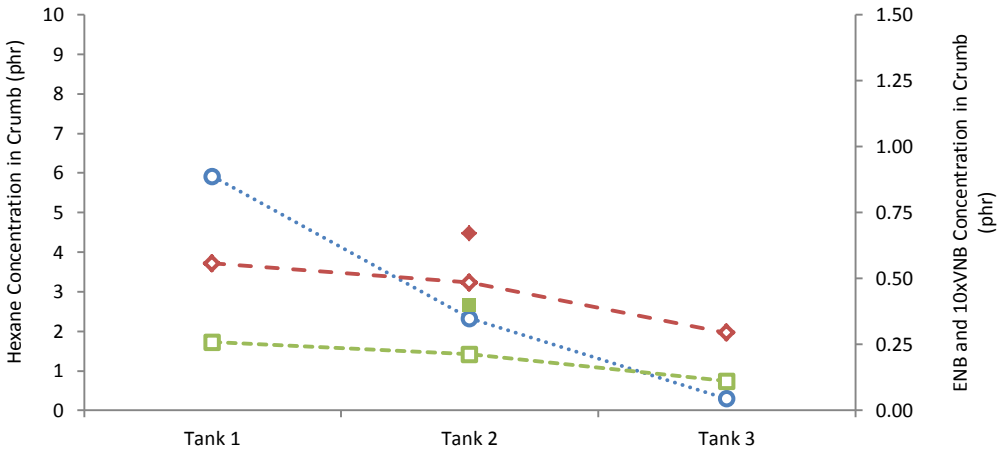

Figure 2b: Updated model predictions and measured results for data set 3

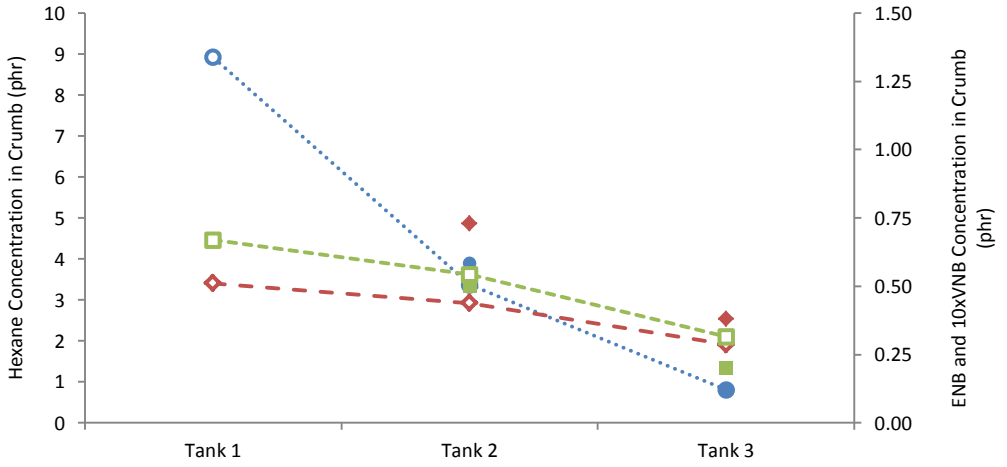

Figure 2c: Updated model predictions and measured results for data set 4

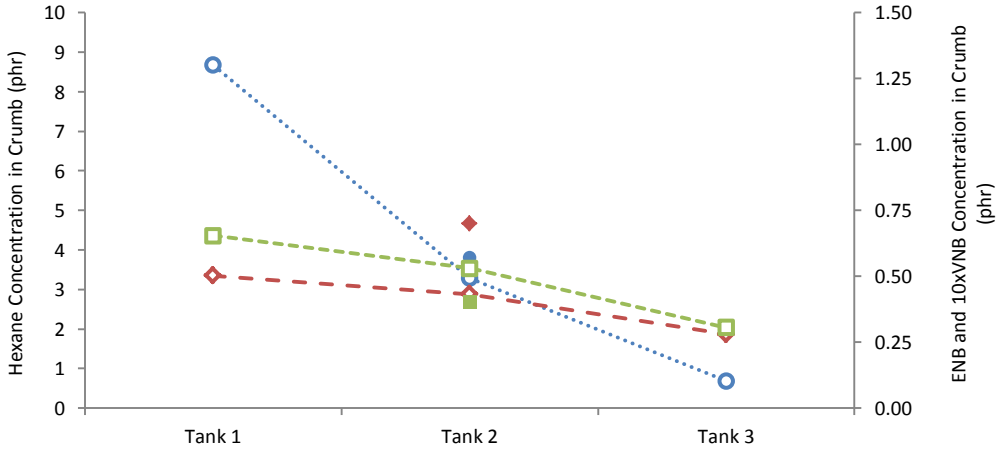

Figure 2d: Updated model predictions and measured results for data set 5

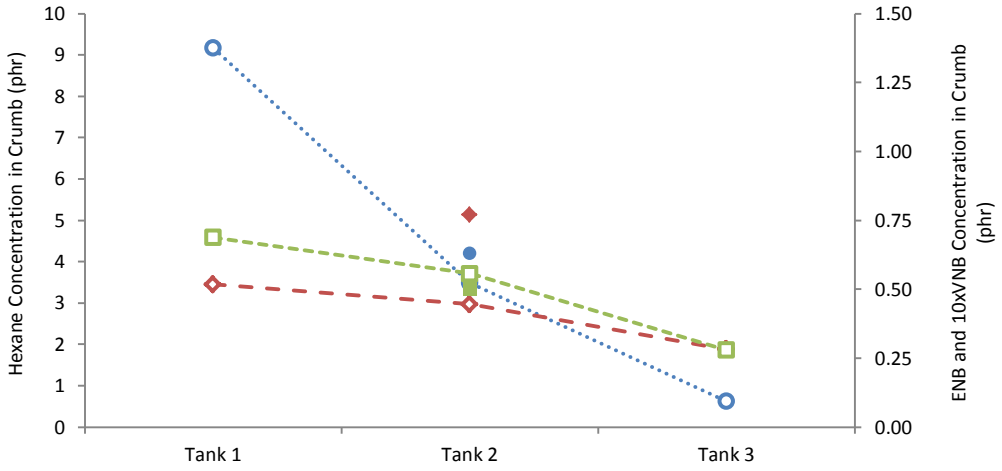

Figure 2e: Updated model predictions and measured results for data set 6

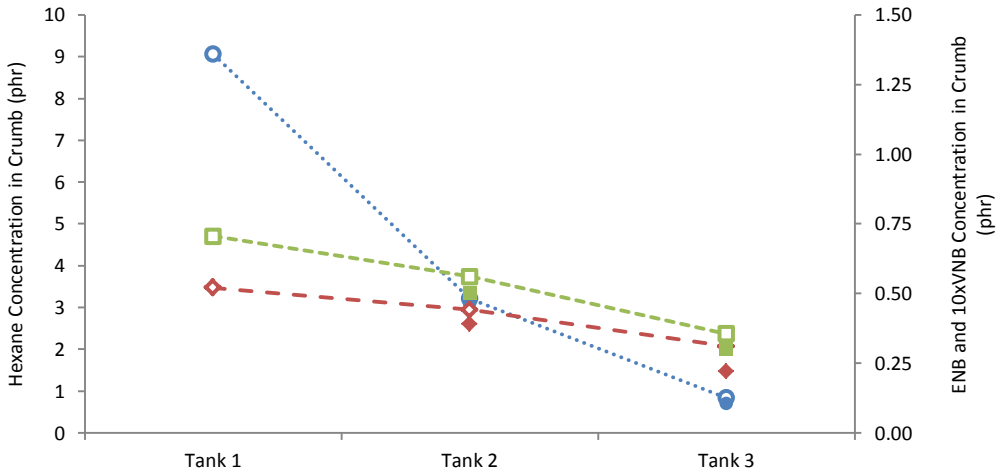

Figure 2f: Updated model predictions and measured results for data set 7

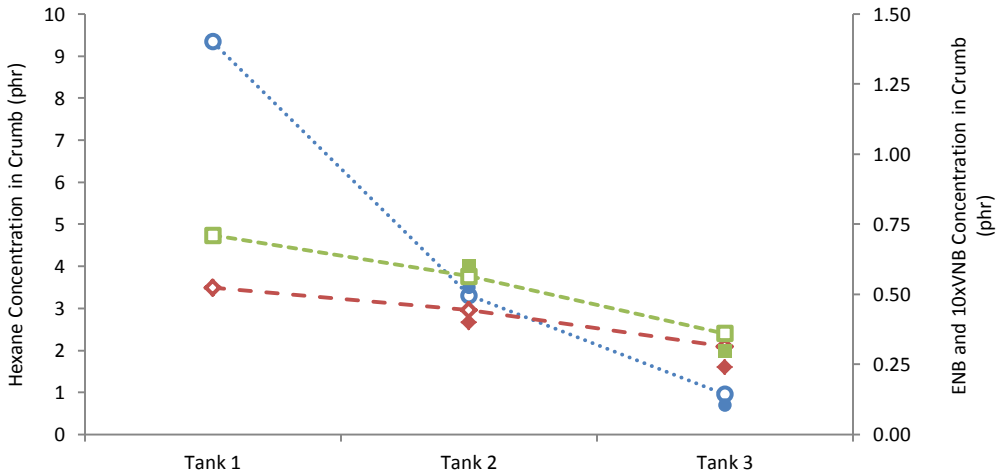

Figure 2g: Updated model predictions and measured results for data set 8

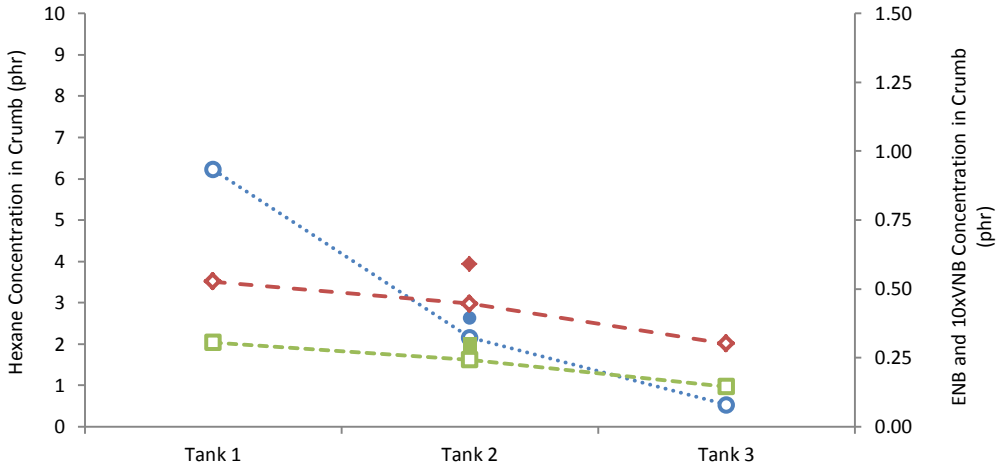

Figure 2h: Updated model predictions and measured results for data set 9

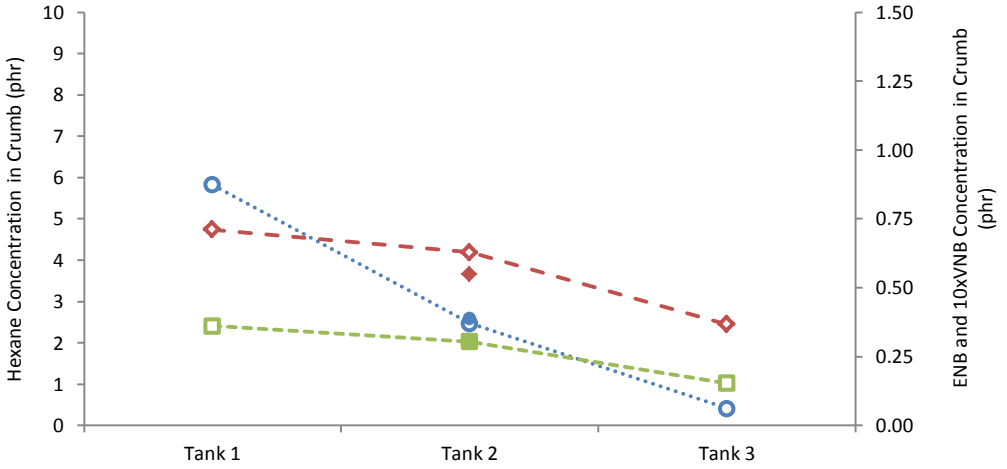

Figure 2i: Updated model predictions and measured results for data set 10

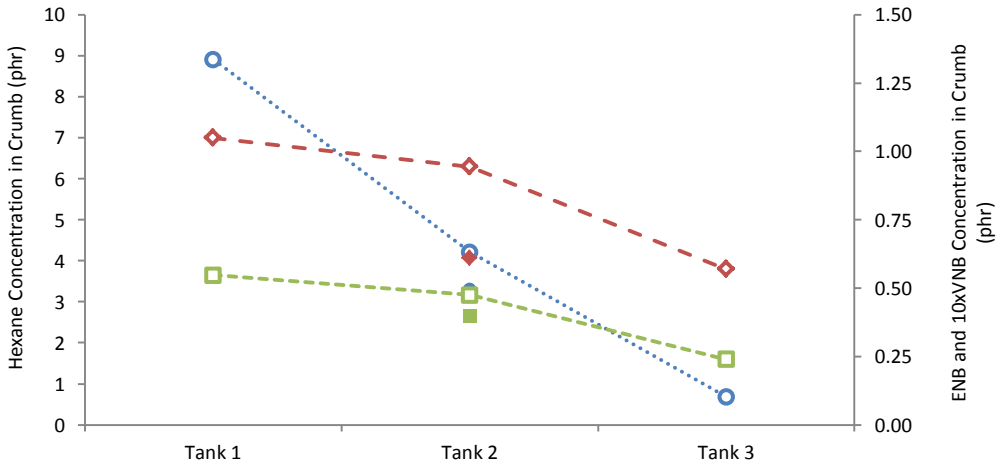

Figure 2j: Updated model predictions and measured results for data set 11

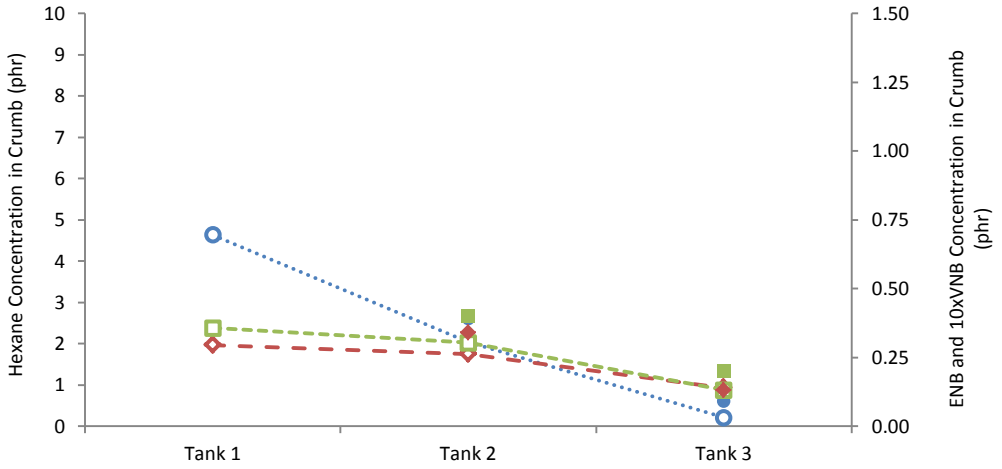

Figure 2k: Updated model predictions and measured results for data set 12

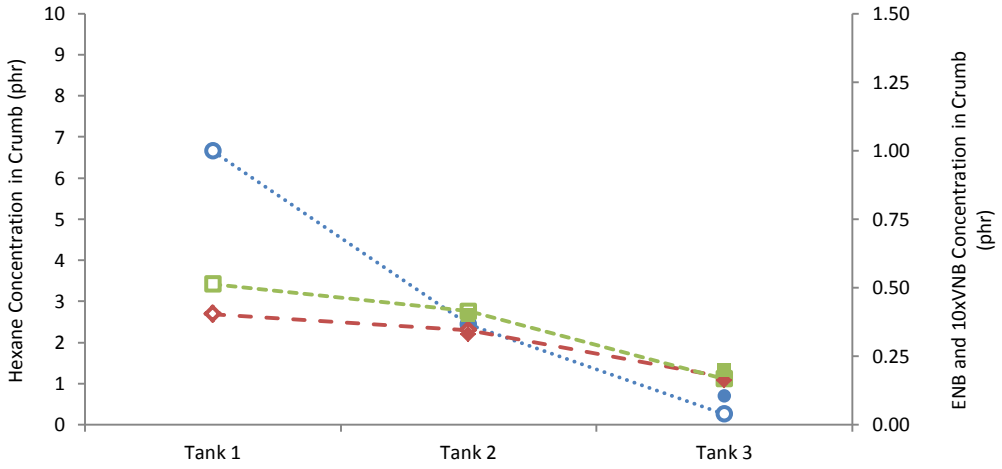

Figure 2l: Updated model predictions and measured results for data set 13

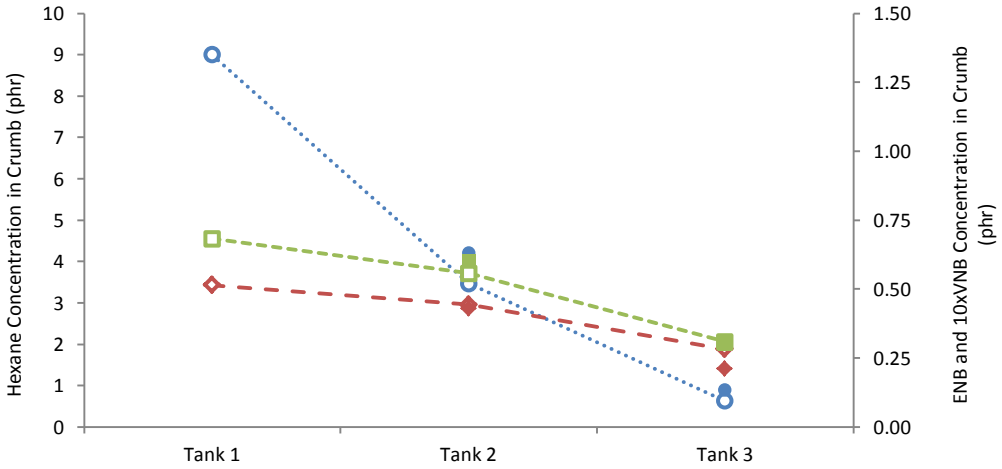

Figure 2m: Updated model predictions and measured results for data set 14

Appendix C:
Three-Tank Model Preliminary Parameter Tuning Residuals

Shown in Figures 3a to 20c are residuals from the predicted and measured $\bar{m}_{j,i}$ values versus the input variables used in the three-tank process for all 14 industrial data sets. The model predictions were determined using the initial parameter values in Table 14 and seven updated tuning parameters in Table 17. Possible trends are discussed following part c of each figure.

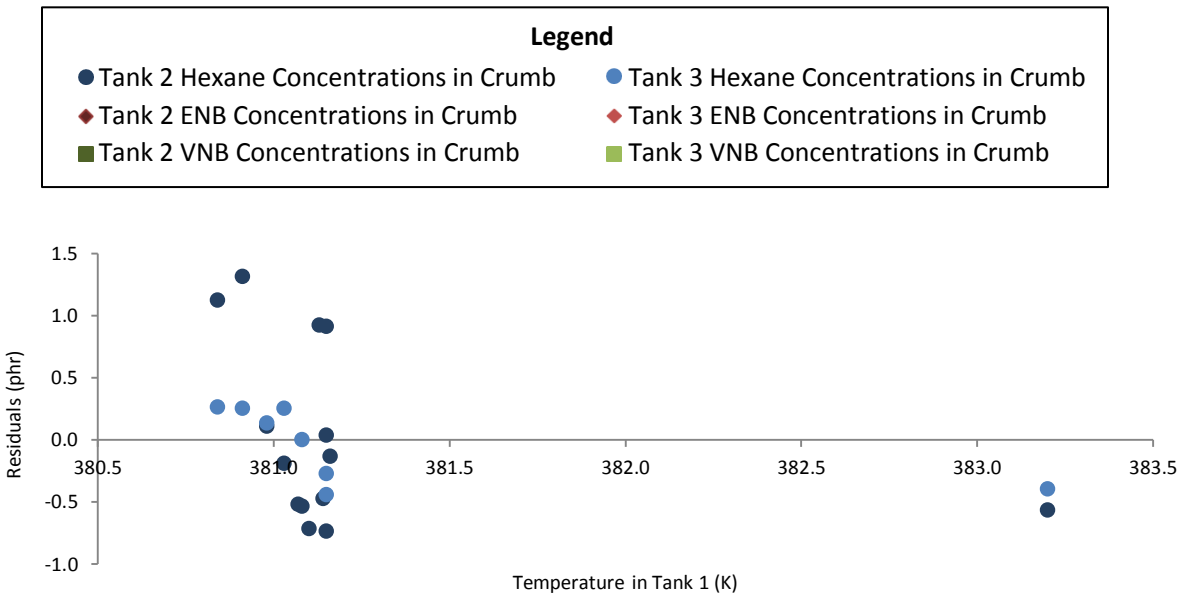

Figure 3a: $\bar{m}_{C6,i}$ residuals for the three-tank process as a function of temperature in tank 1

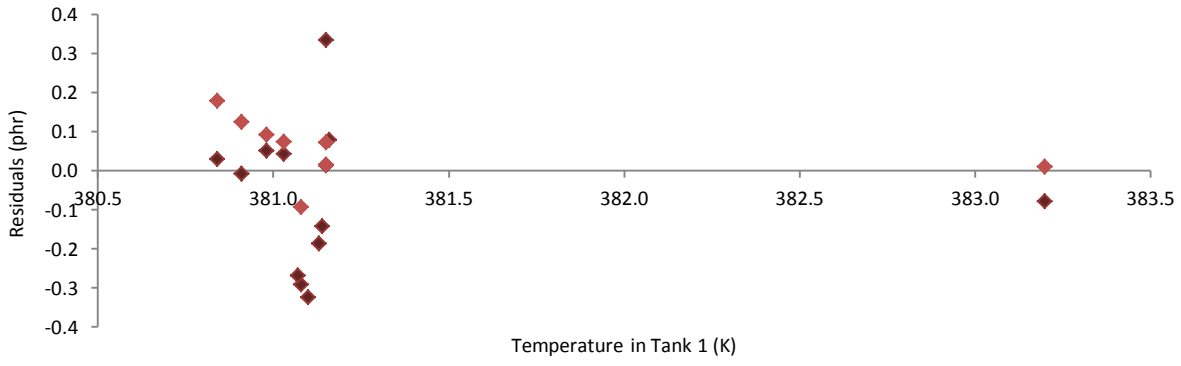

Figure 3b: $\bar{m}_{ENB,i}$ residuals for the three-tank process as a function of temperature in tank 1

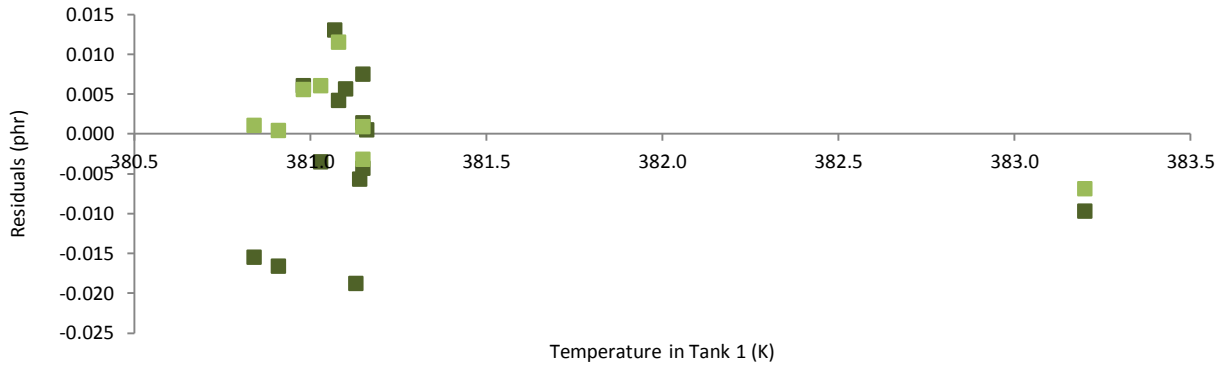

Figure 3c: $\bar{m}_{VNB,i}$ residuals for the three-tank process as a function of temperature in tank 1

No trends were observed in the $\bar{m}_{j,i}$ residuals as a function of the temperature in tank 1.

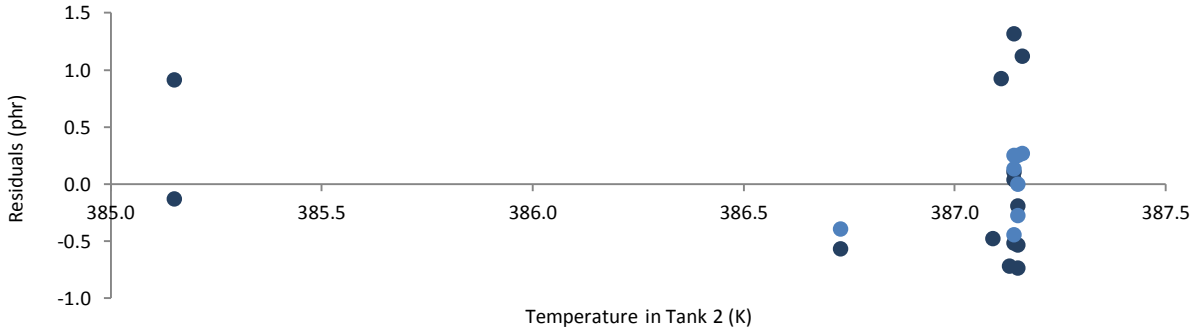

Figure 4a: $\bar{m}_{C6,i}$ residuals for the three-tank process as a function of temperature in tank 2

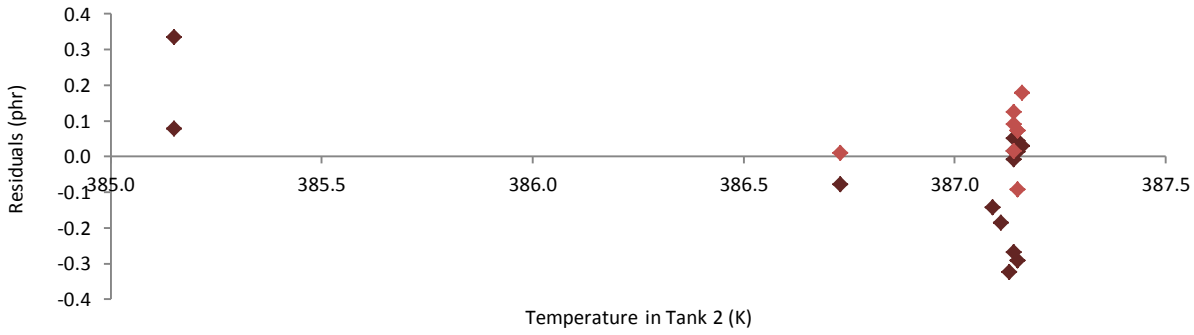

Figure 4b: $\bar{m}_{ENB,i}$ residuals for the three-tank process as a function of temperature in tank 2

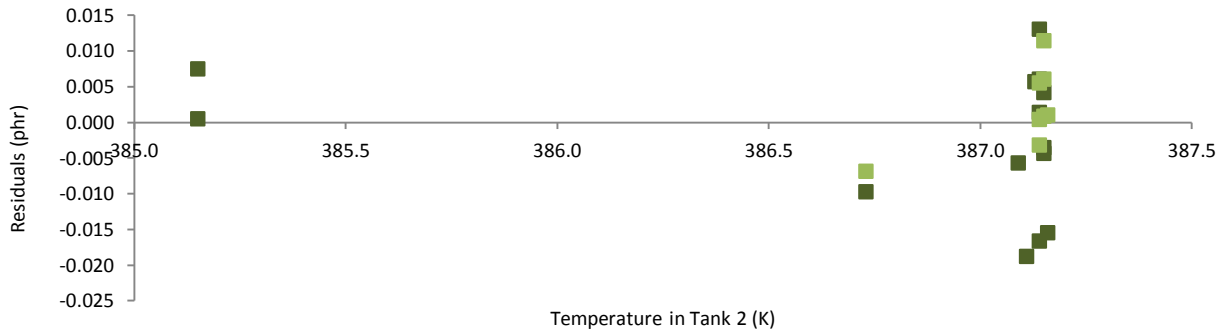

Figure 4c: $\bar{m}_{VNB,i}$ residuals for the three-tank process as a function of temperature in tank 2

At lower temperatures in tank 2, predicted $\bar{m}_{ENB,2}$ values may be too low (see Figure 4b). Perhaps the temperature effect for ENB solubility and/or diffusivity is too strong in the model, causing the $\bar{m}_{ENB,2}$ predictions to be too low. More data from the four-tank process will provide more information on this possible trend; therefore, no modifications will be made to the three-tank model at this stage. No trends were observed in the $\bar{m}_{C6,i}$, $\bar{m}_{ENB,3}$, and $\bar{m}_{VNB,i}$ residuals as a function of the temperature in tank 2.

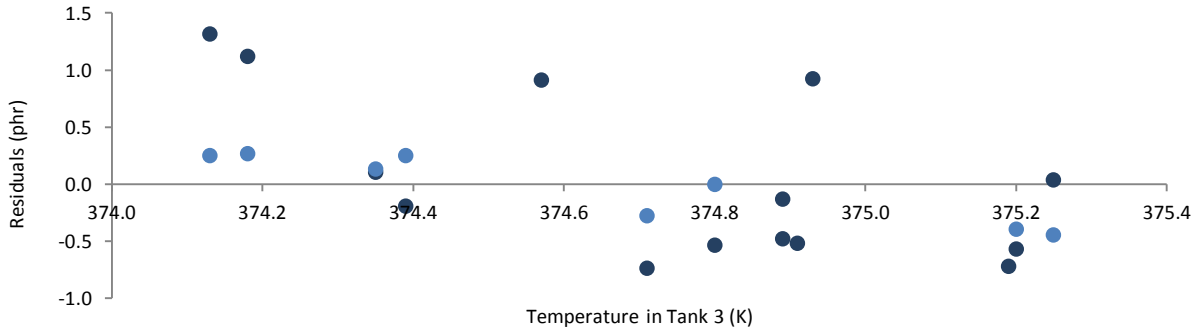

Figure 5a: $\bar{m}_{C6,i}$ residuals for the three-tank process as a function of temperature in tank 3

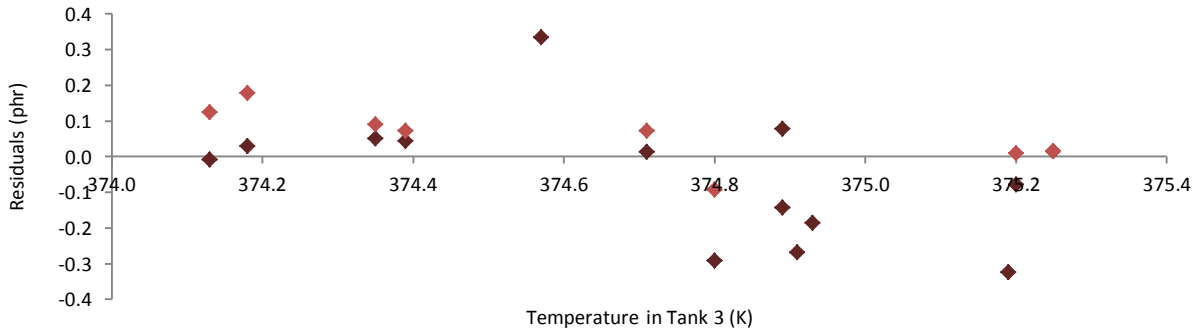

Figure 5b: $\bar{m}_{ENB,i}$ residuals for the three-tank process as a function of temperature in tank 3

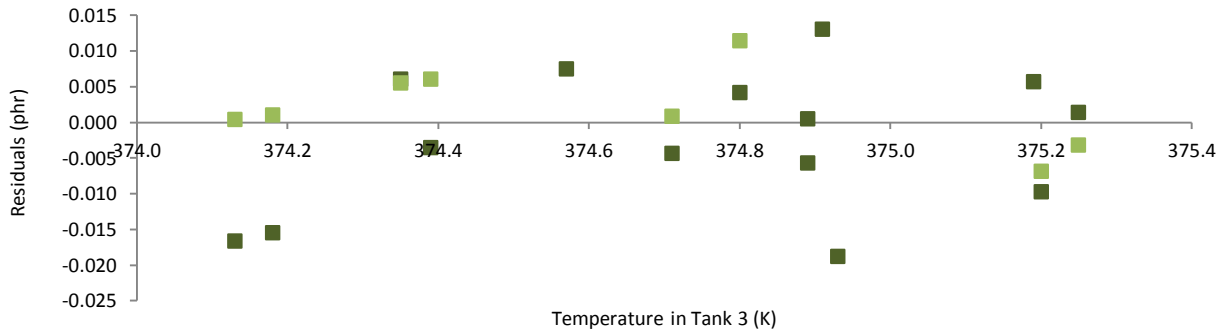

Figure 5c: $\bar{m}_{VNB,i}$ residuals for the three-tank process as a function of temperature in tank 3

No trends were observed in the $\bar{m}_{j,i}$ residuals as a function of the temperature in tank 3.

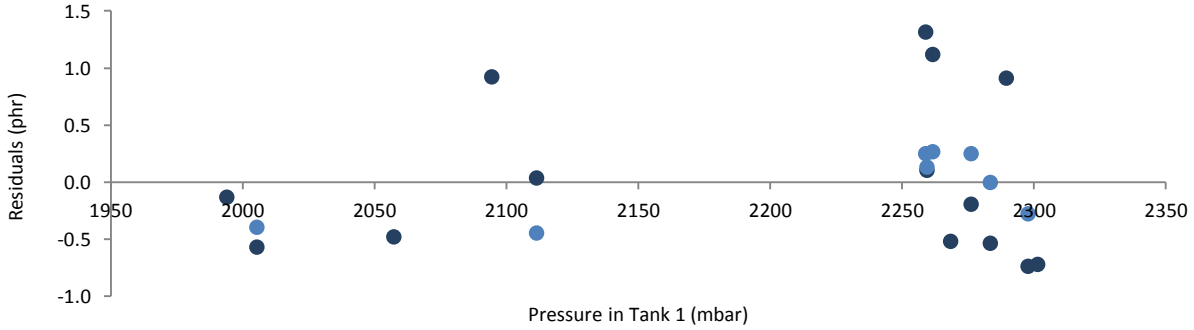

Figure 6a: $\bar{m}_{C6,i}$ residuals for the three-tank process as a function of pressure in tank 1

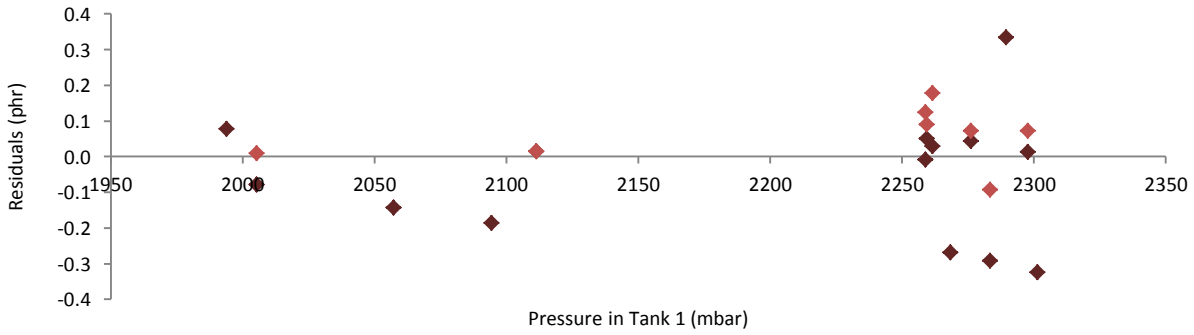

Figure 6b: $\bar{m}_{ENB,i}$ residuals for the three-tank process as a function of pressure in tank 1

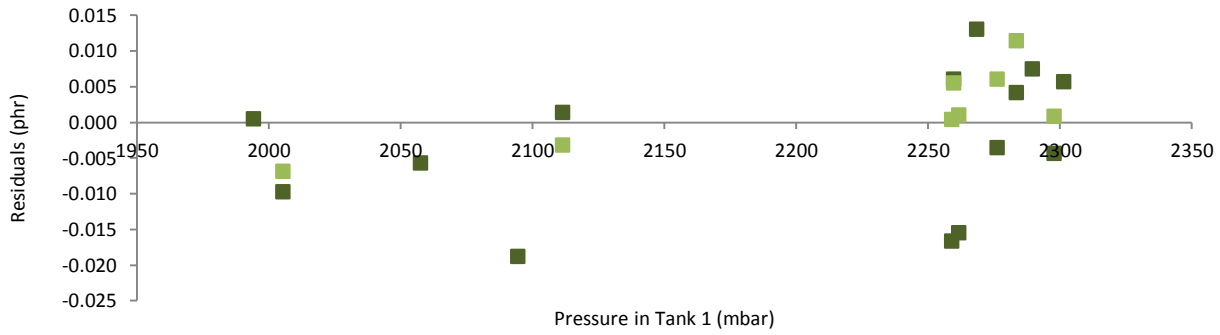

Figure 6c: $\bar{m}_{VNB,i}$ residuals for the three-tank process as a function of pressure in tank 1

At high pressures in tank 1, predicted $\bar{m}_{VNB,3}$ values may be too high (see Figure 6c). Perhaps the pressure in tank 1 needs to be lower in order to lower the $y_{VNB,1}$ and to increase the diffusion of VNB out of the crumb. More data from the four-tank process will provide more information on this possible trend; therefore, no modifications will be made to the three-tank model at this stage but the four-tank residuals as a function of pressure in tank 1 will be thoroughly analysed. No trends were observed in the $\bar{m}_{C6,i}$, $\bar{m}_{ENB,i}$, and $\bar{m}_{VNB,2}$ residuals as a function of the pressure in tank 1.

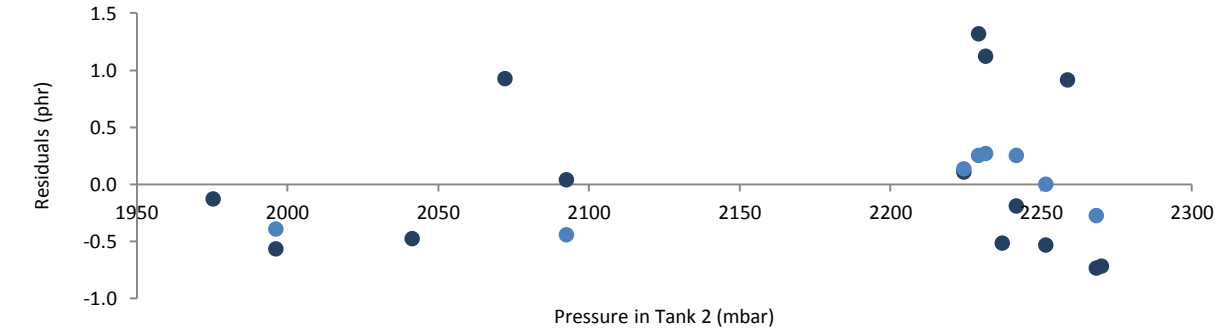

Figure 7a: $\bar{m}_{C6,i}$ residuals for the three-tank process as a function of pressure in tank 2

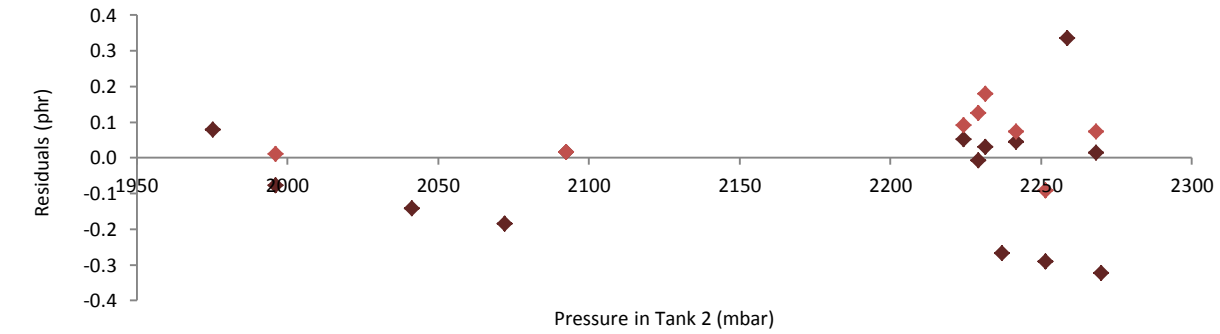

Figure 7b: $\bar{m}_{ENB,i}$ residuals for the three-tank process as a function of pressure in tank 2

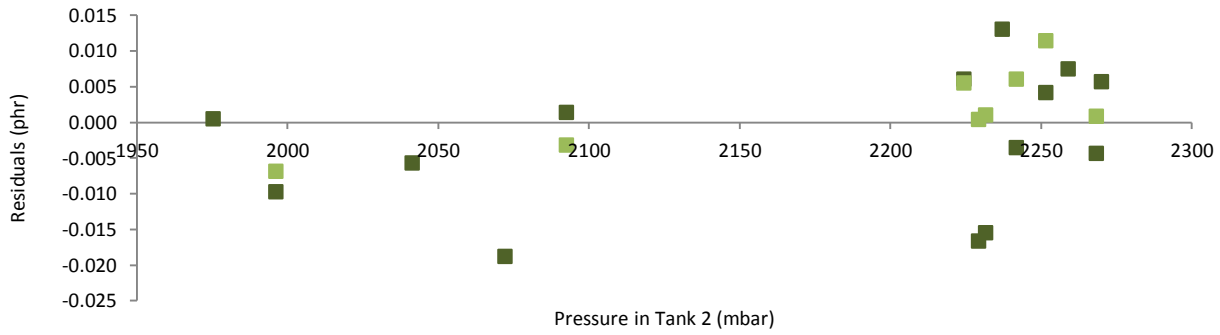

Figure 7c: $\bar{m}_{VNB,i}$ residuals for the three-tank process as a function of pressure in tank 2

At high pressures in tank 2, predicted $\bar{m}_{VNB,3}$ values may be too high (see Figure 7c). Perhaps the pressure in tank 2 needs to be lower in order to lower the $y_{VNB,1}$ and to increase the diffusion of VNB out of the crumb. More data from the four-tank process will provide more information on this possible trend; therefore, no modifications will be made to the three-tank model at this stage but the four-tank residuals as a function of pressure in tank 1 will be thoroughly analysed. No trends were observed in the $\bar{m}_{C6,i}$, $\bar{m}_{ENB,i}$, and $\bar{m}_{VNB,2}$ residuals as a function of the pressure in tank 2.

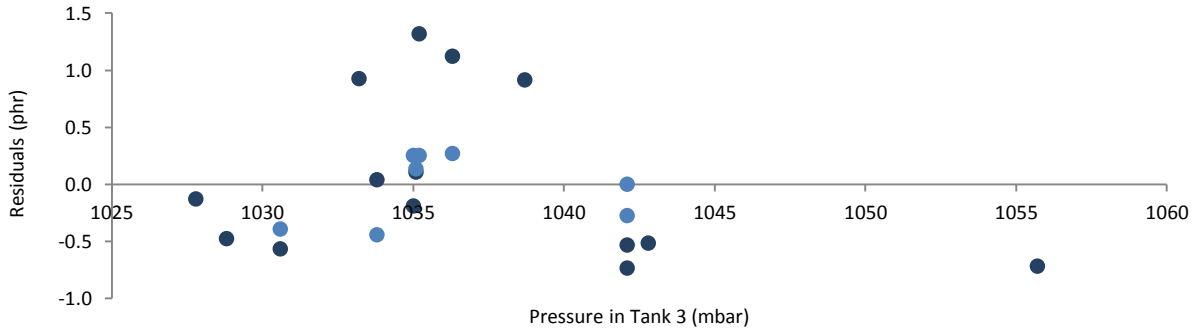

Figure 8a: $\bar{m}_{C6,i}$ residuals for the three-tank process as a function of pressure in tank 3

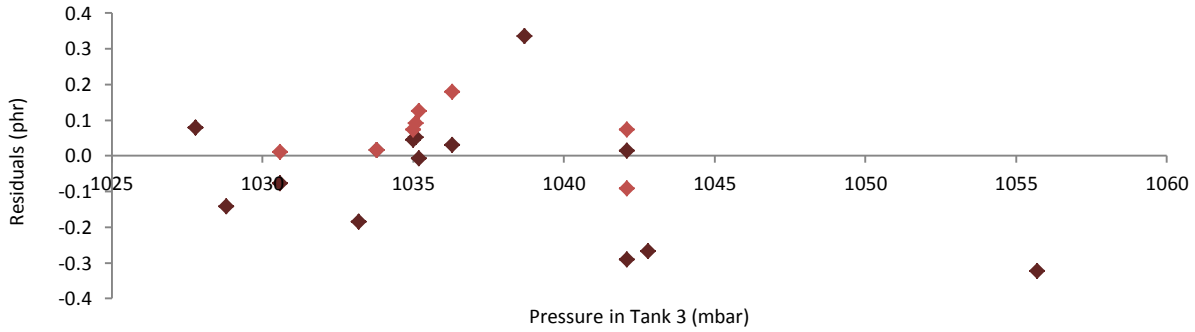

Figure 8b: $\bar{m}_{ENB,i}$ residuals for the three-tank process as a function of pressure in tank 3

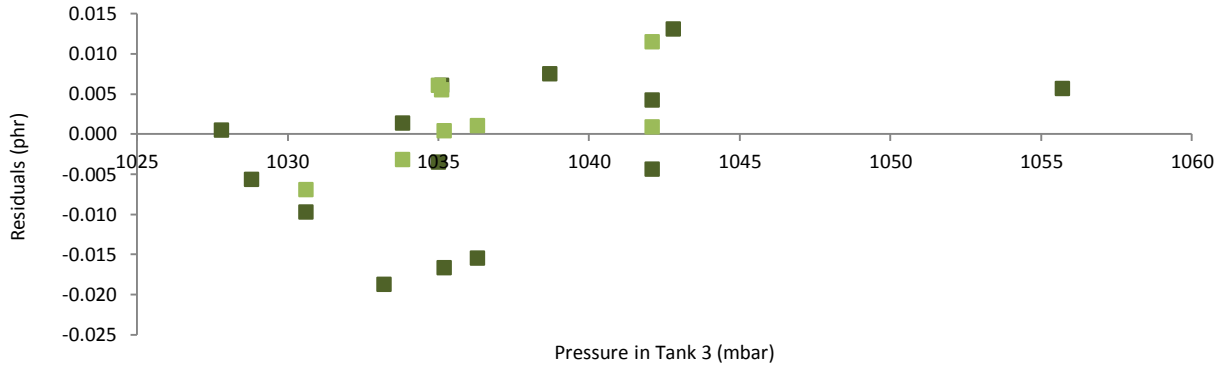

Figure 8c: $\bar{m}_{VNB,i}$ residuals for the three-tank process as a function of pressure in tank 3

No trends were observed in the $\bar{m}_{j,i}$ residuals as a function of the pressure in tank 3.

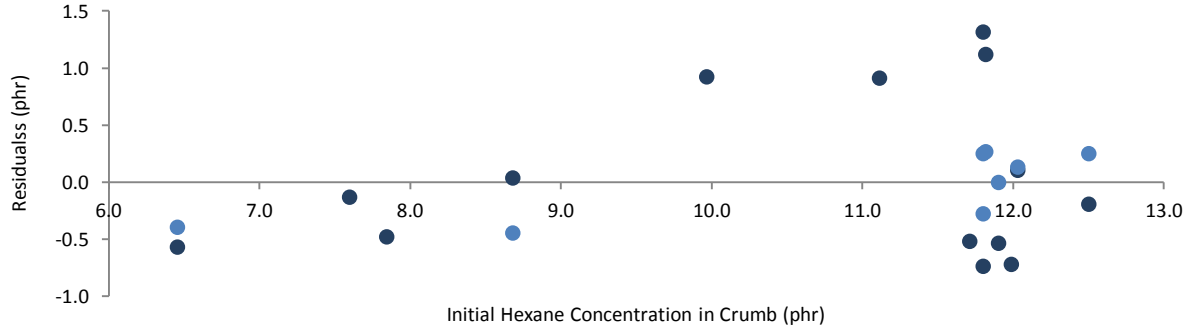

Figure 9a: $\bar{m}_{C6,i}$ residuals for the three-tank process as a function of the initial hexane concentration in the crumb

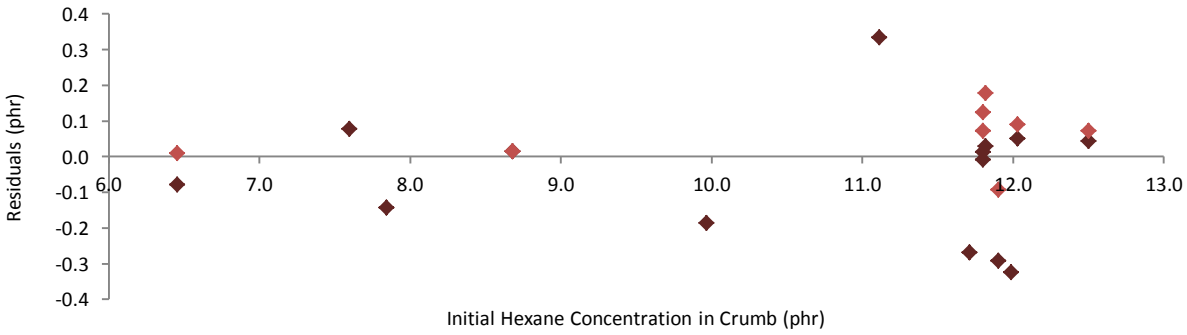

Figure 9b: $\bar{m}_{ENB,i}$ residuals for the three-tank process as a function of the initial hexane concentration in the crumb

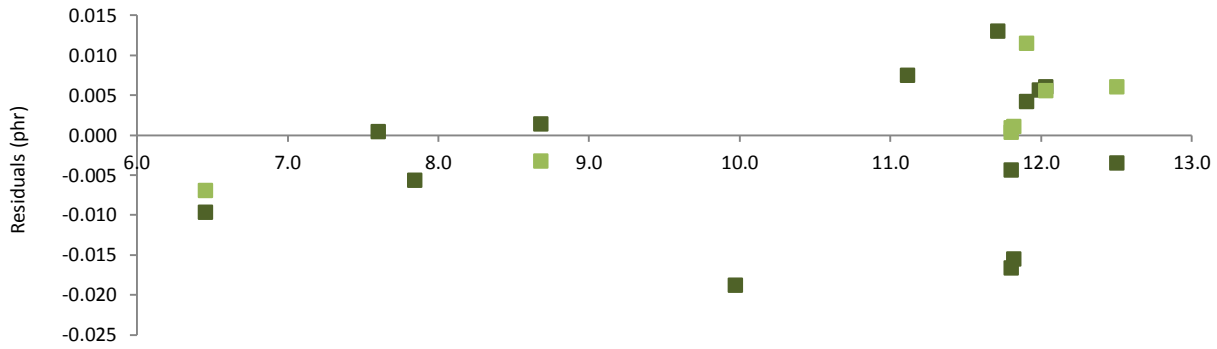

Figure 9c: $\bar{m}_{VNB,i}$ residuals for the three-tank process as a function of the initial hexane concentration in the crumb

No trends were observed in the $\bar{m}_{j,i}$ residuals as a function of the initial hexane concentration in the crumb.

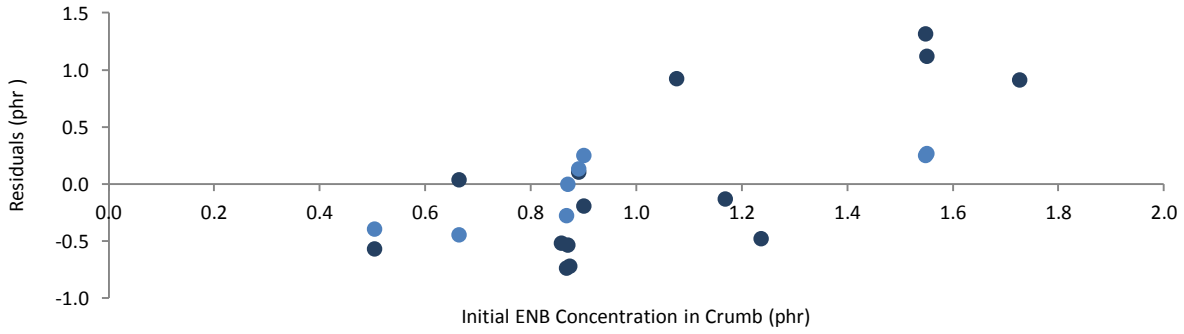

Figure 10a: $\bar{m}_{C6,i}$ residuals for the three-tank process as a function of the initial ENB concentration in the crumb

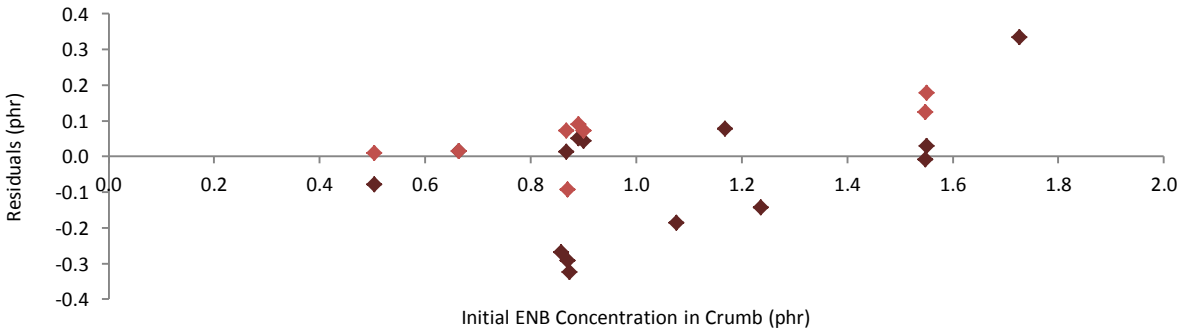

Figure 10b: $\bar{m}_{ENB,i}$ residuals for the three-tank process as a function of the initial ENB concentration in the crumb

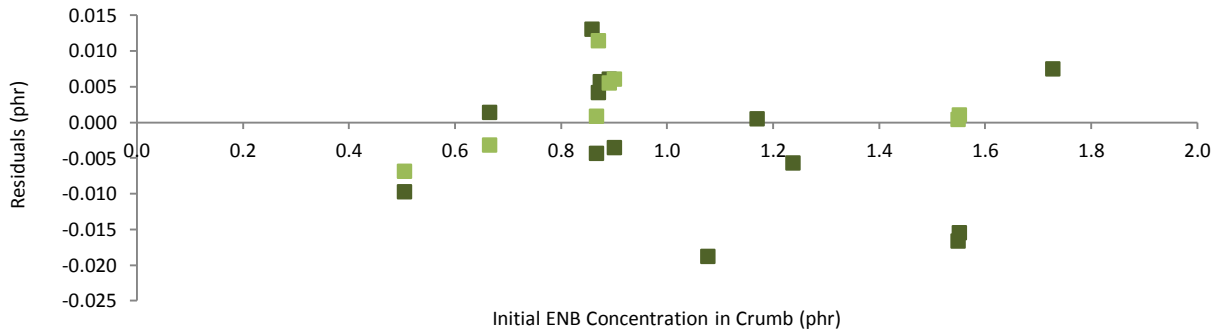

Figure 10c: $\bar{m}_{VNB,i}$ residuals for the three-tank process as a function of the initial ENB concentration in the crumb

At high values of $m_{ENB,0}$, predicted $\bar{m}_{C6,2}$ values may be too high (see Figure 10a). No corrective action can be made for this trend since there is no obvious cause and effect for this relationship. No trends were observed in the $\bar{m}_{C6,3}$, $\bar{m}_{ENB,i}$, and $\bar{m}_{VNB,i}$ residuals as a function of $m_{ENB,0}$ values.

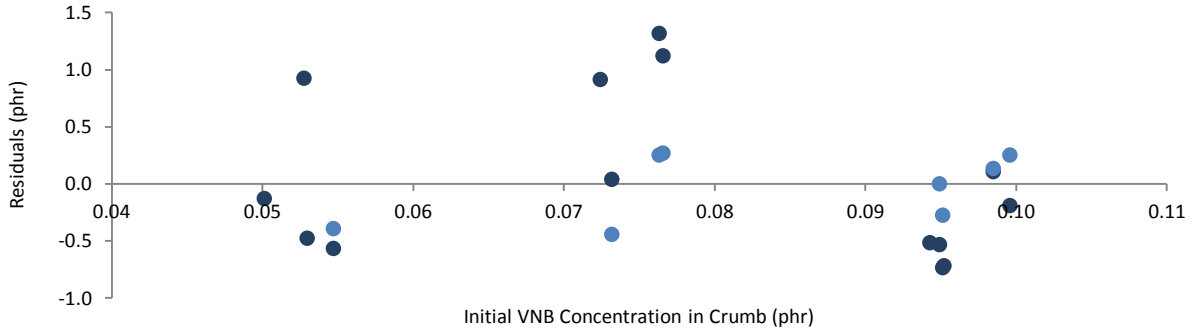

Figure 11a: $\bar{m}_{C6,i}$ residuals for the three-tank process as a function of the initial VNB concentration in the crumb

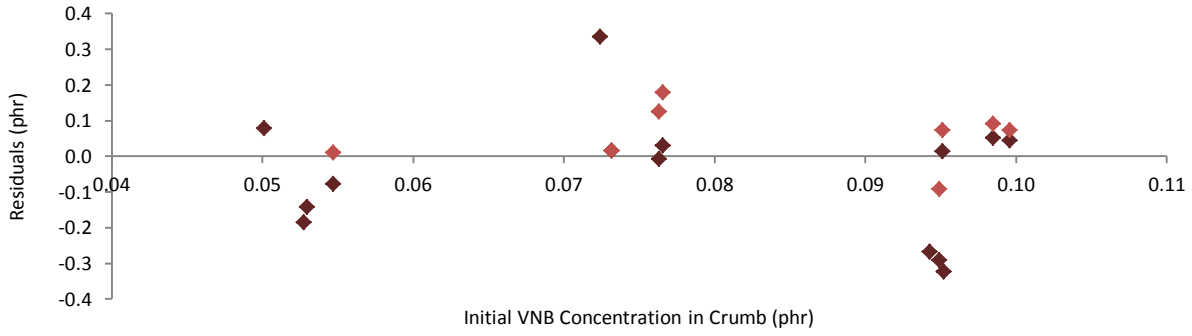

Figure 11b: $\bar{m}_{ENB,i}$ residuals for the three-tank process as a function of the initial VNB concentration in the crumb

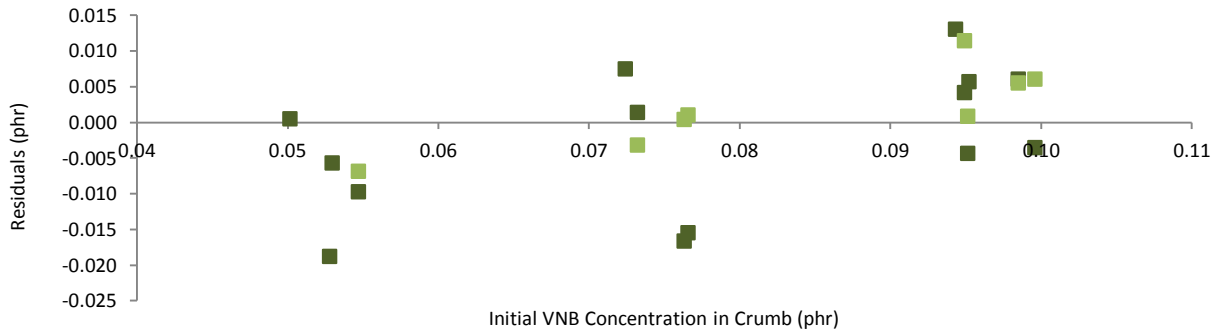

Figure 11c: $\bar{m}_{VNB,i}$ residuals for the three-tank process as a function of the initial VNB concentration in the crumb

At high values of $m_{VNB,0}$, both the predicted $\bar{m}_{VNB,2}$ and $\bar{m}_{VNB,3}$ values may be too high (see Figure 11c). Perhaps the VNB solubility and/or diffusivity are too small in the model. More data from the four-tank process will provide more information on this possible trend; therefore, no modifications will be made to the three-tank model at this stage. No trends were observed in the $\bar{m}_{C6,i}$ and $\bar{m}_{ENB,i}$ residuals as a function of $m_{VNB,0}$ values.

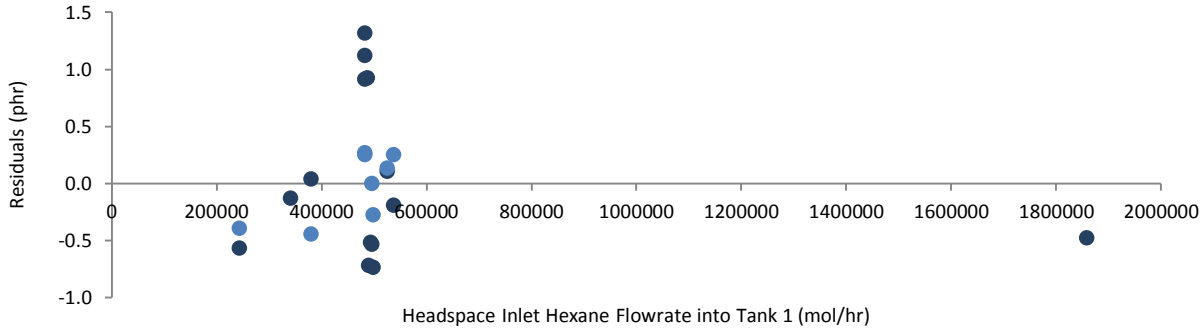

Figure 12a: $\bar{m}_{C6,i}$ residuals for the three-tank process as a function of the headspace inlet hexane flowrate into tank 1

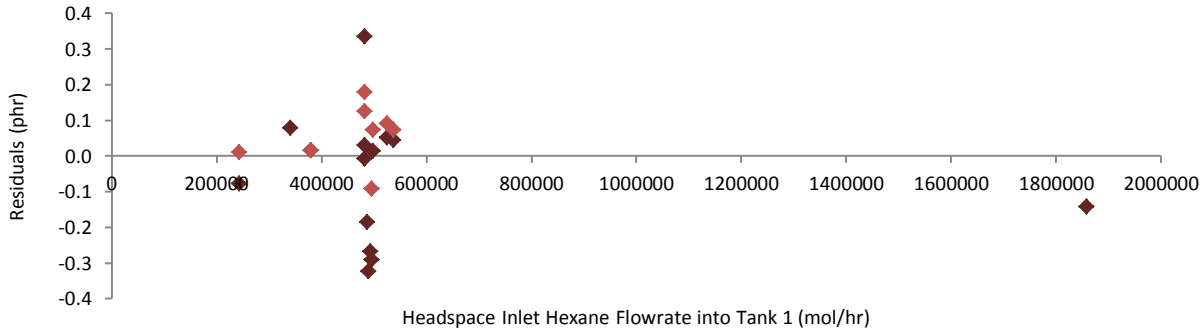

Figure 12b: $\bar{m}_{ENB,i}$ residuals for the three-tank process as a function of the headspace inlet hexane flowrate into tank 1

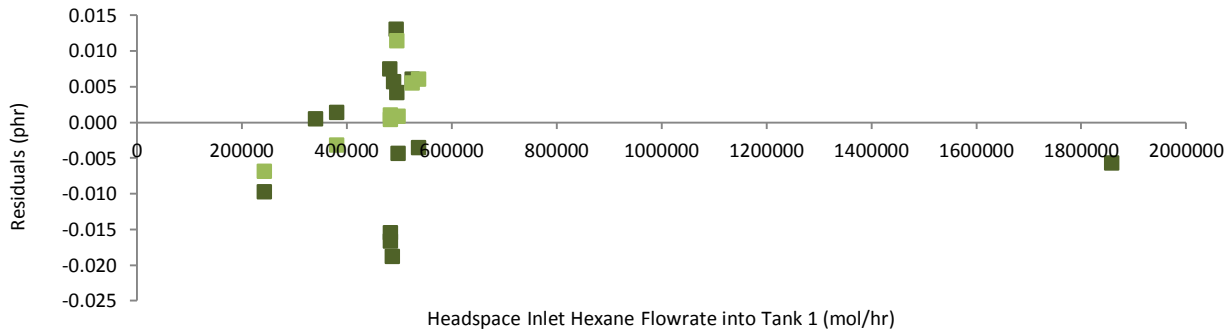

Figure 12c: $\bar{m}_{VNB,i}$ residuals for the three-tank process as a function of the headspace inlet hexane flowrate into tank 1

No trends were observed in the $\bar{m}_{j,i}$ residuals as a function of F_{preC6} values.

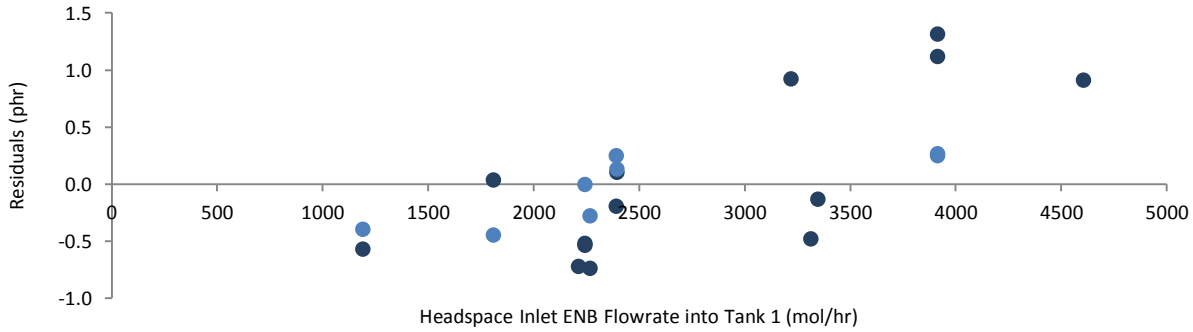

Figure 13a: $\bar{m}_{C6,i}$ residuals for the three-tank process as a function of the headspace inlet ENB flowrate into tank 1

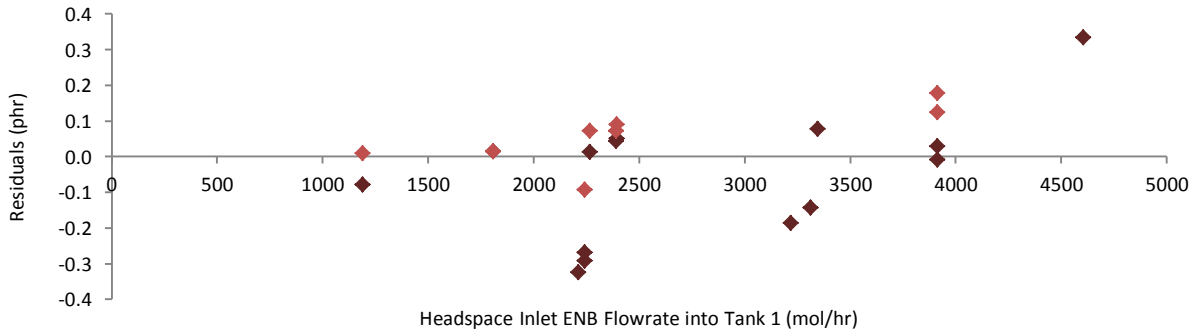

Figure 13b: $\bar{m}_{ENB,i}$ residuals for the three-tank process as a function of the headspace inlet ENB flowrate into tank 1

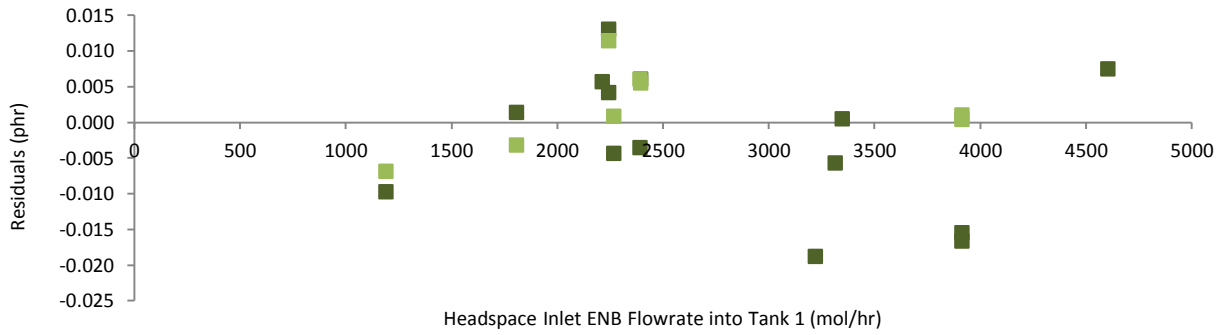

Figure 13c: $\bar{m}_{VNB,i}$ residuals for the three-tank process as a function of the headspace inlet ENB flowrate into tank 1

At high values of F_{preENB}, predicted $\bar{m}_{C6,2}$ values may be too high (see Figure 13a). No corrective action can be made for this trend since there is no obvious cause and effect for this relationship. No trends were observed in the $\bar{m}_{C6,3}$, $\bar{m}_{ENB,i}$ and $\bar{m}_{VNB,i}$ residuals as a function of F_{preENB} values.

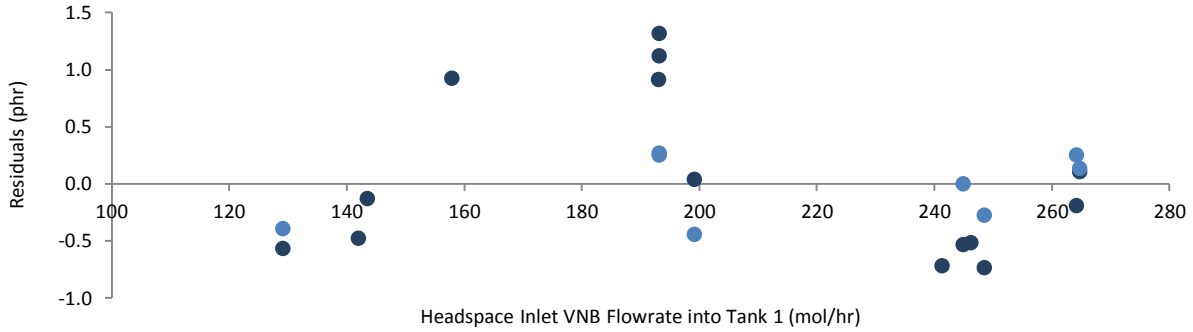

Figure 14a: $\bar{m}_{C6,i}$ residuals for the three-tank process as a function of the headspace inlet VNB flowrate into tank 1

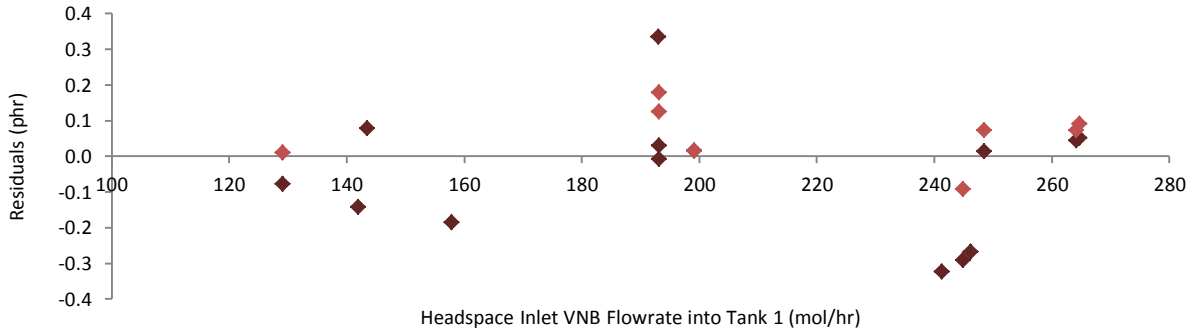

Figure 14b: $\bar{m}_{ENB,i}$ residuals for the three-tank process as a function of the headspace inlet VNB flowrate into tank 1

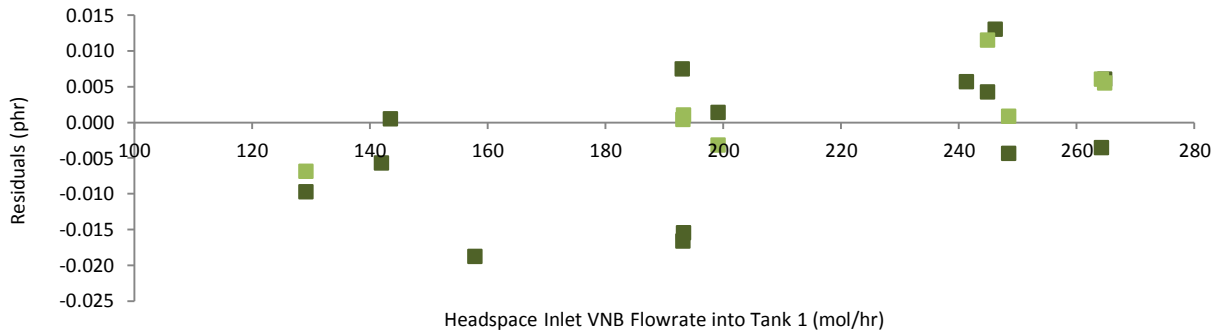

Figure 14c: $\bar{m}_{VNB,i}$ residuals for the three-tank process as a function of the headspace inlet VNB flowrate into tank 1

At high values of F_{preVNB}, both predicted $\bar{m}_{VNB,2}$ and $\bar{m}_{VNB,3}$ values may be too high (see Figure 14c). Perhaps the VNB solubility and/or diffusivity are too small in the model. More data from the four-tank process will provide more information on this possible trend; therefore, no modifications will be made to the three-tank model at this stage. No trends were observed in the $\bar{m}_{C6,i}$ and $\bar{m}_{ENB,i}$ residuals as a function of F_{preVNB} values.

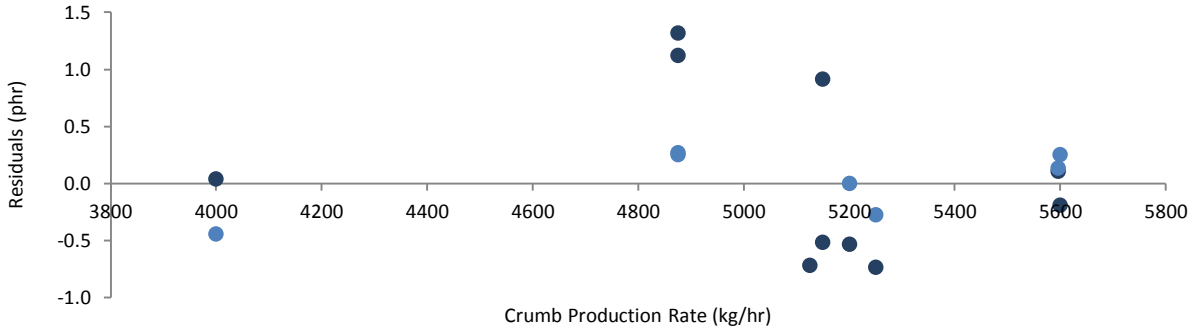

Figure 15a: $\bar{m}_{C6,i}$ residuals for the three-tank process as a function of the crumb production rate

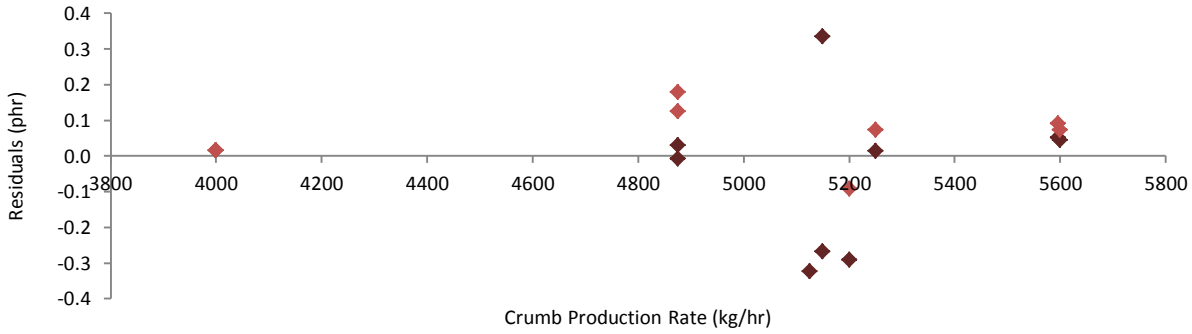

Figure 15b: $\bar{m}_{ENB,i}$ residuals for the three-tank process as a function of the crumb production rate

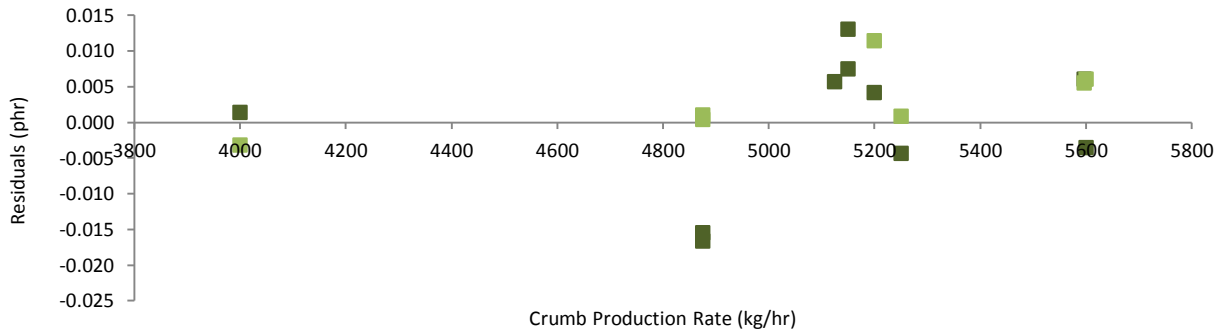

Figure 15c: $\bar{m}_{VNB,i}$ residuals for the three-tank process as a function of the crumb production rate

No trends were observed in the $\bar{m}_{j,i}$ residuals as a function of the crumb production rate.

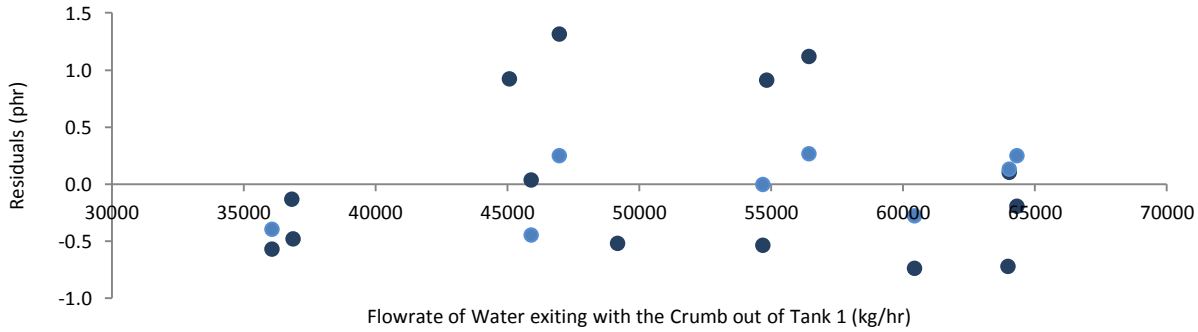

Figure 16a: $\bar{m}_{C6,i}$ residuals for the three-tank process as a function of the flowrate of water exiting with the crumb out of tank 1

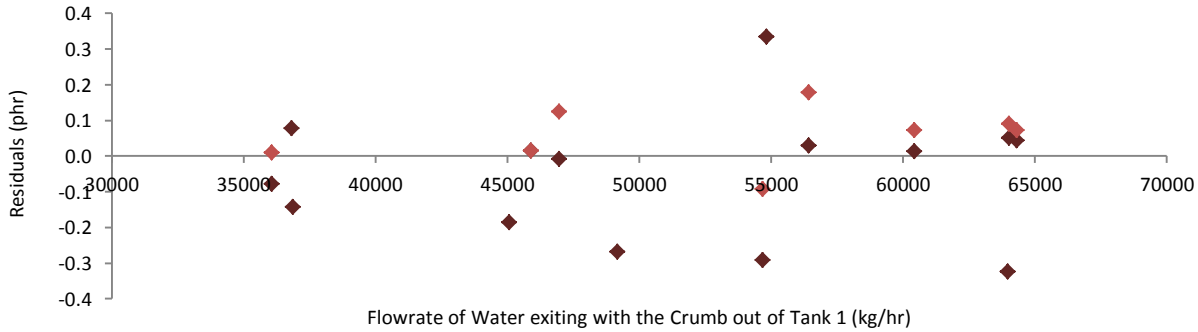

Figure 16b: $\bar{m}_{ENB,i}$ residuals for the three-tank process as a function of the flowrate of water exiting with the crumb out of tank 1

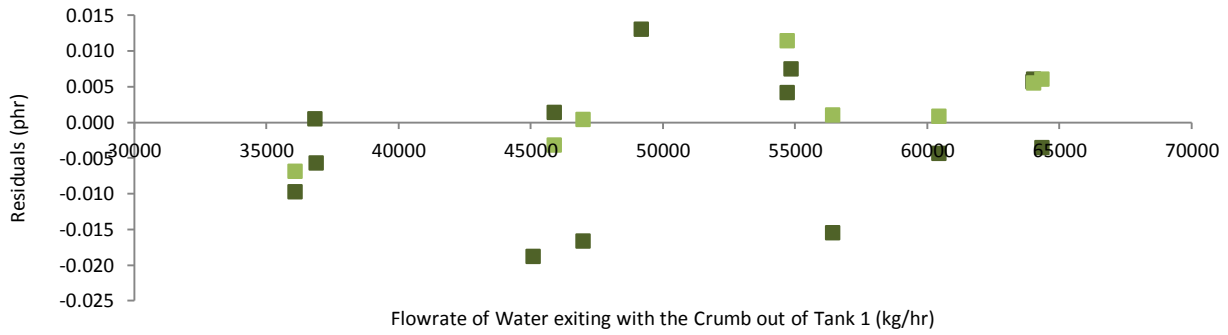

Figure 16c: $\bar{m}_{VNB,i}$ residuals for the three-tank process as a function of the flowrate of water exiting with the crumb out of tank 1

No trends were observed in the $\bar{m}_{j,i}$ residuals as a function of the water exiting with the crumb out of tank 1.

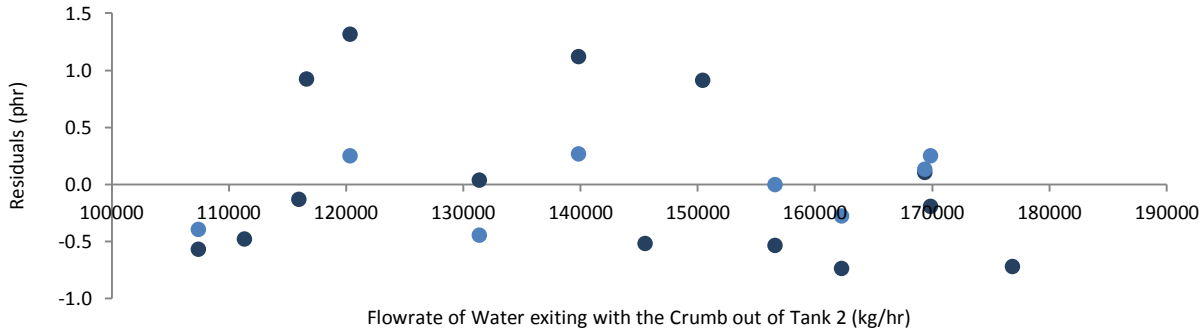

Figure 17a: $\bar{m}_{C6,i}$ residuals for the three-tank process as a function of the flowrate of water exiting with the crumb out of tank 2

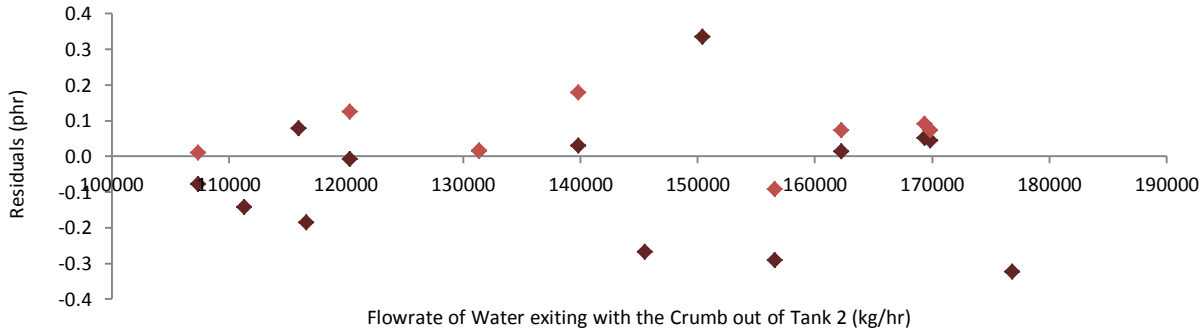

Figure 17b: $\bar{m}_{ENB,i}$ residuals for the three-tank process as a function of the flowrate of water exiting with the crumb out of tank 2

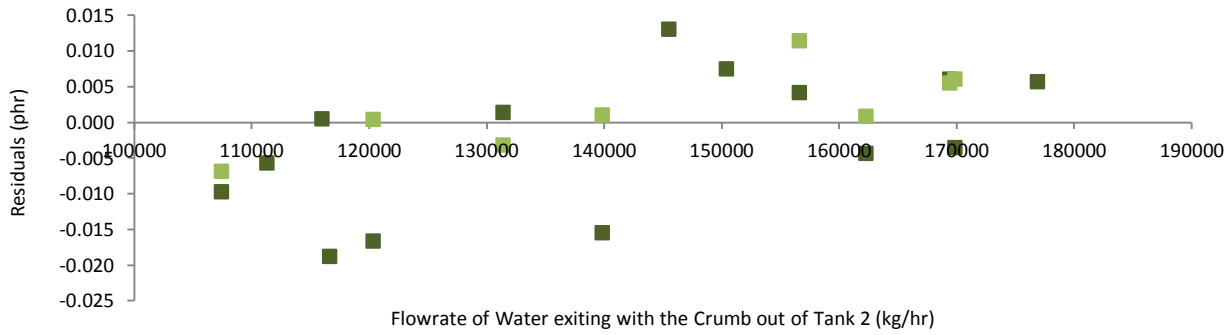

Figure 17c: $\bar{m}_{VNB,i}$ residuals for the three-tank process as a function of the flowrate of water exiting with the crumb out of tank 2

At high flowrates of water exiting with the crumb out of tank 2, both predicted $\bar{m}_{VNB,2}$ and $\bar{m}_{VNB,3}$ values may be too high (see Figure 17c). At high flowrates of water, τ_2 and τ_3 values will be lower; perhaps the VNB solubility and/or diffusivity are too small in the model, causing predicted $\bar{m}_{VNB,2}$ and $\bar{m}_{VNB,3}$ values to be too high. More data from the four-tank process will provide more information on this possible trend; therefore, no modifications will be made to the three-tank model at this stage.
No trends were observed in the $\bar{m}_{C6,i}$ and $\bar{m}_{ENB,i}$ residuals as a function of flowrate of water exiting with the crumb out of tank 2.

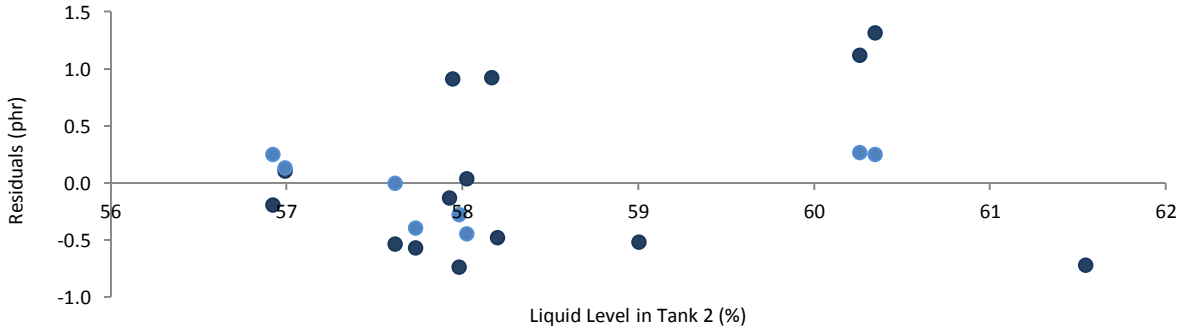

Figure 18a: $\bar{m}_{C6,i}$ residuals for the three-tank process as a function of the liquid level in tank 2

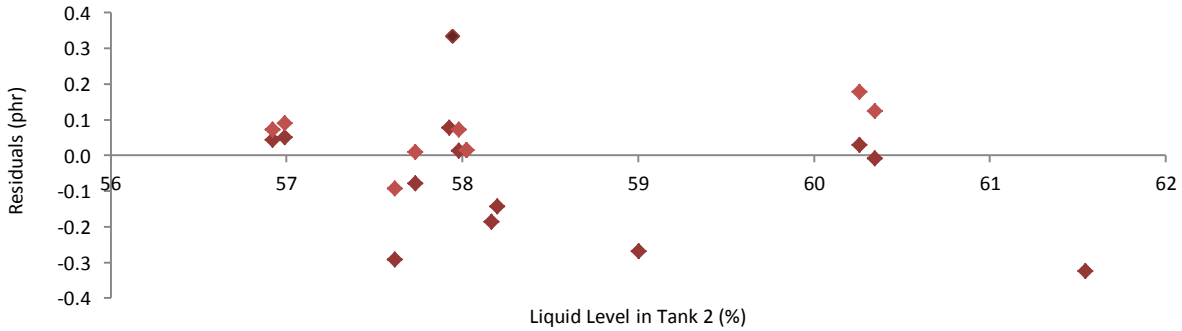

Figure 18b: $\bar{m}_{ENB,i}$ residuals for the three-tank process as a function of the liquid level in tank 2

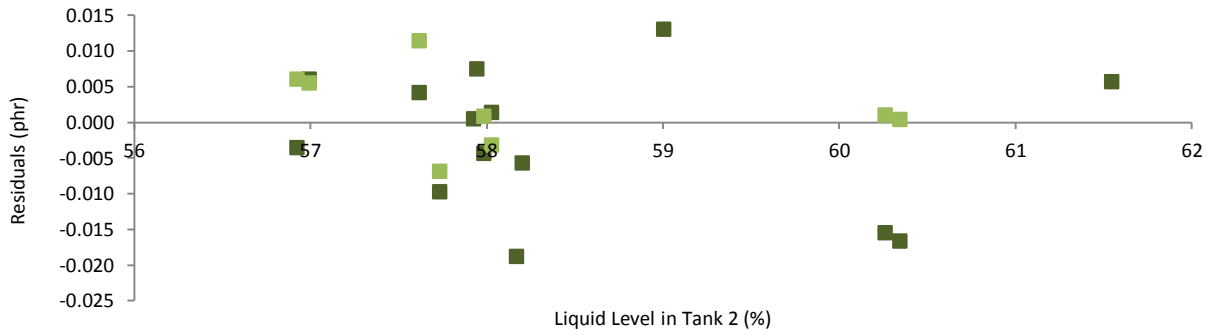

Figure 18c: $\bar{m}_{VNB,i}$ residuals for the three-tank process as a function of the liquid level in tank 2

No trends were observed in the $\bar{m}_{j,i}$ residuals as a function of the liquid level in tank 2.

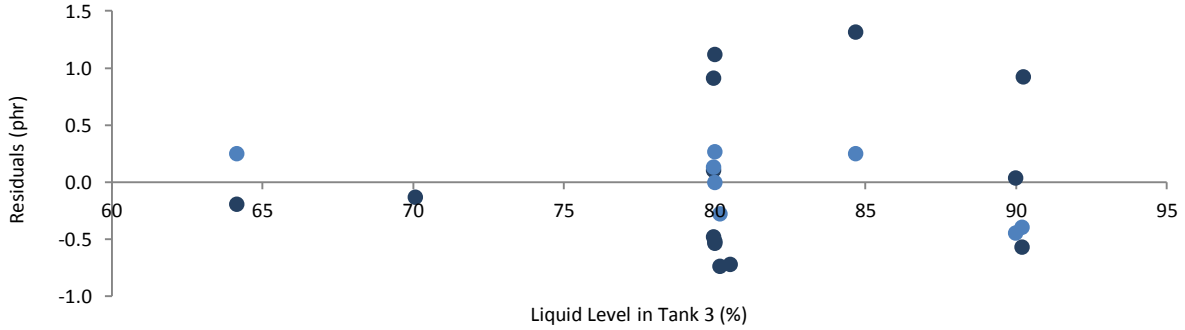

Figure 19a: $\bar{m}_{C6,i}$ residuals for the three-tank process as a function of the liquid level in tank 3

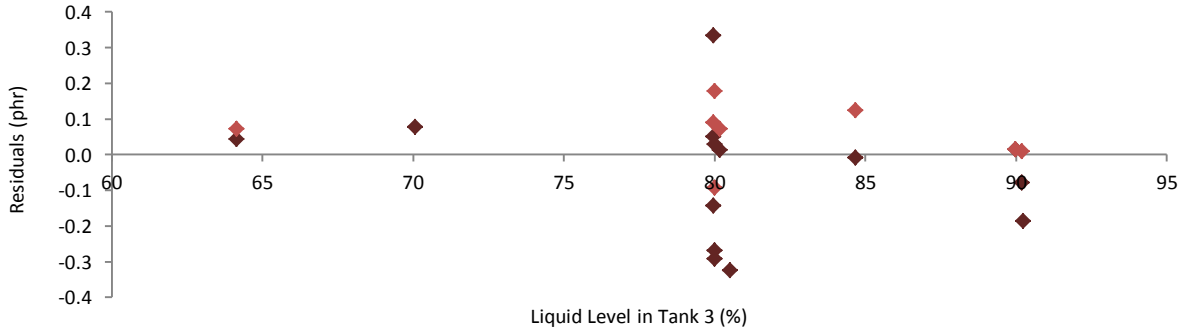

Figure 19b: $\bar{m}_{ENB,i}$ residuals for the three-tank process as a function of the liquid level in tank 3

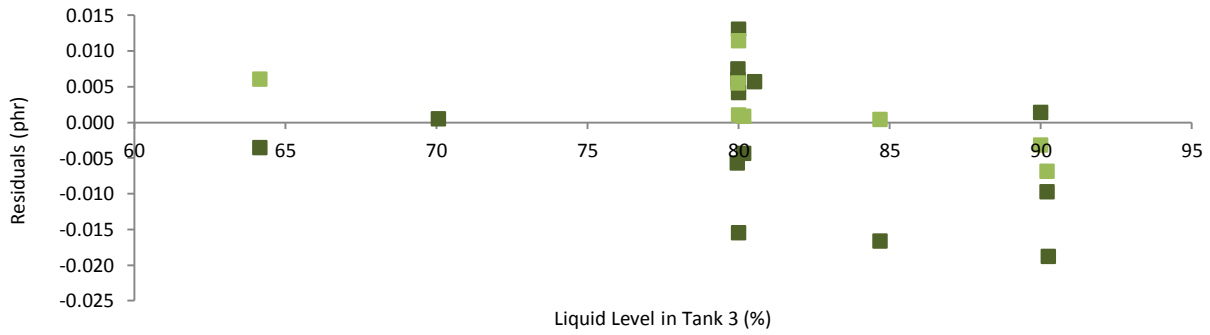

Figure 19c: $\bar{m}_{VNB,i}$ residuals for the three-tank process as a function of the liquid level in tank 3

No trends were observed in the $\bar{m}_{j,i}$ residuals as a function of the liquid level in tank 3.

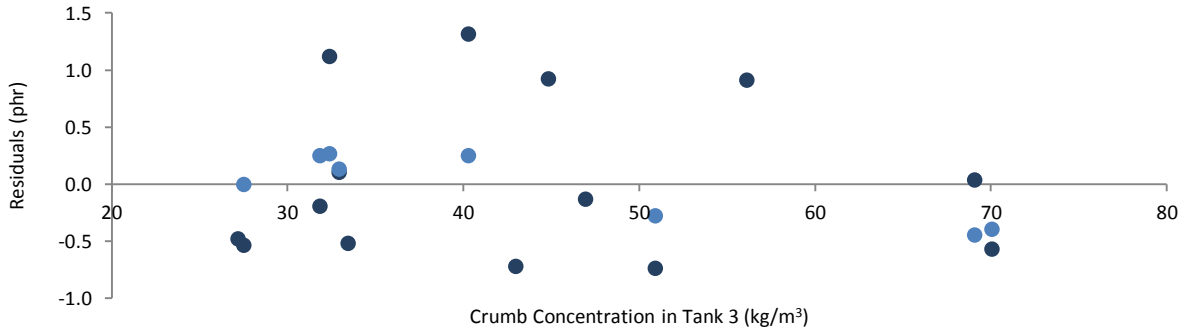

Figure 20a: $\bar{m}_{C6,i}$ residuals for the three-tank process as a function of the crumb concentration in tank 3

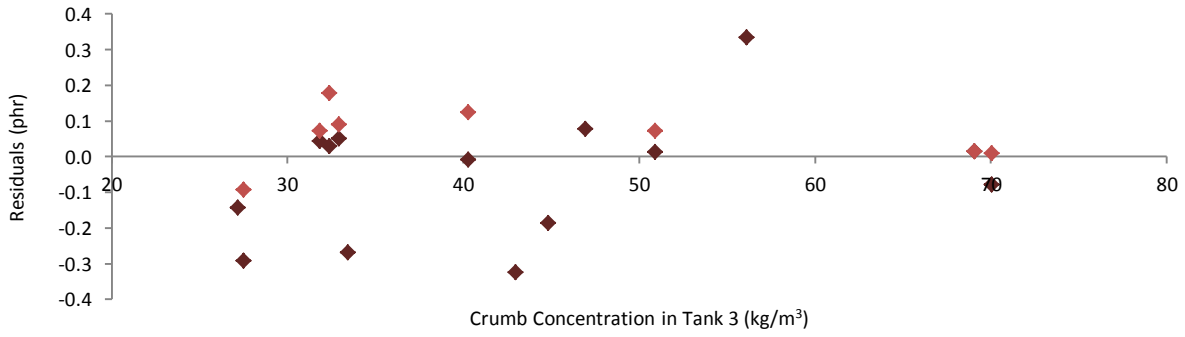

Figure 20b: $\bar{m}_{ENB,i}$ residuals for the three-tank process as a function of the crumb concentration in tank 3

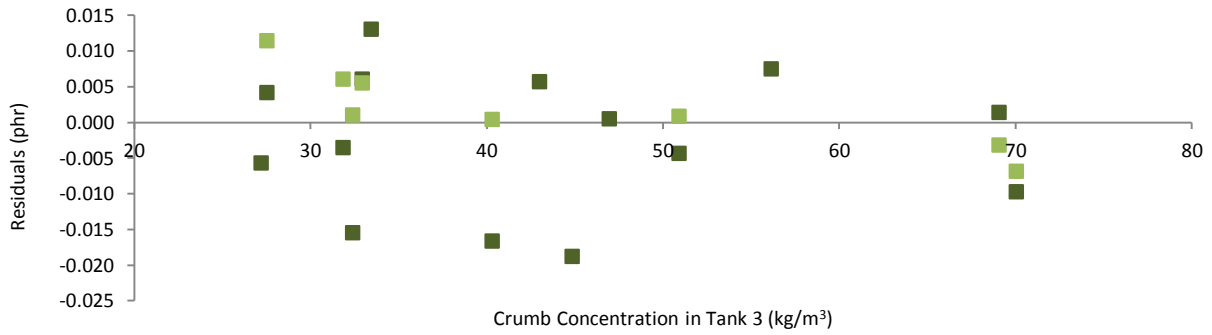

Figure 20c: $\overline{m}_{VNB,i}$ residuals for the three-tank process as a function of the crumb concentration in tank 3

At high crumb concentrations in tank 3, predicted $\overline{m}_{VNB,3}$ values may be too low (see Figure 20c). At high crumb concentrations, τ_3 values will be lower; perhaps the VNB solubility and/or diffusivity are too small in the model, causing predicted $\overline{m}_{VNB,3}$ values to be too high. More data from the four-tank process will provide more information on this possible trend; therefore, no modifications will be made to the three-tank model at this stage. No trends were observed in the $\overline{m}_{C6,i}$, $\overline{m}_{ENB,i}$ and $\overline{m}_{VNB,2}$ residuals as a function of crumb concentration in tank 3.

In summary, some trends were observed in the residuals using the updated three-tank process model; however, these trends are minor and can be further examined after conducting an additional phase of parameter estimation using the combined three- and four-tank process data sets. It is possible the solubility and/or diffusivity for VNB is too low but further VNB solubility and diffusivity parameter adjustment will occur in the next phase of parameter estimation.

Appendix D:
Four-Tank Model Preliminary Simulation Results

Shown in Figures 4a to 4j are model predictions and measured data for $\bar{m}_{j,i}$ values from the four-tank processes for 10 industrial data sets. Figure 14 in Chapter 5 provides information about the 11th data set. The model predictions shown were determined using the initial parameter values in Tables 18, 19 & 20. Dashed lines are used to guide the eye.

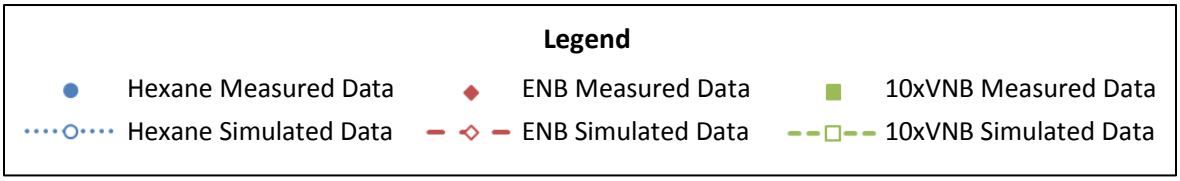

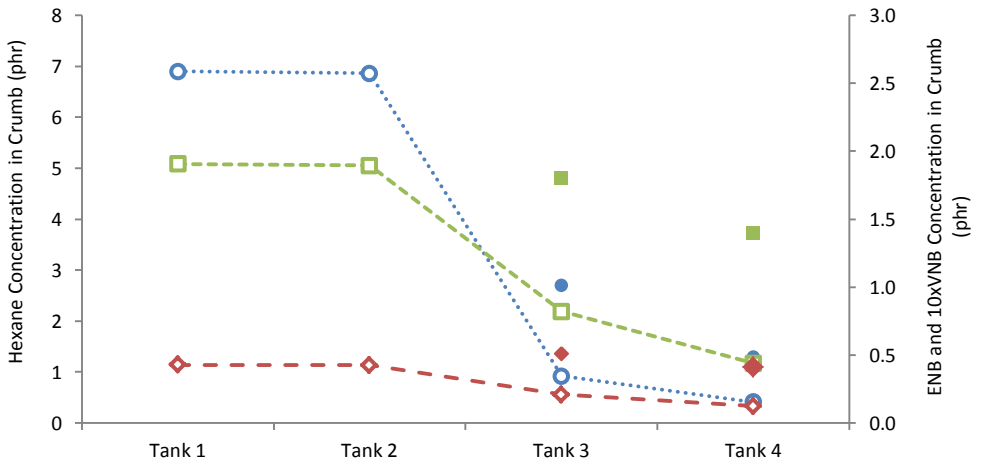

Figure 4a: Model predictions and measured results for data set 2

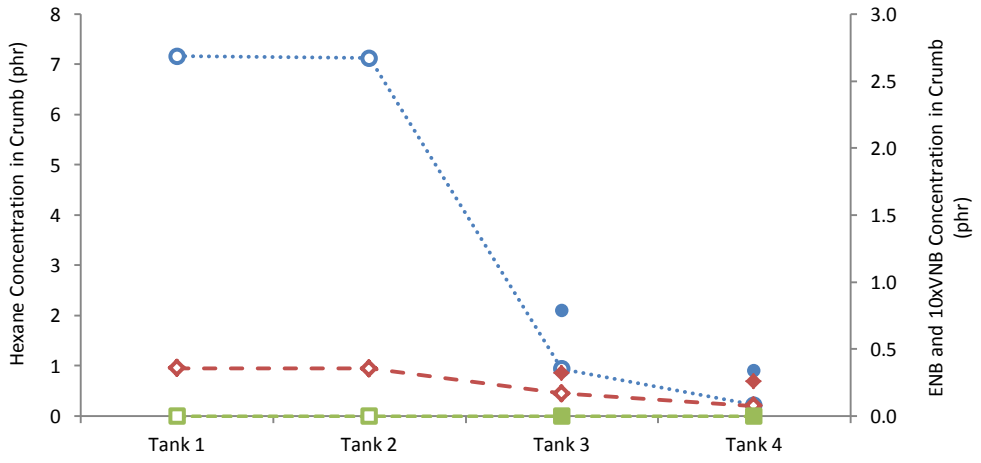

Figure 4b: Model predictions and measured results for data set 3

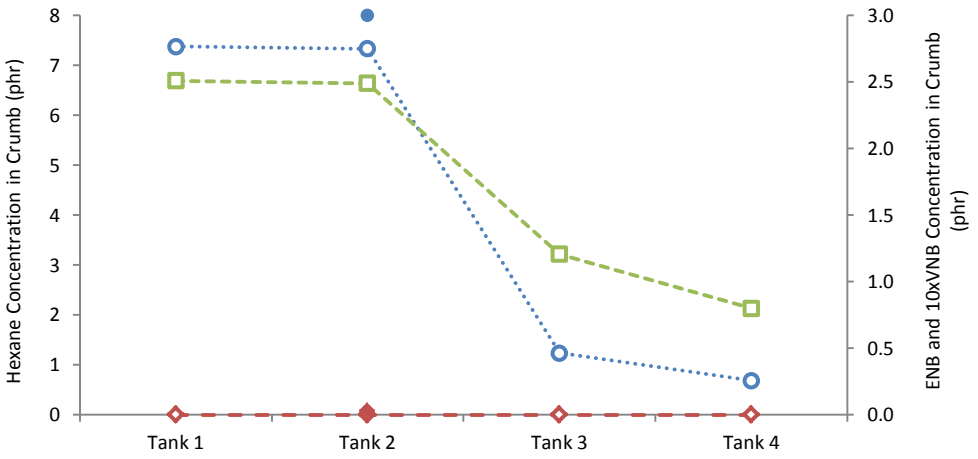

Figure 4c: Model predictions and measured results for data set 4

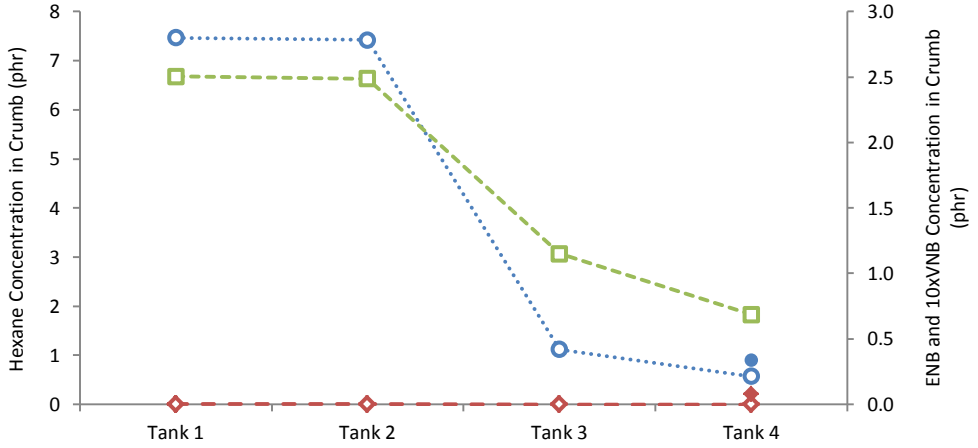

Figure 4d: Model predictions and measured results for data set 5

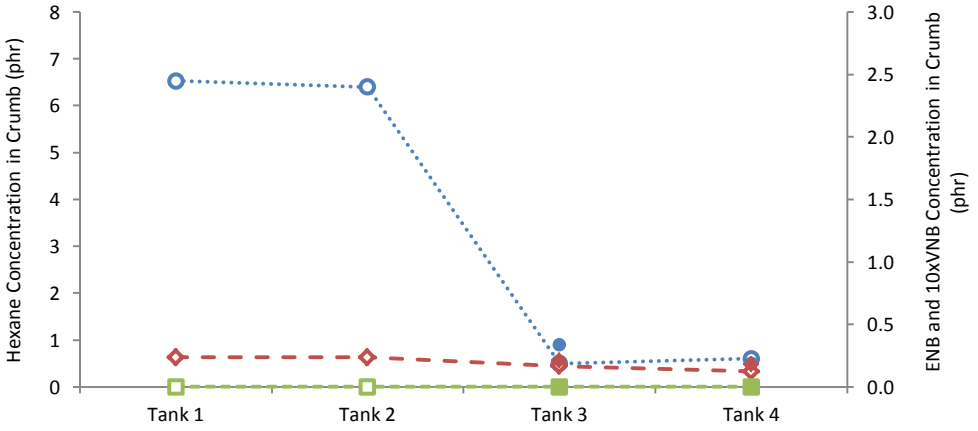

Figure 4e: Model predictions and measured results for data set 6

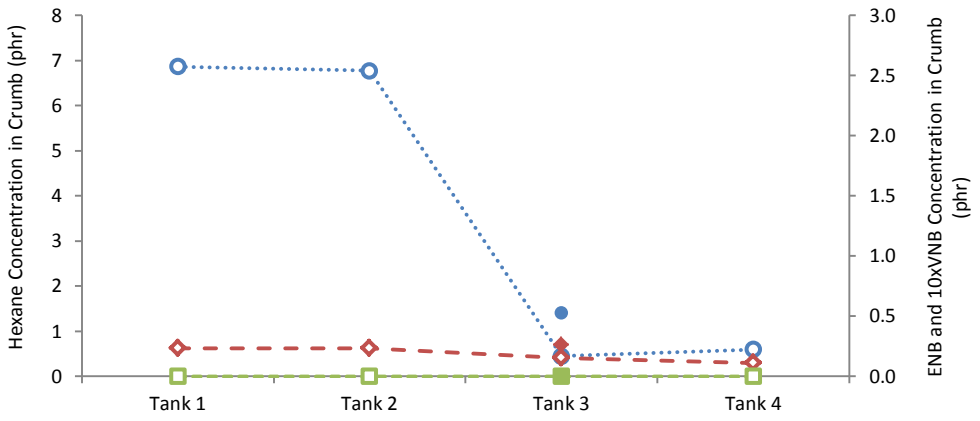

Figure 4f: Model predictions and measured results for data set 7

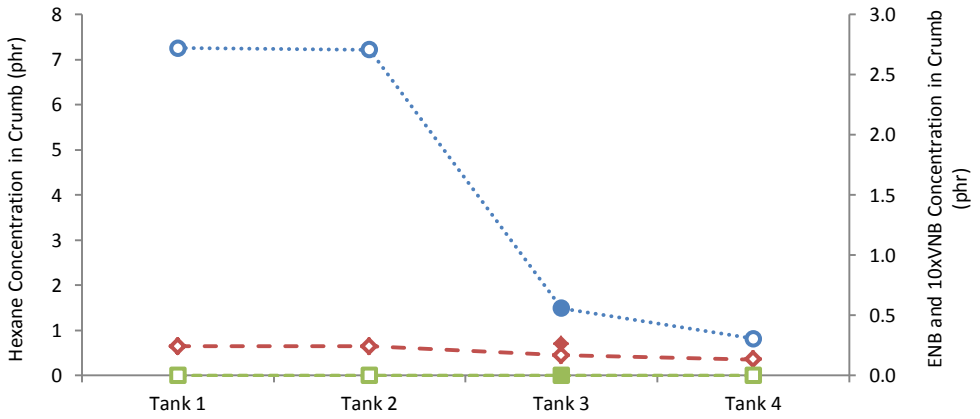

Figure 4g: Model predictions and measured results for data set 8

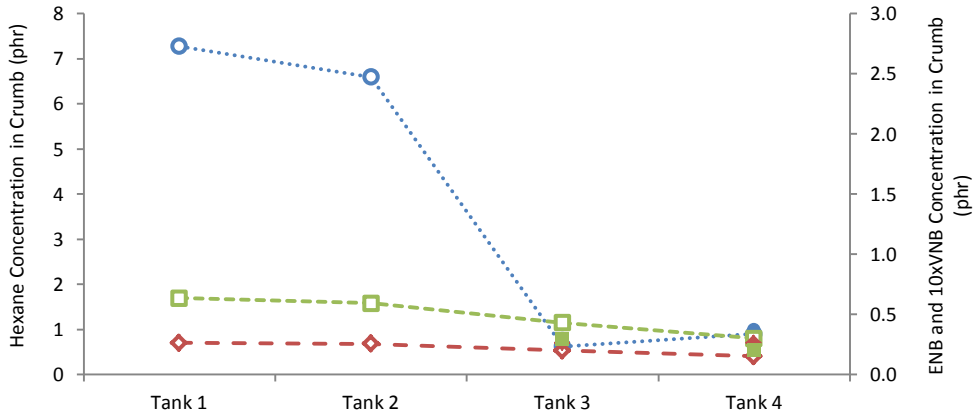

Figure 4h: Model predictions and measured results for data set 9

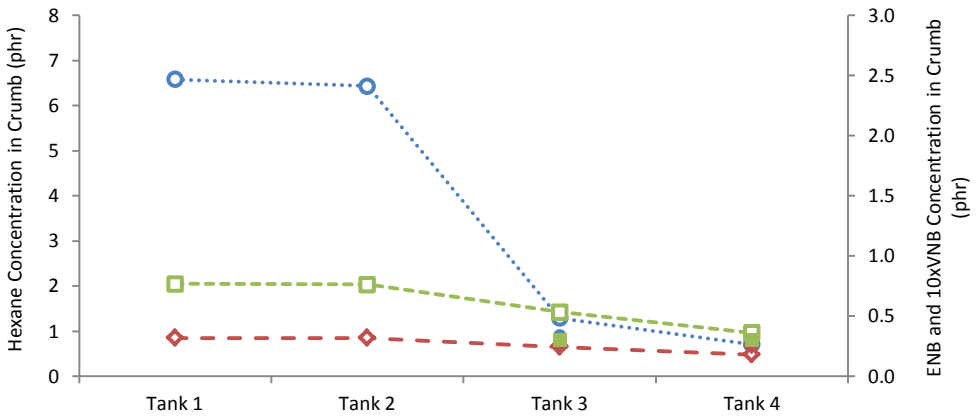

Figure 4i: Model predictions and measured results for data set 10

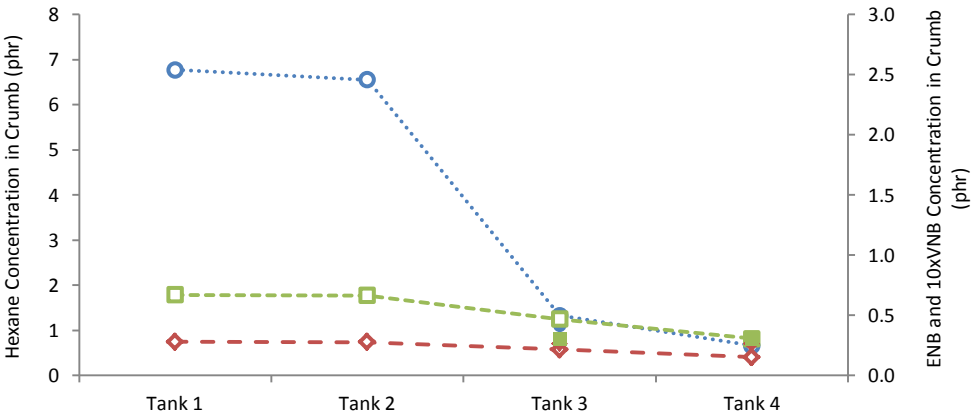

Figure 4j: Model predictions and measured results for data set 11

Appendix E:
Four-Tank Model Simulation Results after Preliminary Parameter Tuning

Shown in Figures 5a to 5k are model predictions and measured data for $\overline{m}_{j,i}$ values from the four-tank processes for 11 industrial data sets. The model predictions shown were determined using the initial parameter values in Tables 18, 19, 20, and updated estimated parameters in Tables 24 & 25. Dashed lines are used to guide the eye.

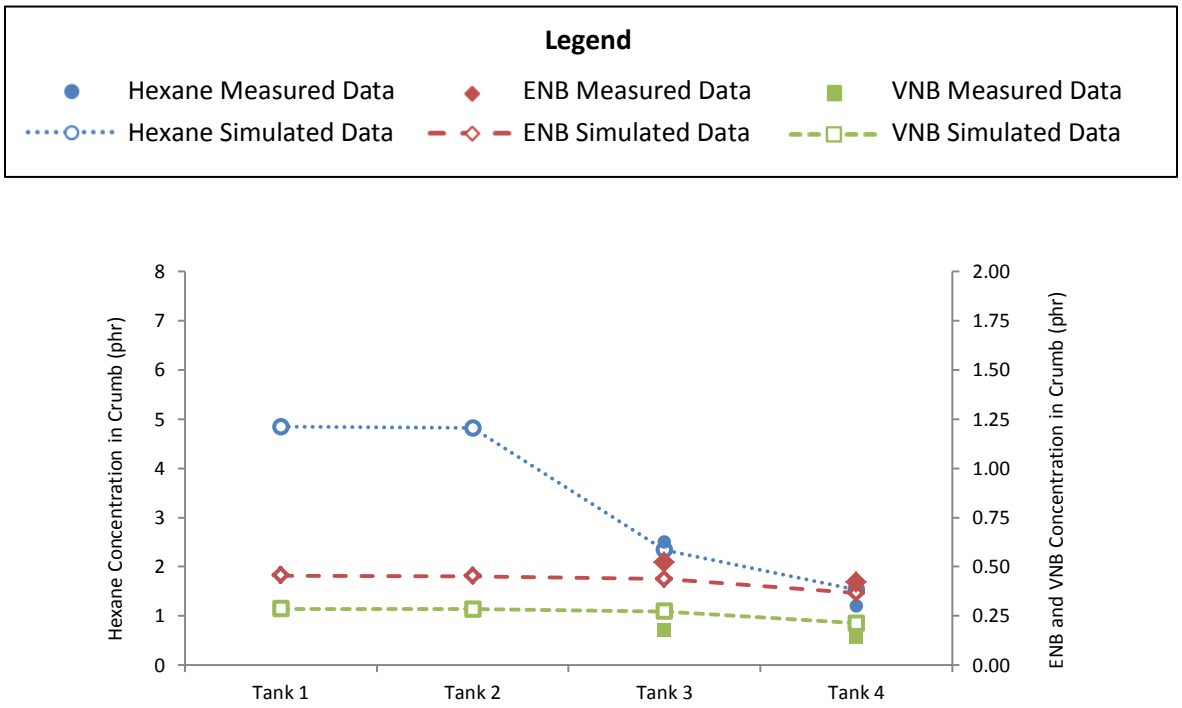

Figure 5a: Updated model predictions and measured results for data set 1

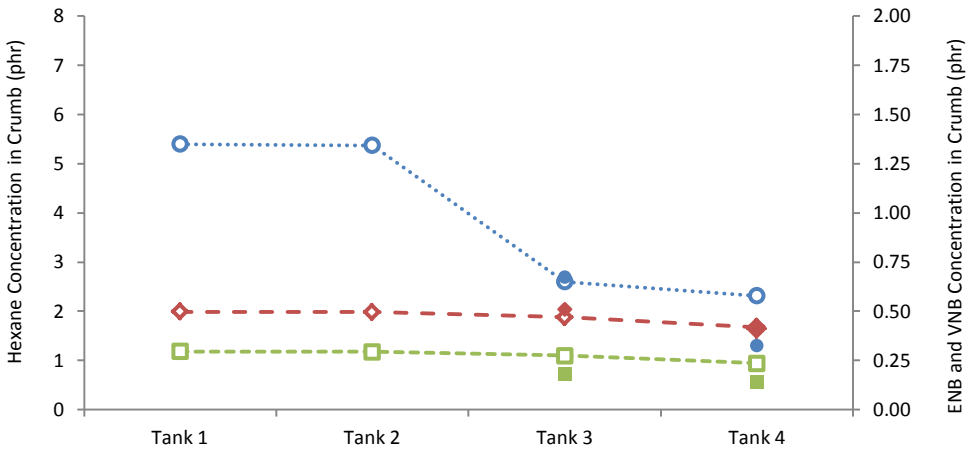

Figure 5b: Updated model predictions and measured results for data set 2

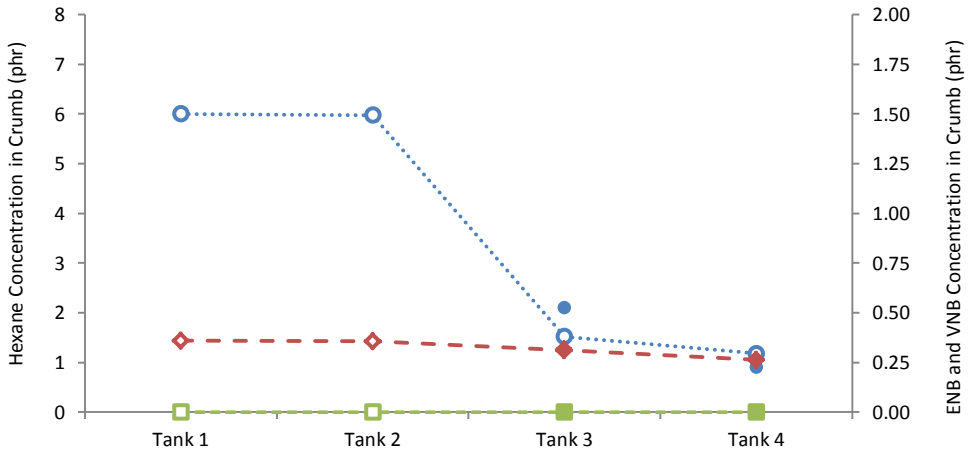

Figure 5c: Updated model predictions and measured results for data set 3

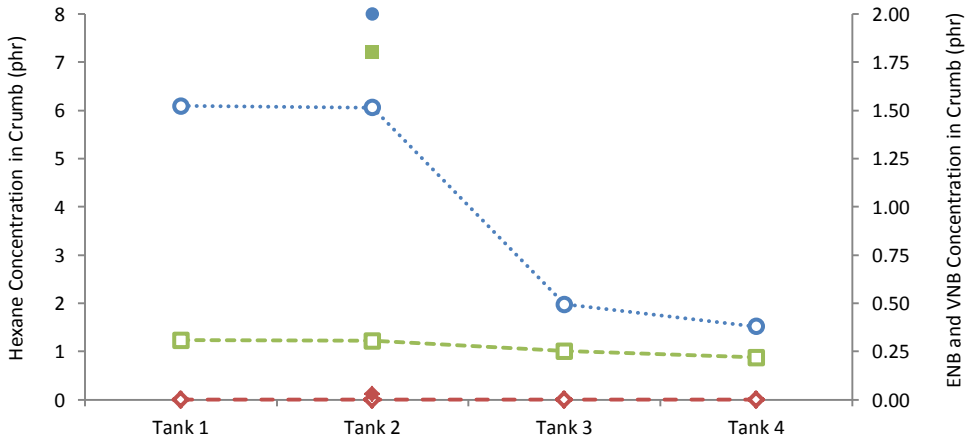

Figure 5d: Updated model predictions and measured results for data set 4

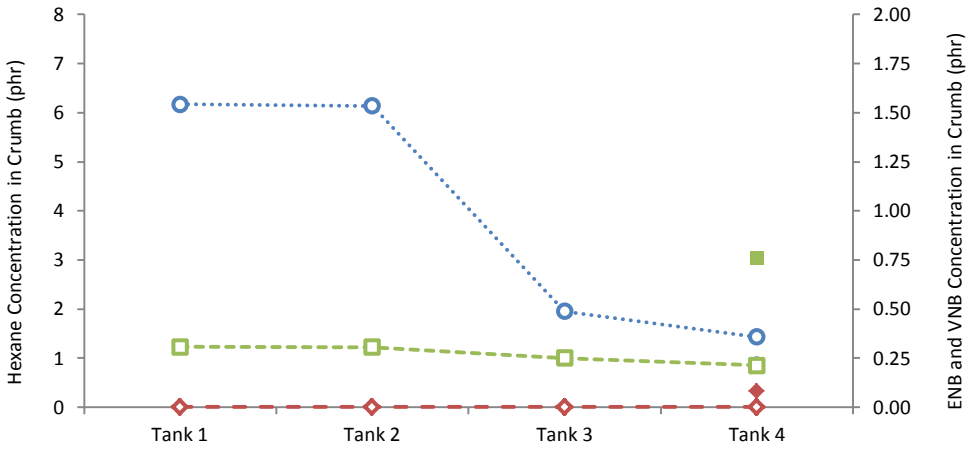

Figure 5e: Updated model predictions and measured results for data set 5

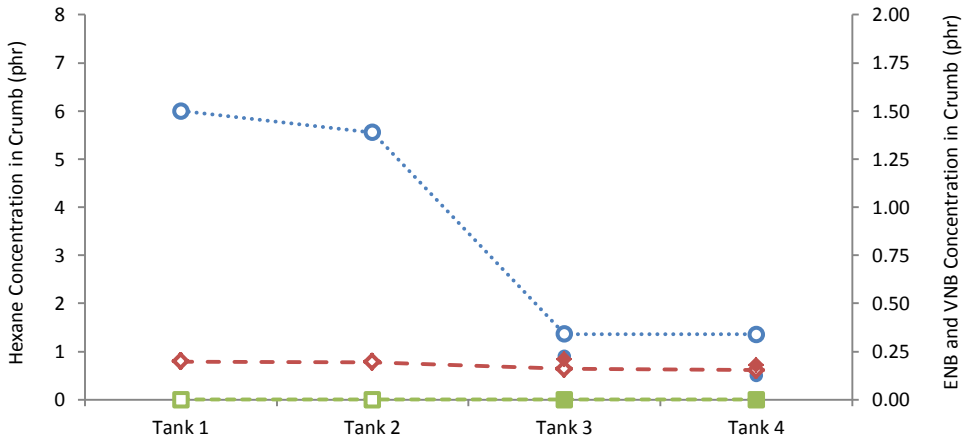

Figure 5f: Updated model predictions and measured results for data set 6

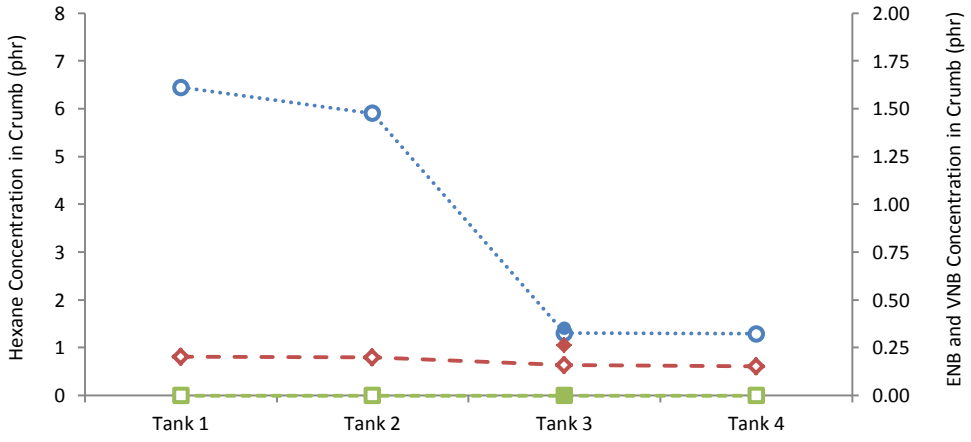

Figure 5g: Updated model predictions and measured results for data set 7

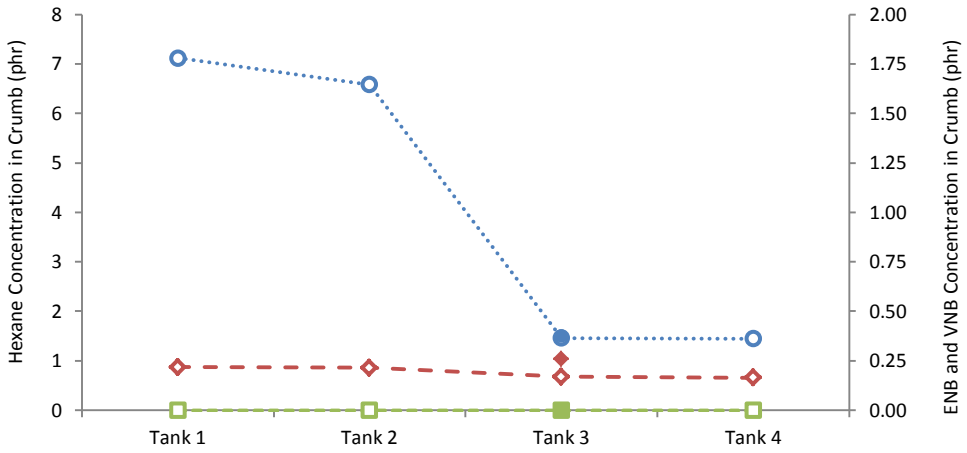

Figure 5h: Updated model predictions and measured results for data set 8

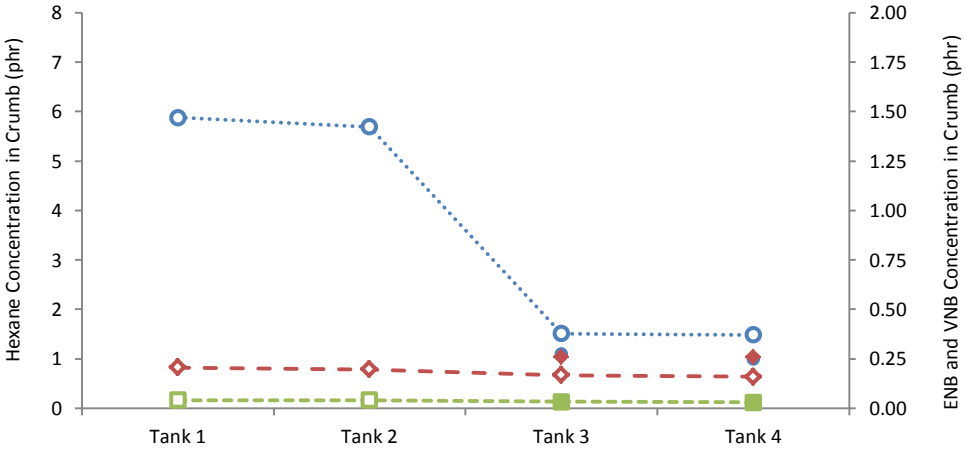

Figure 5i: Updated model predictions and measured results for data set 9

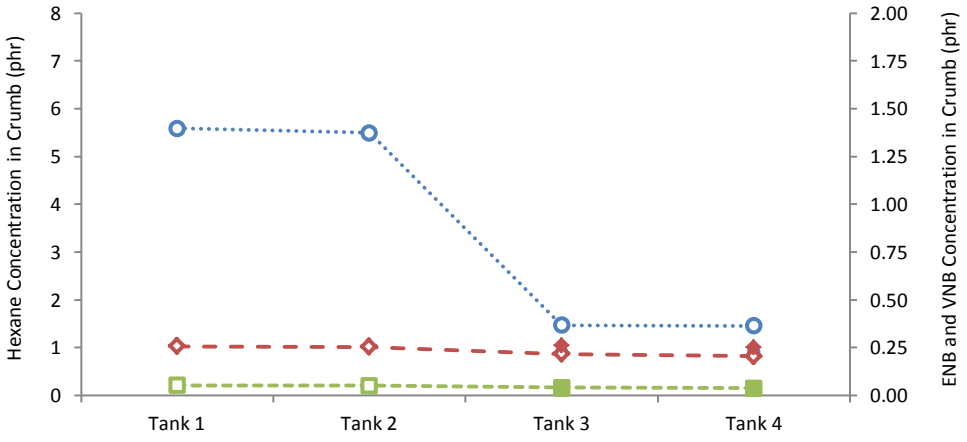

Figure 5j: Updated model predictions and measured results for data set 10

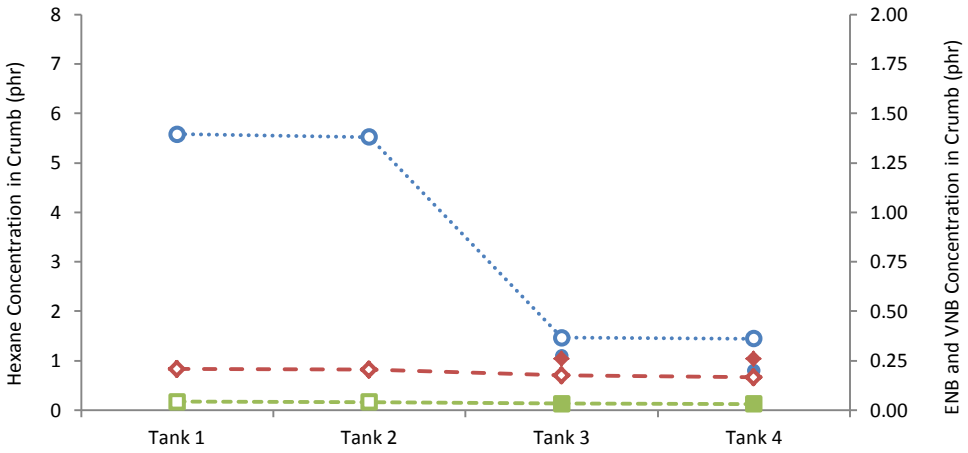

Figure 5k: Updated model predictions and measured results for data set 11

Appendix F:
Three-Tank Model Simulation Results after Final Parameter Tuning

Shown in Figures 6a to 6m are model predictions and measured data for $\overline{m}_{j,i}$ values from the three-tank process for 13 industrial data sets. Figure 18 in Chapter 5 provides information about the 14th data set. The model predictions shown were determined using the initial parameter values in Table 14 and updated estimated parameters in Table 28. Dashed lines are used to guide the eye.

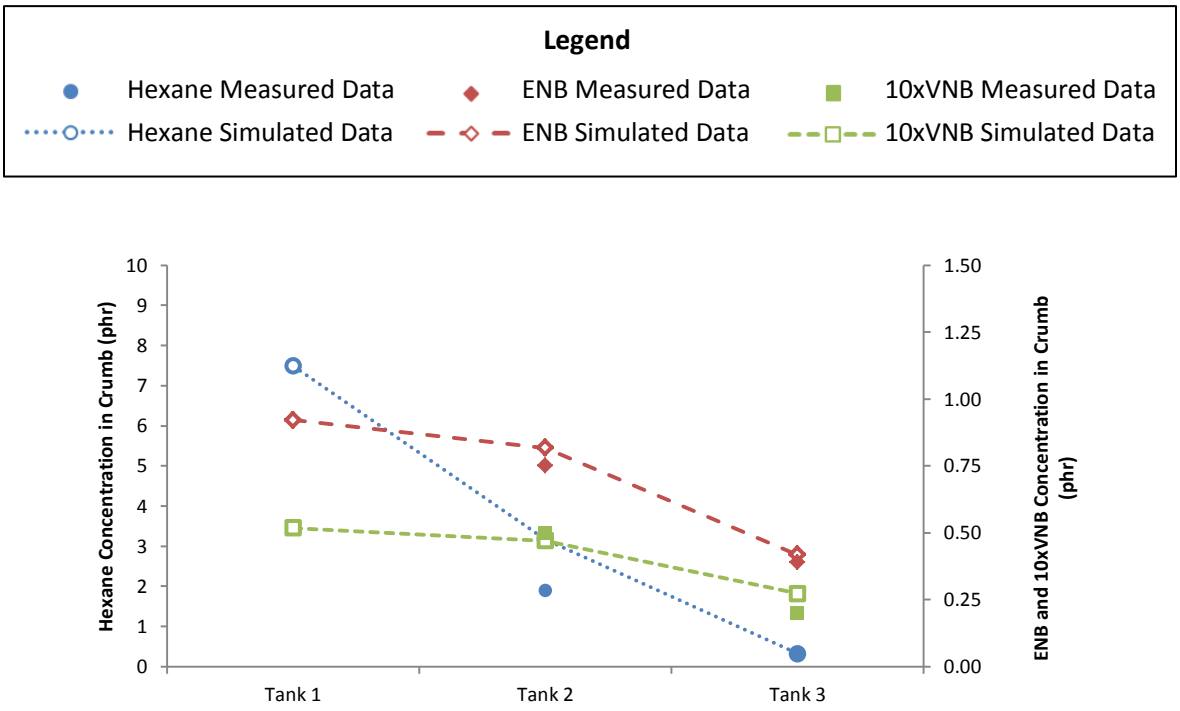

Figure 6a: Updated model predictions and measured results for data set 2 from the three-tank process

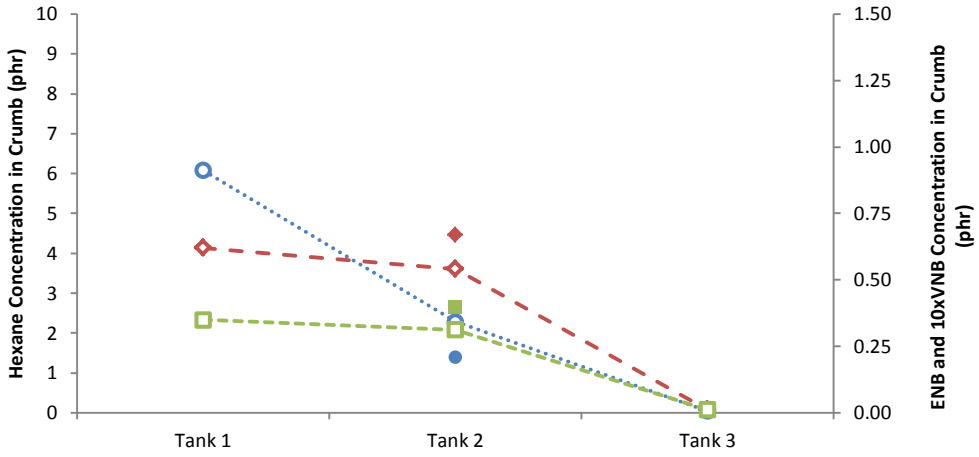

Figure 6b: Updated model predictions and measured results for data set 3 from the three-tank process

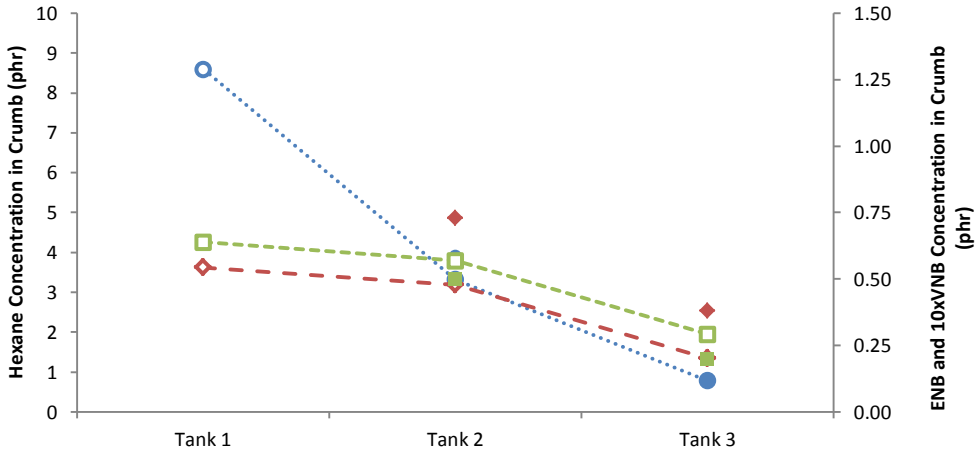

Figure 6c: Updated model predictions and measured results for data set 4 from the three-tank process

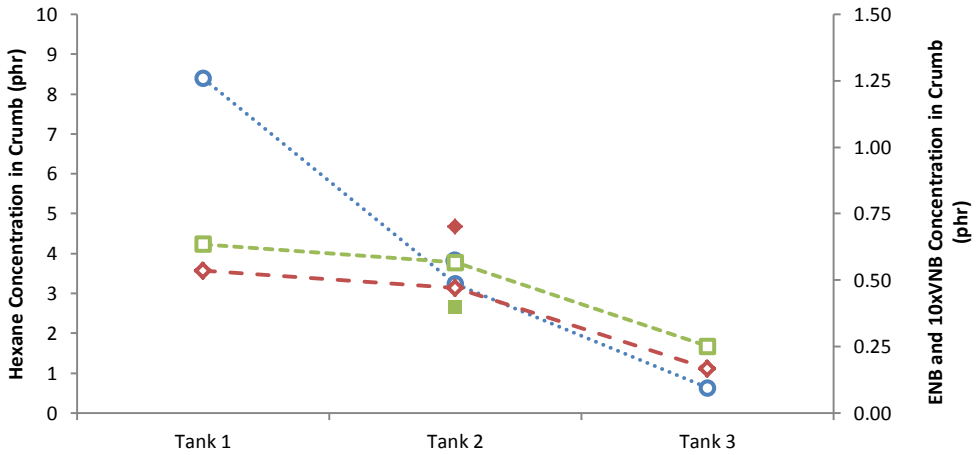

Figure 6d: Updated model predictions and measured results for data set 5 from the three-tank process

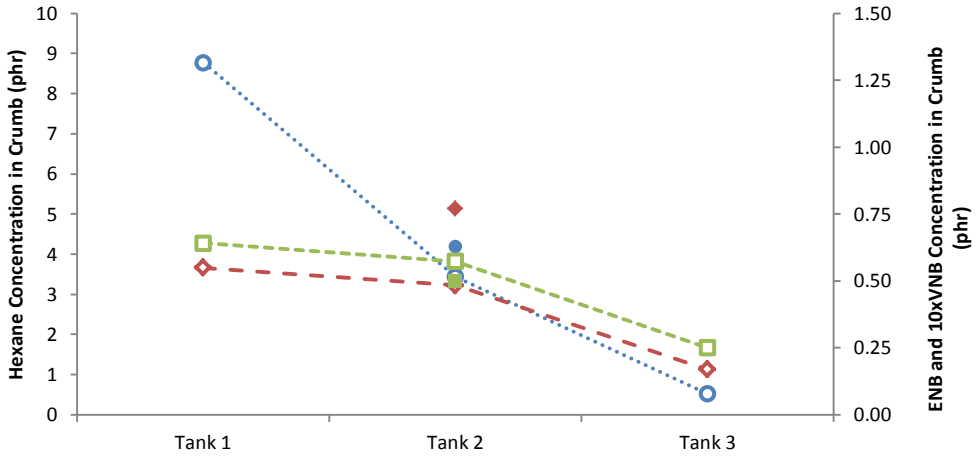

Figure 6e: Updated model predictions and measured results for data set 6 from the three-tank process

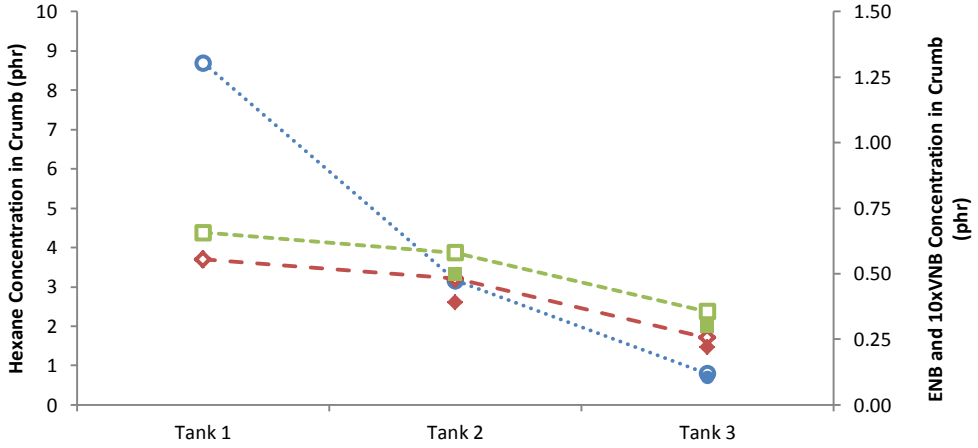

Figure 6f: Updated model predictions and measured results for data set 7 from the three-tank process

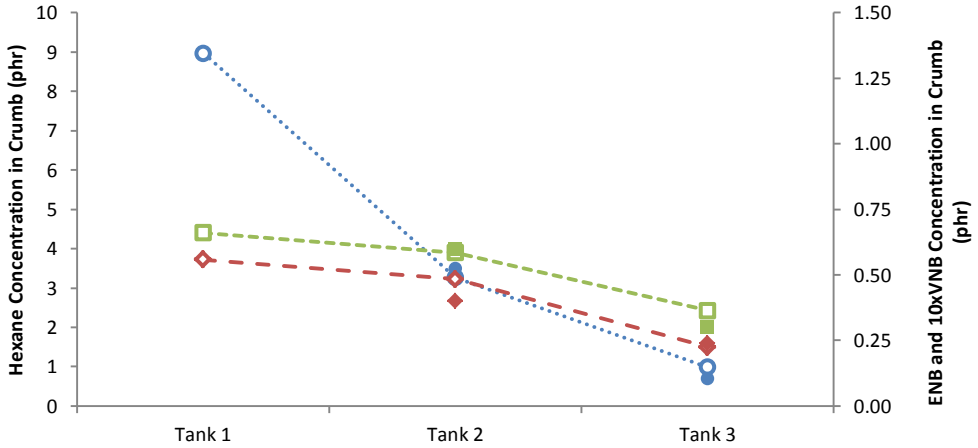

Figure 6g: Updated model predictions and measured results for data set 8 from the three-tank process

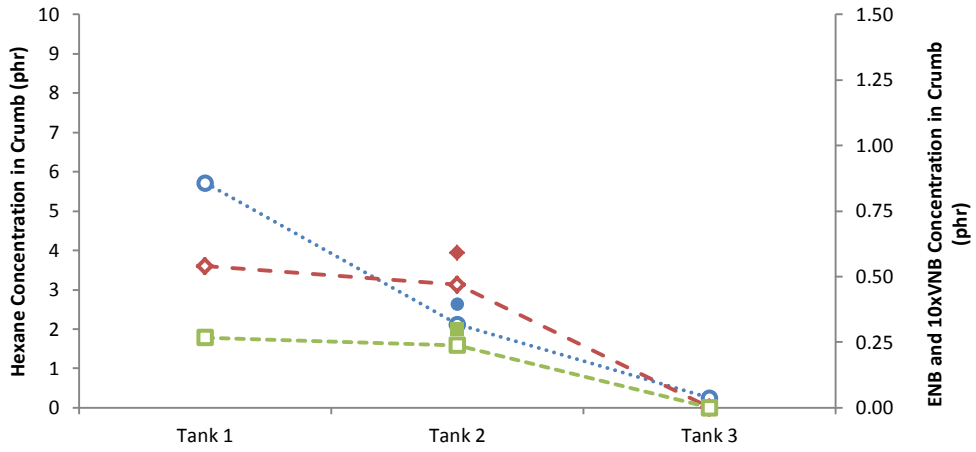

Figure 6h: Updated model predictions and measured results for data set 9 from the three-tank process

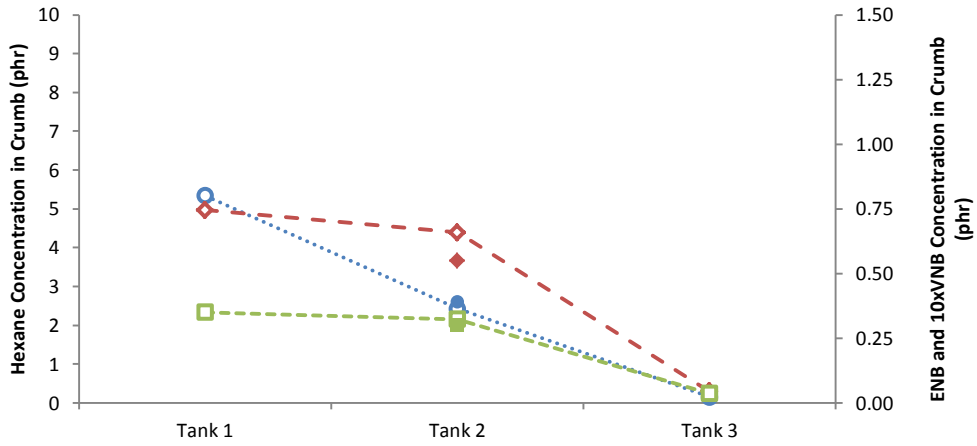

Figure 6i: Updated model predictions and measured results for data set 10 from the three-tank process

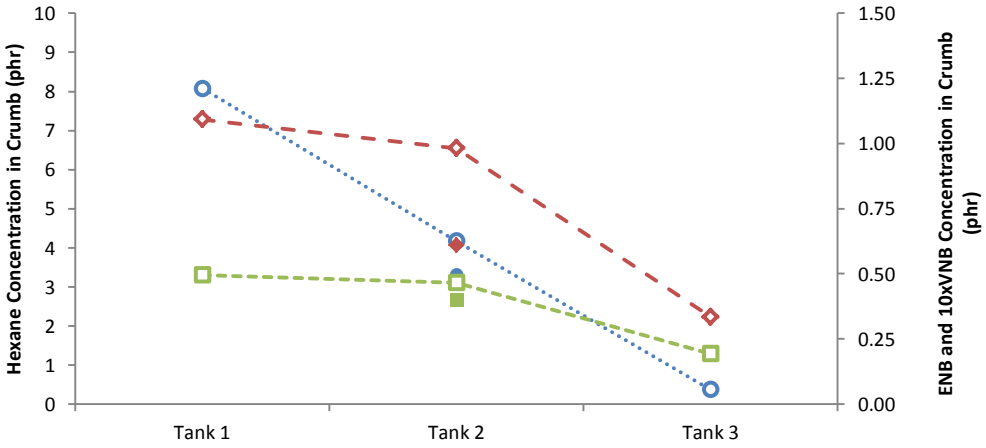

Figure 6j: Updated model predictions and measured results for data set 11 from the three-tank process

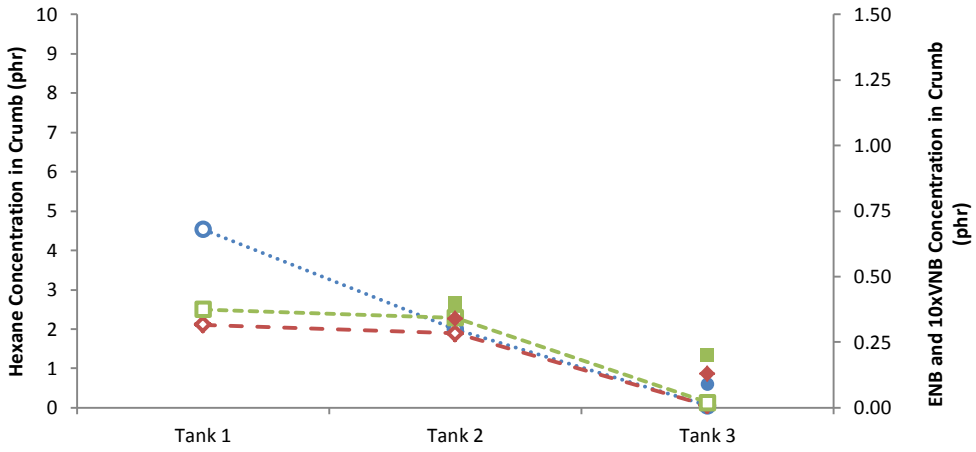

Figure 6k: Updated model predictions and measured results for data set 12 from the three-tank process

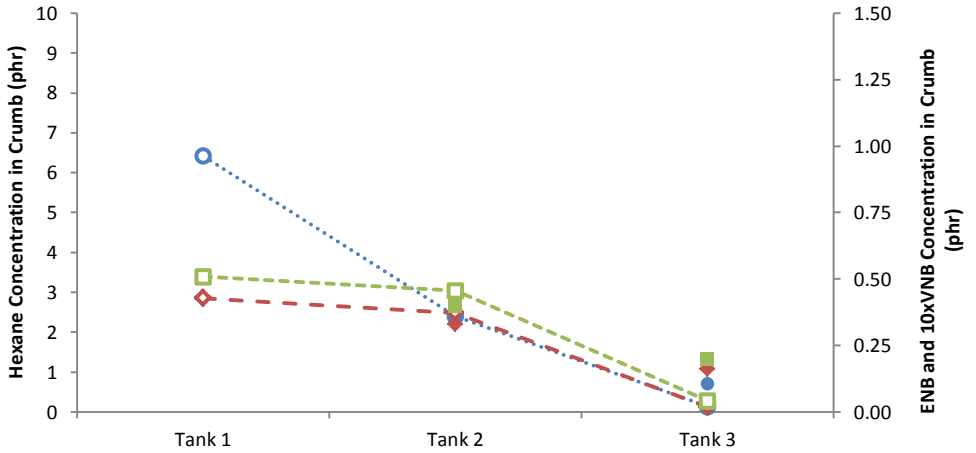

Figure 6l: Updated model predictions and measured results for data set 13 from the three-tank process

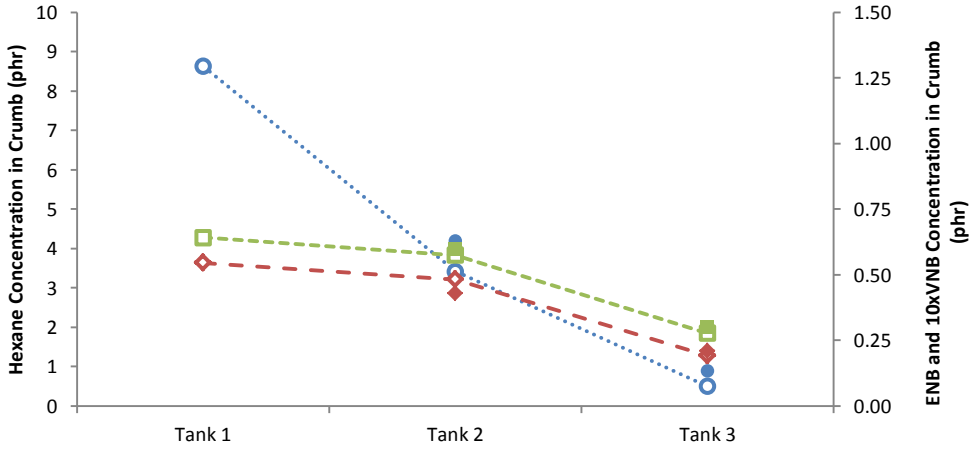

Figure 6m: Updated model predictions and measured results for data set 14 from the three-tank process

Appendix G:
Four-Tank Model Simulation Results after Final Parameter Tuning

Shown in Figures 7a to 7i are model predictions and measured data for $\bar{m}_{j,i}$ values from the four-tank processes for nine industrial data sets. Figures 19 and 20 in Chapter 5 provide information about the tenth and eleventh data sets. The model predictions shown were determined using the initial parameter values in Tables 14, 19, 20, and the updated estimated parameters in Table 28. Dashed lines are used to guide the eye.

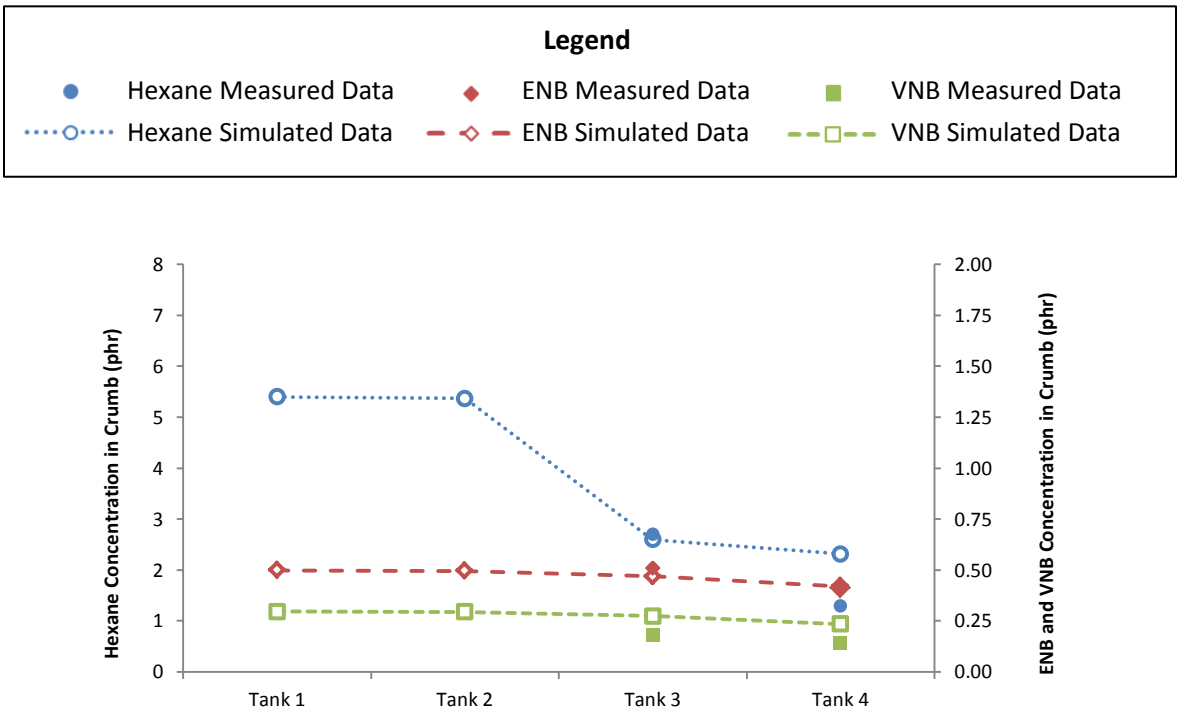

Figure 7a: Updated model predictions and measured results for data set 2 from four-tank process A

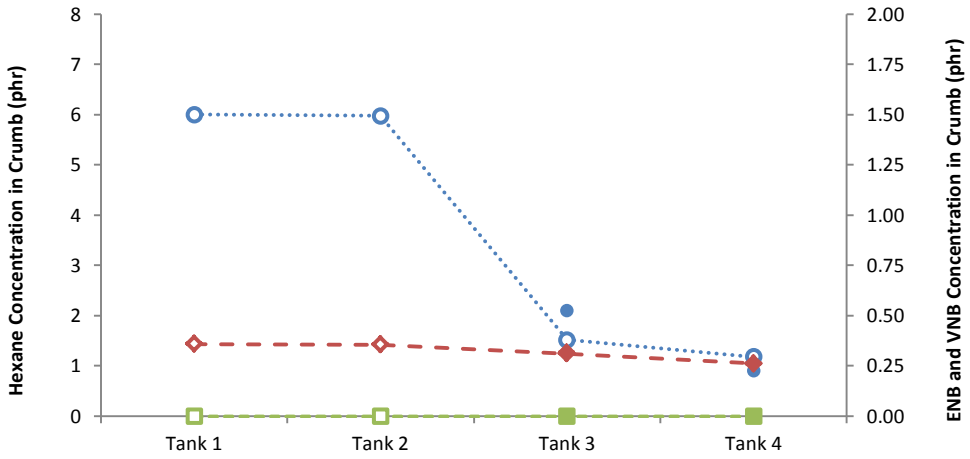

Figure 7b: Updated model predictions and measured results for data set 3 from four-tank process A

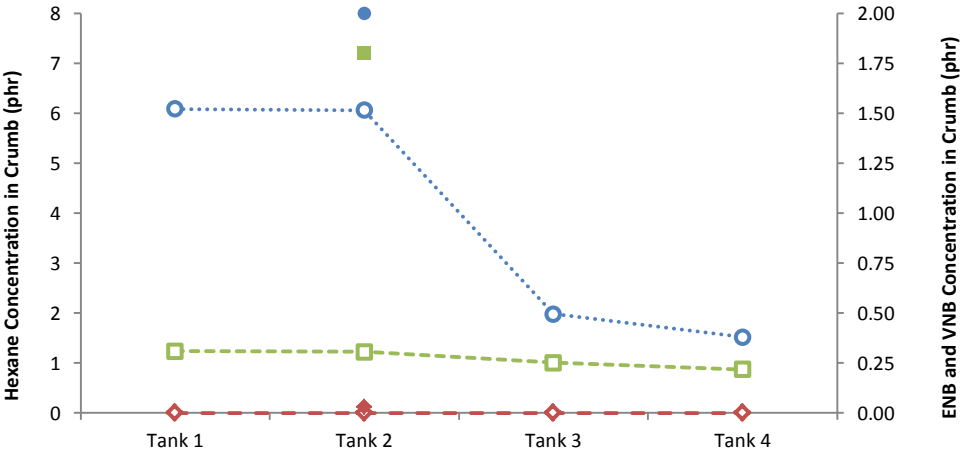

Figure 7c: Updated model predictions and measured results for data set 4 from four-tank process A

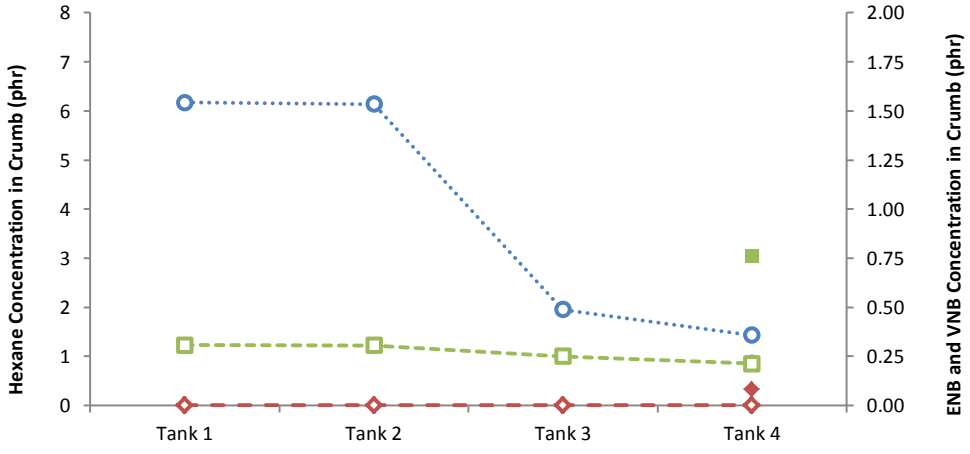

Figure 7d: Updated model predictions and measured results for data set 5 from four-tank process A

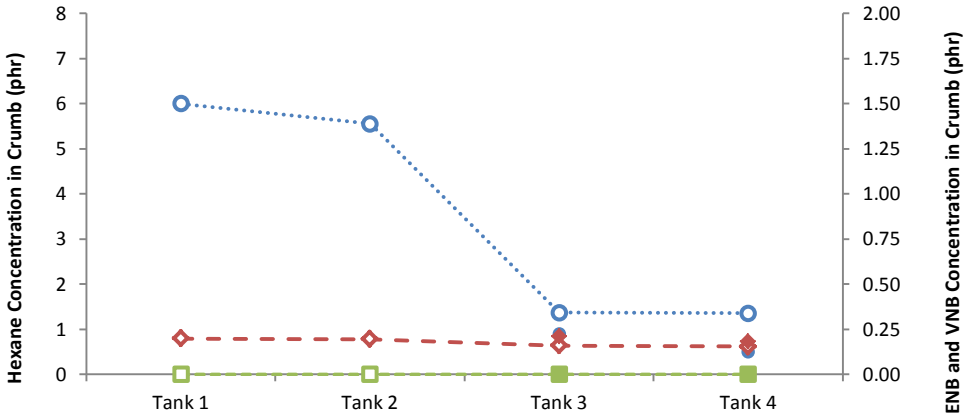

Figure 7e: Updated model predictions and measured results for data set 7 from four-tank process B

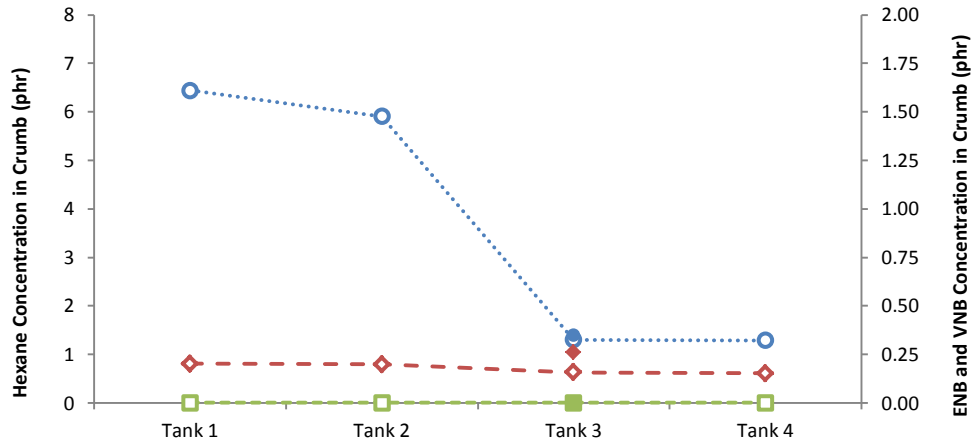

Figure 7f: Updated model predictions and measured results for data set 8 from four-tank process B

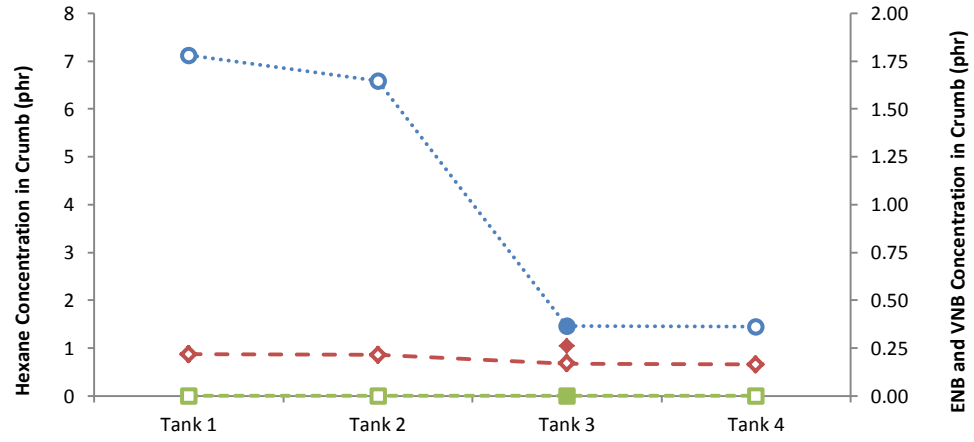

Figure 7g: Updated model predictions and measured results for data set 9 from four-tank process B

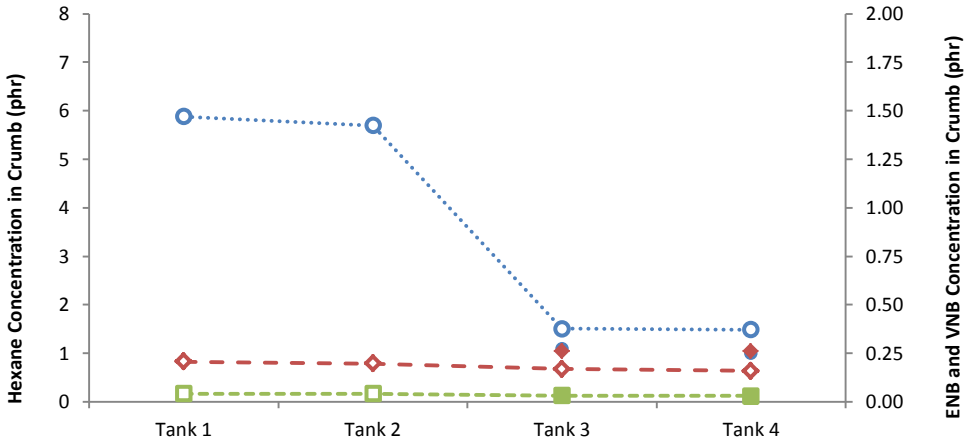

Figure 7h: Updated model predictions and measured results for data set 10 from four-tank process B

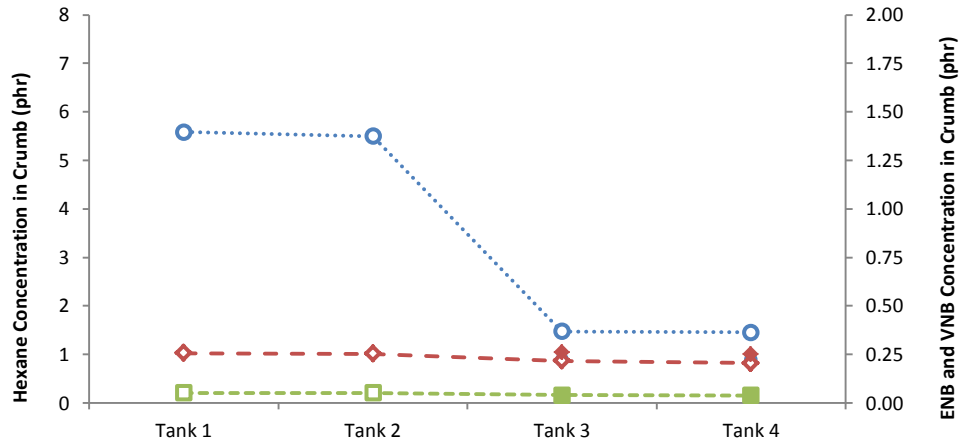

Figure 7i: Updated model predictions and measured results for data set 11 from four-tank process B

Appendix H:
Residence Time Distribution and Time Bins

Figure 8 indicates the residence time distribution for a single CFST as well as the 48 time bins and corresponding fraction of particles in each. Note that the residence time used for this example has a value of 1. Table A indicates the associated time-value for the right-edges of the bins.

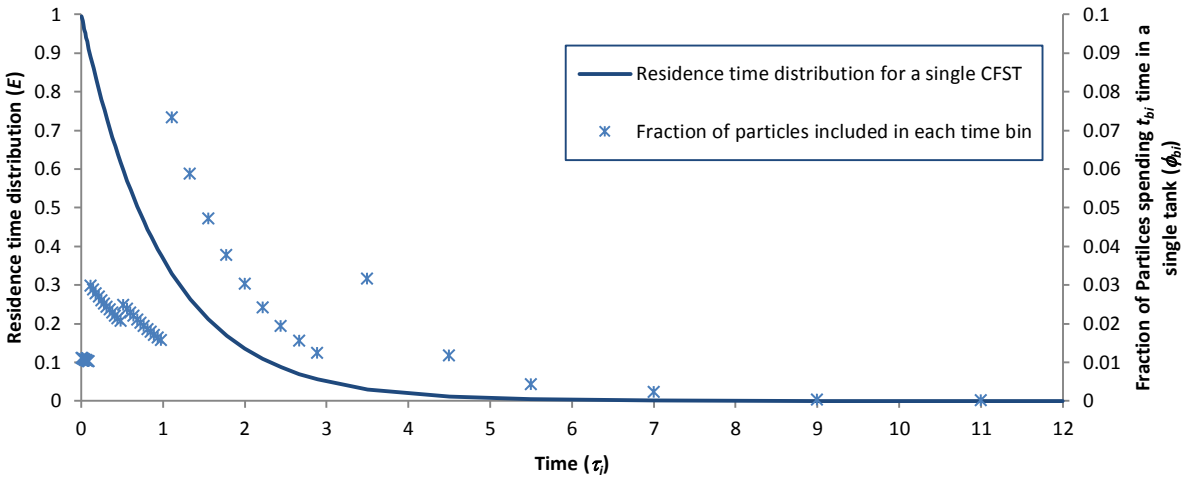

Figure 8: Time bins and residence time distribution for a single CFST. Note that the residence time (τ_i) for this example is 1.

Table A: The time associated with the right-edges of the 48 time bins.

Bin Number	t_{biR}	Bin Number	t_{biR}	Bin Number	t_{biR}
1	0.0111 τ_i	17	0.3667 τ_i	33	1.0000 τ_i
2	0.0222 τ_i	18	0.4000 τ_i	34	1.2222 τ_i
3	0.0333 τ_i	19	0.4333 τ_i	35	1.4444 τ_i
4	0.0444 τ_i	20	0.4667 τ_i	36	1.6667 τ_i
5	0.0556 τ_i	21	0.5000 τ_i	37	1.8889 τ_i
6	0.0667 τ_i	22	0.5417 τ_i	38	2.1111 τ_i
7	0.0778 τ_i	23	0.5833 τ_i	39	2.3333 τ_i
8	0.0889 τ_i	24	0.6250 τ_i	40	2.5556 τ_i
9	0.1000 τ_i	25	0.6667 τ_i	41	2.7778 τ_i
10	0.1333 τ_i	26	0.7083 τ_i	42	3.0000 τ_i
11	0.1667 τ_i	27	0.7500 τ_i	43	4.0000 τ_i
12	0.2000 τ_i	28	0.7917 τ_i	44	5.0000 τ_i
13	0.2333 τ_i	29	0.8333 τ_i	45	6.0000 τ_i
14	0.2667 τ_i	30	0.8750 τ_i	46	8.0000 τ_i
15	0.3000 τ_i	31	0.9167 τ_i	47	10.0000 τ_i
16	0.3333 τ_i	32	0.9583 τ_i	48	12.0000 τ_i